

The shell model as a unified view of nuclear structure

E. Caurier*

*Institut de Recherches Subatomiques, IN2P3-CNRS, Université Louis Pasteur, F-67037
Strasbourg, France*

G. Martínez-Pinedo†

*ICREA and Institut d'Estudis Espacials de Catalunya, Universitat Autònoma de Barcelona,
E-08193 Bellaterra, Spain*

F. Nowacki‡

*Institut de Recherches Subatomiques, IN2P3-CNRS, Université Louis Pasteur, F-67037
Strasbourg, France*

A. Poves§

*Departamento de Física Teórica, Universidad Autónoma, Cantoblanco, 28049, Madrid,
Spain*

A. P. Zuker||

*Institut de Recherches Subatomiques, IN2P3-CNRS, Université Louis Pasteur, F-67037
Strasbourg, France*

(Published 16 June 2005)

The last decade has witnessed both quantitative and qualitative progress in shell-model studies, which have resulted in remarkable gains in our understanding of the structure of the nucleus. Indeed, it is now possible to diagonalize matrices in determinantal spaces of dimensionality up to 10^9 using the Lanczos tridiagonal construction, whose formal and numerical aspects are analyzed in this review. In addition, many new approximation methods have been developed in order to overcome the dimensionality limitations. New effective nucleon-nucleon interactions have been constructed that contain both two- and three-body contributions. The former are derived from realistic potentials (i.e., potentials consistent with two-nucleon data). The latter incorporate the pure monopole terms necessary to correct the bad saturation and shell-formation properties of the realistic two-body forces. This combination appears to solve a number of hitherto puzzling problems. The present review concentrates on those results which illustrate the global features of the approach: the universality of the effective interaction and the capacity of the shell model to describe simultaneously all the manifestations of the nuclear dynamics, either single-particle or collective in nature. The review also treats in some detail the problems associated with rotational motion, the origin of quenching of the Gamow-Teller transitions, double- β decays, the effect of isospin nonconserving nuclear forces, and the specificities of neutron-rich nuclei. Many other calculations—which appear to have “merely” spectroscopic interest—are touched upon briefly, although the authors are fully aware that much of the credibility of the shell model rests on them.

CONTENTS

I. Introduction	428	II. The Interaction	433
A. The three pillars of the shell model	428	A. Effective interactions	434
B. Competing views of nuclear structure	429	B. The monopole Hamiltonian	435
1. Collective versus microscopic	429	1. Bulk properties. Factorable forms	436
2. Mean field versus diagonalizations	430	2. The soft potential $V_{\text{low } k}$	437
3. Realistic versus phenomenological	430	3. Shell formation	437
C. The valence space	431	C. The multipole Hamiltonian	439
D. About this review: The unified view	432	D. Universality of the realistic interactions	441
		III. The Solution of the Secular Problem in a Finite Space	442
		A. The Lanczos method	442
		B. The choice of the basis	443
		C. The Glasgow m -scheme code	444
		D. The m -scheme code ANTOINE	444
		E. The coupled code NATHAN	445
		F. No-core shell model	446
		G. Present possibilities	447
		IV. The Lanczos Basis	447
		A. Level densities	447

*Electronic address: etienne.caurier@ires.in2p3.fr

†Electronic address: martinez@ieec.uab.es

‡Electronic address: frederic.nowacki@ires.in2p3.fr

§Electronic address: alfredo.poves@uam.es

||Electronic address: andres.zuker@ires.in2p3.fr

B. The ground state	449
1. The exp(S) method	449
2. Other numerical approximation methods	450
3. Monte Carlo methods	451
C. Lanczos strength functions	451
V. The $0\hbar\omega$ Calculations	452
A. The monopole problem and the three-body interaction	452
B. The pf shell	455
1. Spectroscopic factors	456
2. Isospin nonconserving forces	456
3. Pure spectroscopy	457
C. Gamow-Teller and magnetic dipole strength	457
1. The meaning of the valence space	459
2. Quenching	459
VI. Spherical Shell-Model Description of Nuclear Rotations	460
A. Rotors in the pf shell	461
B. Quasi-SU(3)	462
C. Heavier nuclei: Quasi+pseudo SU(3)	464
D. The ^{36}Ar and ^{40}Ca superdeformed bands	465
E. Rotational bands of unnatural parity	466
VII. Description of Very Neutron-Rich Nuclei	467
A. $N=8$: ^{11}Li , halos	467
B. $N=20$: ^{32}Mg , deformed intruders	468
C. $N=28$: Vulnerability	469
D. $N=40$: From “magic” ^{68}Ni to deformed ^{64}Cr	471
VIII. Other Regions and Themes	472
A. Astrophysical applications	472
B. $\beta\beta$ decays	475
C. Charge radius shifts in the calcium isotopes	476
D. Shell-model calculations in heavier nuclei	477
E. Random Hamiltonians	478
IX. Conclusion	479
Acknowledgments	479
Appendix A: Basic Definitions and Results	479
Appendix B: Full Form of \mathcal{H}_m	480
1. Separation of \mathcal{H}_{mnp} and \mathcal{H}_{m0}	481
2. Diagonal forms of \mathcal{H}_m	482
Appendix C: The Center-of-Mass Problem	482
References	483

I. INTRODUCTION

In the early days of nuclear physics, the nucleus, composed of strongly interacting neutrons and protons confined in a very small volume, did not appear to be a system to which the shell model, so successful in the atoms, could be of much relevance. Other descriptions—based on the analogy with a charged liquid drop—seemed more natural. However, experimental evidence of independent particle behavior in nuclei soon began to accumulate, such as the extra binding related to some precise values of the number of neutrons and protons (magic numbers) and the systematics of spins and parities.

The existence of shell structure in nuclei had already been noticed in the thirties, but it took more than a decade and numerous papers (see Elliott and Lane, 1957, for the early history) before the correct prescrip-

tion was found by Mayer (1949) and Axel, Jensen, and Suess (1949). To explain the regularities of the nuclear properties associated with *magic numbers*—i.e., specific values of the number of protons Z and neutrons N —the authors proposed a model of independent nucleons confined by a surface-corrected, isotropic harmonic oscillator, plus a strong attractive spin-orbit term,¹

$$U(r) = \frac{1}{2}\hbar\omega r^2 + D\vec{l}^2 + C\vec{l} \cdot \vec{s}. \quad (1)$$

In modern language this proposal amounts to assuming that the main effect of two-body nucleon-nucleon interactions is to generate a spherical mean field. The wave function of the ground state of a given nucleus is then the product of one Slater determinant for the protons and another for the neutrons, obtained by filling the lowest subshells (or “orbits”) of the potential. This primordial shell model is nowadays called the *independent-particle model* (IPM) or *naive shell model*. Its foundation was laid by Brueckner (1954), who showed how the short-range nucleon-nucleon repulsion combined with the Pauli principle could lead to nearly independent particle motion.

As the number of protons and neutrons departs from the magic numbers it becomes indispensable to include in some way the “residual” two-body interaction, to break the degeneracies inherent in the filling of orbits with two or more nucleons. At this point difficulties accumulate: “Jensen himself never lost his skeptical attitude towards the extension of the single-particle model to include the dynamics of several nucleons outside closed shells in terms of a residual interaction” (Weidenmüller, 1990). Nonetheless, some physicists chose to persist. One of our purposes here is to explain and illustrate why it was worth persisting. The key point is that passage from the IPM to the interacting shell model—the shell model for short—is conceptually simple but difficult in practice. In the next section we briefly review the steps involved. Our aim is to give the reader an overall view of the shell model as a subdiscipline of the many-body problem. Italics are used for terms of nuclear jargon when they appear for the first time. The rest of the Introduction will look at the competing views of nuclear structure and establish their connections with the shell model. Throughout, the reader will be directed to the sections of this review where specific topics are discussed.

A. The three pillars of the shell model

The strict validity of the IPM may be limited to closed shells (and single-particle—or hole—states built on them), but it provides a framework with two important components that help in dealing with more complex situations. One is of a mathematical nature: the oscillator orbits define a basis of Slater determinants, the m

¹We assume throughout adimensional oscillator coordinates, i.e., $r \rightarrow (m\omega/\hbar)^{1/2}r$.

scheme, in which to formulate the Schrödinger problem in the occupation number representation (Fock space). It is important to realize that the oscillator basis is relevant, not so much because it provides an approximation to the individual nucleon wave functions, but because it provides the natural quantization condition for self-bound systems.

Then, the many-body problem becomes one of diagonalizing a simple matrix. We have a set of determinantal states for A particles, $a_1^\dagger \cdots a_{iA}^\dagger |0\rangle = |\phi_I\rangle$, and a Hamiltonian containing kinetic and potential energies \mathcal{K} and \mathcal{V} , respectively,

$$\mathcal{H} = \sum_{ij} \mathcal{K}_{ij} a_i^\dagger a_j - \sum_{\substack{i \leq j \\ k \leq l}} \mathcal{V}_{ijkl} a_i^\dagger a_j^\dagger a_k a_l. \quad (2)$$

This Hamiltonian adds one or two particles in orbits i, j and removes one or two from orbits k, l , subject to the Pauli principle ($\{a_i^\dagger a_j\} = \delta_{ij}$). The eigensolutions of the problem $|\Phi_a\rangle = \sum_{I, a} c_{I, a} |\phi_I\rangle$, are the result of diagonalizing the matrix $\langle \phi_I | \mathcal{H} | \phi_I \rangle$, whose off-diagonal elements are either 0 or $\pm \mathcal{V}_{ijkl}$. However, the dimensionalities of the matrices—though not infinite, since a cutoff is inherent to a nonrelativistic approach—are so large as to make the problem intractable, except for the lightest nuclei. Stated in these terms, the nuclear many-body problem does not differ much from other many-fermion problems in condensed matter, quantum liquids, or cluster physics, with which it quite often shares concepts and techniques. The differences come from the interactions, which in the nuclear case are particularly complicated, but paradoxically quite weak, in the sense that they produce sufficiently little mixing of basic states that the zeroth-order approximations bear a significant resemblance to reality.

This is the second far-reaching physical component of the IPM: the basis can be taken to be small enough to be often tractable. Here some elementary definitions are needed: The (neutron and proton) *major oscillator shells* of principal quantum number $p=0, 1, 2, 3, \dots$, called s, p, sd, pf, \dots , respectively, of energy $\hbar\omega(p+3/2)$, contain orbits of total angular momentum $j=1/2, 3/2, \dots, p+1/2$, each with its possible j_z projections, for a total degeneracy $D_j=2j+1$ for each subshell, and $D_p=(p+1)(p+2)$ for the major shells. [One should not confuse the $p=1$ shell— p shell in the old spectroscopic notation—with the generic harmonic-oscillator shell of energy $\hbar\omega(p+3/2)$.]

When for a given nucleus the particles are restricted to have the lowest possible values of p compatible with the Pauli principle, we speak of a $0\hbar\omega$ space. When the many-body states are allowed to have components involving basis states with up to N oscillator quanta more than those pertaining to the $0\hbar\omega$ space, we speak of a $N\hbar\omega$ space (often referred to as a *no-core space*).

For nuclei up to $A \approx 60$, the major oscillator shells provide physically meaningful $0\hbar\omega$ spaces. The simplest possible example will suggest why this is so. Starting from the first of the magic numbers, $N=Z=2$, ${}^4\text{He}$ is no

doubt a closed shell. Adding one particle should produce a pair of single-particle levels: $p_{3/2}$ and $p_{1/2}$. Indeed, this is what is found in ${}^5\text{He}$ and ${}^5\text{Li}$. What about ${}^6\text{Li}$? The lowest configuration, $p_{3/2}^2$, should produce four states of angular momentum and isospin $JT=0, 1, 10, 21, 30$. They are experimentally observed. There is also a $JT=20$ level that requires the $p_{3/2}p_{1/2}$ configuration. Hence the idea of choosing as basis p^m (p stands generically for $p_{3/2}p_{1/2}$) for nuclei up to the next closure, $N=Z=8$, i.e., ${}^{16}\text{O}$. Obviously, the general Hamiltonian in Eq. (2) must be transformed into an “effective” one adapted to the restricted basis, the *valence space*. When this is done, the results are very satisfactory (Cohen and Kurath, 1965). The argument extends to the sd and pf shells.

We have now identified two of the three “pillars” of the shell model: a good valence space and an effective interaction adapted to it. The third is a shell-model code capable of coping with the secular problem. In Sec. I.C we shall examine the reasons for the success of the classical $0\hbar\omega$ shell-model spaces and propose extensions capable of dealing with more general cases. The interaction will be touched upon in Sec. I.B.3 and discussed at length in Sec. II. The codes will be the subject of Sec. III.

B. Competing views of nuclear structure

Because shell-model work is so computer intensive, it is instructive to compare its history and recent developments with the competing—or alternative—views of nuclear structure that demand less (or no) computing power.

1. Collective versus microscopic

The early shell model was hard to reconcile with the idea of the compound nucleus and the success of the liquid-drop model. With the discovery of rotational motion (Bohr, 1952; Bohr and Mottelson, 1953) which was at first as surprising as the IPM, the reconciliation seemed to become harder. Resolution came with the realization that collective rotors are associated with “intrinsic states” very well approximated by deformed mean-field determinants (Nilsson, 1955), from which the exact eigenstates can be extracted by projection to good angular momentum (Peierls and Yoccoz, 1957), an early and spectacular example of spontaneous symmetry breaking. When nuclear superfluidity was added to the picture (Bohr *et al.*, 1958), the unified model was born, a basic paradigm that remains valid.

Compared with the impressive architecture of the unified model, what the shell model could offer were some striking but isolated examples that pointed to the soundness of a many-particle description. Among them, let us mention the elegant work of Talmi and Unna (1960), the $f_{7/2}^n$ model of McCullen, Bayman, and Zamick (1964)—probably the first successful diagonalization involving both neutrons and protons—and the Cohen and Kurath (1965) fit to the p shell, the first of the classical $0\hbar\omega$

regions. It is worth noting that this calculation involved spaces of m -scheme dimensionalities, d_m , of the order of 100, while at fixed total angular momentum and isospin $d_{JT} \approx 10$.

The microscopic origin of rotational motion was found by Elliott (1958a, 1958b). The interest in this contribution was immediate, but it took quite a few years to realize that Elliott's quadrupole force and the underlying SU(3) symmetry were the foundation, rather than an example, of rotational motion (see Sec. VI).

It is fair to say that for almost 20 years after its inception, in the mind of many physicists, the shell model still suffered from an implicit separation of roles, which assigned it the task of accurately describing a few especially important nuclei, while the overall coverage of the nuclear chart was understood to be the domain of the unified model.

A somewhat intermediate path was opened by the well-known *interacting Boson model* of Arima and Iachello (1975) and its developments, which we do not discuss here. The interested reader can find the details in Iachello and Arima (1987).

2. Mean field versus diagonalizations

The first realistic² matrix elements of Kuo and Brown (1966) and the first modern shell-model code by French *et al.* (1969) came almost simultaneously and opened the way for the first generation of “large-scale” calculations, which at the time meant $d_{JT} \approx 100$ –600. They made it possible to describe the neighborhood of ¹⁶O (Zuker, Buck, and McGrory, 1968) and the lower part of the *sd* shell (Halbert *et al.*, 1971). However, the increases in tractable dimensionalities were insufficient to promote the shell model to the status of a general description, and the role separation mentioned above persisted. Moreover, the work done exhibited serious problems, which could be traced to the realistic matrix elements themselves (see Sec. I.B.3).

However, a fundamental idea emerged at the time: the existence of an underlying universal two-body interaction, which would permit replacement of the unified model description by a fully microscopic one, based on mean-field theory. The first breakthrough came when Baranger and Kumar (1968) proposed a new form of the unified model by showing that Elliott's quadrupole force could be derived from the Kuo-Brown matrix elements. Adding a pairing interaction and a spherical mean field, they proceeded to perform Hartree-Fock-Bogoliubov calculations in the first of a successful series of papers (Kumar and Baranger, 1968). Their work could be described as shell model by other means, as it was restricted to valence spaces of two contiguous major shells.

This limitation was overcome when Vautherin and Brink (1972) and Dechargé and Gogny (1980) initiated the two families of Hartree-Fock (HF) calculations

which became known as the Skyrme and Gogny approaches, respectively. These remain to this day the only tools capable of giving microscopic descriptions throughout the Periodic Table. They were later joined by the relativistic HF approach (Serot and Walecka, 1986). For a review of the three variants see Bender, Heenen, and Reinhard (2003). See also Péru, Girod, and Berger (2000) and Rodriguez-Guzmán, Egido, and Robledo (2000), and references therein, for recent work with the Gogny force, which is the one with the closer connection with realistic interactions (Secs. VI.A and II.D).

Since single determinantal states can hardly be expected to describe many-body solutions, everybody admits the need to go beyond the mean field. Nevertheless, as it provides such a good approximation to the wave functions (typically about 50%) it suggests efficient truncation schemes, as will be explained in Secs. IV.B.1 and IV.B.2.

3. Realistic versus phenomenological

Nowadays, many regions of the table of nuclides remain beyond the direct reach of the shell model, but enough has happened in the last decade to transform it into a unified view. Many steps—as outlined in Sec. I.D—are needed to substantiate this claim. Here we introduce the first: A unified view requires a unique interaction. Its free parameters must be few and well defined, so as to make the calculations independent of the quantities they are meant to explain. Here, because we touch upon a different competing view of special interest for shell-model experts, we recall the remarks at the end of the first paragraph of Sec. I.B.2.

The exciting prospect that realistic matrix elements might lead to parameter-free spectroscopy did not materialize. As the growing sophistication of numerical methods allowed treatment of an increasing number of particles in the *sd* shell, the results became disastrous. Then, two schools of thought on the status of phenomenological corrections emerged. In one of them, all matrix elements were considered to be free parameters. In the other, only average matrix elements, or *centroids*—related to the bad saturation and shell formation properties of the two-body potentials—needed to be fitted (the monopole way). The former led to the *universal sd interaction* (Wildenthal, 1984), which enjoyed immense success and for ten years set the standard for shell-model calculations in a large valence space (Brown and Wildenthal, 1988; see Brown, 2001, for a recent review). The second, which we adopt here, was initiated in Eduardo Pasquini's Ph.D. thesis (1976), where the first calculations in the full *pf* shell, involving both neutrons and protons, were done.³ Twenty years later, we know that the minimal monopole corrections proposed in his work are sufficient to provide results of a quality comparable

²Realistic interactions are those consistent with data obtained in two- (and nowadays three-) nucleon systems.

³Two months after receiving his Ph.D., Pasquini and his wife “disappeared” in Argentina. Hence his work is only publicly available in condensed form (Pasquini and Zuker, 1978).

to those of the universal sd interaction for nuclei in $f_{7/2}$ region.

However, there were still problems with the monopole way: they showed up around and beyond ^{56}Ni , as well as in the failure to be competitive with the universal sd interaction in the sd shell (note that the universal sd interaction contains nonmonopole two-body corrections to the realistic matrix elements). The solution was found only recently with the introduction of three-body forces. This far-reaching development will be explained in detail in Secs. II, II.B, and V.A. Here we shall only anticipate the conclusions of these sections by offering two syllogisms. First, the case for realistic two-body interactions is so strong that we have to accept them as they are. Little is known about three-body forces except that they exist. Therefore problems with calculations involving only two-body forces must be blamed on the absence of three-body forces. This argument raises (at least) one question: What is to be made of all the calculations, using only two-body forces, that give satisfactory results? The answer lies in the second syllogism: All clearly identifiable problems are of monopole origin. They can be solved reasonably well by phenomenological changes of the monopole matrix elements. Therefore fitted interactions can differ from realistic ones basically through monopole matrix elements. (We speak of R compatibility in this case.) The two syllogisms become fully consistent by noting that the inclusion of three-body monopole terms always improves the performance of the forces that adopt the monopole way.

For the $0\hbar\omega$ spaces, the Cohen-Kurath (1965), the Chung-Wildenthal (Wildenthal and Chung, 1979) and the FPD6 (Richter *et al.*, 1991) interactions appear to be R compatible. The universal sd (Wildenthal, 1984) interaction is R incompatible. The recent set of pf -shell matrix elements (GXPF1), proposed by Honma *et al.* (2002, 2004) turns out to be R incompatible in a subtle way. This will be analyzed in Secs. V.A and V.B.

C. The valence space

The choice of valence space should reflect a basic physical fact: that the most significant components of the low-lying states of nuclei can be accounted for by many-body states involving the excitation of particles in a few orbitals around the Fermi level. The history of the shell model is that of the interplay between experiment and theory to establish the validity of this concept. Our present understanding can be roughly summed up by saying that “a few” orbitals means essentially one or two contiguous major shells.⁴

For a single major shell, the classical $0\hbar\omega$ spaces, exact solutions are now available from which instructive conclusions can be drawn. Consider, for instance, the spectrum of ^{41}Ca from which we want to extract the single-

particle states of the pf shell. Remember that in ^5Li we expected to find two states and indeed found two. Now, in principle, we expect four states. They are certainly in the data. However, they must be retrieved from a jungle of some 140 levels seen below 7 MeV. Moreover, the $f_{7/2}$ ground state is the only one that is a pure single-particle state. The others are split, even severely in the case of the highest ($f_{5/2}$) (Endt and van der Leun, 1990; Sec. V.B.1 contains an interesting example of the splitting mechanism). So, how can we expect the pf shell to be a good valence space? For a few particles above ^{40}Ca it is certainly not. However, as we shall show, it turns out that above $A=46$, the lowest $(pf)^m$ configurations⁵ are sufficiently detached from all others as to generate wave functions that can evolve to the exact ones through low-order perturbation theory.

The ultimate ambition of shell-model theory is to get exact solutions. Those provided by the sole valence space are, so to speak, the tip of the iceberg in terms of number of basic states involved. The rest may be so well hidden as to make us believe in the literal validity of the shell-model description in a restricted valence space. For instance, the magic closed shells are good valence spaces consisting of a single state. This does not mean that a magic nucleus is 100% closed shell; 50% or 60% should be enough, as we shall see in Sec. IV.B.1. In Sec. V.C.1 it will be argued that the $0\hbar\omega$ valence spaces account for basically the same percentage of the full wave functions. Conceptually the valence space may be thought of as defining a representation intermediate between the Schrödinger one, in which the operators are fixed and the wave function contains all the information, and the Heisenberg one, where the reverse is true.

At best, $0\hbar\omega$ spaces can describe only a limited number of low-lying states of the same (“natural”) parity. Two contiguous major shells can most certainly cope with all levels of interest, but they lead to intractably large spaces and suffer from a center-of-mass problem (analyzed in Appendix C). Here, a physically sound pruning of the space is suggested by the IPM. What made a success of the model is its explanation of the observed magic numbers by the addition of a spin-orbit term to the harmonic-oscillator (HO) field (for shell formation, see Sec. II.B.2). If we separate a major shell into two parts, $\text{HO}(p)=p_{>} \oplus r_p$, where $p_{>}$ is the largest subshell having $j=p+1/2$, and r_p is the “rest” of the harmonic-oscillator p shell, we can define the *extruded-intruded* (EI) spaces as $\text{EI}(p)=r_p \oplus (p+1)_{>}$. The $(p+1)_{>}$ orbit is expelled from $\text{HO}(p+1)$ by the spin-orbit interaction and intrudes into $\text{HO}(p)$. The EI spaces are well established entities when only one *fluid* (proton or neutron) is active, giving rise to the shell closures at proton number or neutron number 28, 50, 82, and 126. These nuclei are “spherical,” amenable to exact diagonalizations, and fairly well understood (see, for example, Abzouzi *et al.*, 1991).

⁴Three major shells are necessary to deal with superdeformation.

⁵A configuration is a set of states having a fixed number of particles in each orbit.

As soon as both fluids are active, *deformation effects* become appreciable, leading to coexistence between spherical and deformed states and eventually to dominance of the latter. To cope with this situation we propose *extended EI spaces* defined as $\text{EEI}(p) = r_p \oplus \Delta_{p+1}$, where $\Delta_p = p_{>} \oplus (p_{>-2}) \oplus \dots$, i.e., the $\Delta j=2$ sequence of orbits that contain $p_{>}$, which are needed to account for rotational motion, as explained in Sec. VI. The $\text{EEI}(1)$ ($p_{1/2}, d_{5/2}, s_{1/2}$) space was successful in describing the full low-lying spectra for $A=15-18$ (Zuker *et al.*, 1968, 1969). It is only recently that the $\text{EEI}(2)$ ($s_{1/2}, d_{3/2}, f_{7/2}, p_{3/2}$) space (region around ^{40}Ca) has become tractable (see Secs. VI.D and VII.C). $\text{EEI}(3)$ is the natural space for the proton-rich region centered in ^{80}Zr . For heavier nuclei exact diagonalizations are not possible, but the EEI spaces provide simple and excellent estimates of quadrupole moments at the beginning of the well-deformed regions (Sec. VI.C).

As presented above, the choice of valence space is primarily a matter of physics. In practice, when exact diagonalizations are impossible, truncations are introduced. They may be based on systematic approaches, such as the approximation schemes discussed in Secs. IV.B.1 and IV.B.2, or on the mean-field methods mentioned in Sec. I.B.2 and analyzed in Sec. VI.A.

D. About this review: The unified view

In this review we highlight several unifying aspects common to the most recent successful shell-model calculations:

- (a) An effective interaction connected with both the two- and three-nucleon bare forces,
- (b) explanation of the global properties of nuclei via the monopole Hamiltonian,
- (c) the universality of the multipole Hamiltonian,
- (d) a description of the collective behavior in the laboratory frame, by means of the spherical shell model,
- (e) a description of resonances using the Lanczos strength function method.

The review is organized so as to treat these in turn. References are given here only for work that will not be mentioned later.

Section II. The basic tool for analyzing an interaction is the monopole-multipole separation. The monopole governs saturation and shell properties; it can be thought of as the correct generalization of Eq. (1). Monopole theory is scattered through many references. Only by the inclusion of three-body forces could a satisfactory formulation be achieved. As this is a very recent and fundamental development that makes possible a unified viewpoint of the monopole-field concept, Sec. II is largely devoted to it. The “residual” multipole force has been extensively described in a single reference, which will be reviewed briefly and updated. The aim of the section is to show how realistic interactions can be

characterized by a small number of parameters.

Section III. The ANTOINE and NATHAN codes have made it possible to evolve from dimensionalities $d_m \sim 5 \times 10^4$ in 1989 to $d_m \sim 10^9$, $d_j \sim 10^8$ nowadays. The gains are partly due to the increase in computing power, but more importantly to the development of new algorithms that take advantage of the enlarged disk and RAM size available in contemporary computers. These algorithmic advances in the construction of tridiagonal Lanczos matrices will be described in Sec. III.

Section IV. The Lanczos construction can be used to eliminate the “black box” aspect of the diagonalizations, to a large extent. We show in Sec. IV how it can be related to the notions of the partition function, evolution operator, and level densities. Furthermore, it can be turned into a powerful truncation method by combining it with coupled-cluster theory. Finally, it describes strength functions with maximal efficiency.

Section V. After describing the three-body mechanism that solves the monopole problem, which had plagued the classical $0\hbar\omega$ calculations, we present some selected examples of *pf*-shell spectroscopy. Special attention is given to Gamow-Teller transitions, one of the main achievements of modern shell-model work.

Section VI. Another major achievement is the recent shell-model description of rotational nuclei. The new generation of gamma detectors, Euroball and Gamma-sphere, has made it possible to access high-spin states in medium-mass nuclei, for which full $0\hbar\omega$ calculations are available. Their remarkable harvest includes a large spectrum of collective manifestations that the spherical shell model can predict or explain, for instance, deformed rotors, backbending, band terminations, and yrast traps. Configurations involving two major oscillator shells have also been shown to account well for the appearance of superdeformed excited bands.

Section VII. A combination of factors make light and medium-light nuclei near the neutron drip line especially interesting: (a) They have recently come under intense experimental scrutiny. (b) They are amenable to shell-model calculations, sometimes even exact no-core ones. (c) They exhibit very interesting behavior, such as halos and sudden onset of deformation. (d) They achieve the highest N/Z ratios attained. (e) When all (or most of) the valence particles are neutrons, the spherical shell-model closures, dictated by the isovector channel of the nuclear interaction alone, may differ from those in the stability valley. These regions suggest some exacting tests for the theoretical descriptions, which the conventional shell-model calculations have passed satisfactorily. For nearly unbound nuclei, the shell-model description has to be supplemented by some refined extensions, such as the shell model in the continuum, which is beyond the scope of this review. References to the subject can be found in Bennaceur *et al.* (1999, 2000), Id Betan *et al.* (2002), and Michel *et al.* (2002, 2003), which deal with the Gamow shell model.

Section VIII. There is a characteristic of the shell model we have not yet discussed: its ability to give more precise quantitative information on nuclear structure.

Shell model wave functions are, in particular, of great use in other disciplines. For example, weak decay rates are crucial for the understanding of several astrophysical processes, and neutrinoless $\beta\beta$ decay is one of the main sources of information about the neutrino masses. In both cases, shell-model calculations play a central role. The last section deals with these subjects, and some others.

Appendix B contains a full derivation of the general form of the monopole field.

Two recent reviews by Brown (2001) and Otsuka, Honma, *et al.* (2001) have made it possible to simplify our task and avoid redundancies. However we did not feel that these reviews excused us from citing and commenting in some detail on important work that bears directly on the subjects we treat.

Sections II and IV and the Appendixes are based on unpublished notes by A. P. Zuker.

II. THE INTERACTION

The following remarks from Abzouzi, Caurier, and Zuker (1991) still provide a good introduction to the subject:

“The use of realistic potentials (i.e., consistent with NN scattering data) in shell-model calculation was pioneered by Kuo and Brown (1966). Of the enormous body of work that followed we would like to extract two observations. The first is that whatever the forces (hard- or soft-core, ancient or new) and the method of regularization—Brueckner G matrix (Kuo and Brown, 1966; Kahana *et al.*, 1969a), Sussex direct extraction (Elliott *et al.* 1968), or Jastrow correlations (Fiase *et al.*, 1988)—the effective matrix elements are extraordinarily similar (Rutsgi *et al.*, 1971; Pasquini and Zuker, 1978). The most recent results (Jiang *et al.* 1989) amount to a vindication of the work of Kuo and Brown (1966). We take this similarity to be the great strength of the realistic interactions, since it confers on them a model-independent status as direct links to the phase shifts.

The second observation is that when used in shell-model calculations and compared with data these matrix elements give results that deteriorate rapidly as the number of particles increases (Halbert *et al.*, 1971; Brown and Wildenthal, 1988). It was found (Pasquini and Zuker, 1978) that in the pf shell a phenomenological cure, confirmed by exact diagonalizations up to $A=48$ (Caurier *et al.*, 1989), amounts to very simple modifications of some average matrix elements (*centroids*) of the Kuo-Brown interaction (Kuo and Brown, 1968).”

Abzouzi *et al.* (1991) were able to obtain good spectroscopy in the p and sd shells only through more radical changes in the centroids, involving substantial three-body terms. In 1991 it was hard to interpret them as effective, and there were insufficient grounds to claim that they were real.

Nowadays, the need of true three-body forces has become irrefutable: In the 1990s several two-body potentials were developed—Nijmegen I and II (Stoks *et al.*, 1993), AV18 (Wiringa *et al.*, 1995), and the charge-dependent Bonn potential (CD-Bonn; Machleidt *et al.*, 1996)—that fit the ≈ 4300 entries in the Nijmegen database (Stoks *et al.*, 1994) with $\chi^2 \approx 1$, and none of them seemed capable of predicting perfectly the nucleon vector analyzing power in elastic (N,d) scattering (the A_y puzzle). Two recent additions to the family of high-precision two-body potentials—a new “CD-Bonn” (Machleidt, 2001) and the chiral Idaho-A and -B (Entem and Machleidt, 2002)—have dispelled any hopes of solving the A_y puzzle with two-body-only interactions (Entem *et al.*, 2002).

Furthermore, quasiexact two-body Green’s function Monte Carlo results (Pudliner *et al.*, 1997; Wiringa *et al.*, 2000), which provided acceptable spectra for $A \leq 8$ (though they had problems with binding energies and spin-orbit splittings), now encounter serious trouble in the spectrum of ^{10}B , as found through the no-core shell-model calculations of Navrátil and Ormand (2002) and Caurier *et al.* (2002), and confirmed by Pieper *et al.* (2002), who also show that the problems can be remedied to a large extent by introducing the new Illinois three-body potentials developed by Pieper *et al.* (2001).

It can be seen that the trouble detected with a two-body-only description—with binding energies, spin-orbit splittings, and spectra—is always related to centroids, which, once associated with operators that depend only on the number of particles in subshells, determine a monopole Hamiltonian \mathcal{H}_m that basically governs Hartree-Fock self-consistency. As we shall show, the full \mathcal{H} can be separated rigorously into $\mathcal{H} = \mathcal{H}_m + \mathcal{H}_M$. The multipole part \mathcal{H}_M includes pairing, quadrupole, and other forces responsible for collective behavior, and—as checked by many calculations—is well given by the two-body potentials.

The preceding paragraph amounts to rephrasing the two observations quoted at the beginning of this section with the proviso that discrepancies with experiment cannot be blamed on the—now nearly perfect—two-body potentials. Hence the necessary “corrections” to \mathcal{H}_m must have a three-body origin. Given that we have no complaint with \mathcal{H}_M , the primary problem is the monopole contribution to the three-body potentials. This is welcome news, because a full three-body treatment would render most shell-model calculations impossible, while the phenomenological study of monopole behavior is quite simple. Furthermore, it is quite justified because there is little *ab initio* knowledge of the three-body potentials.⁶ Therefore whatever information comes from nuclear data beyond $A=3$ is welcome.

In shell-model calculations, the interaction appears as matrix elements, which soon become far more numerous

⁶Experimentally there will never be enough data to determine them. The hope for a few-parameter description comes from chiral perturbation theory (Entem and Machleidt, 2002).

than the number of parameters defining the realistic potentials. Our task will consist in analyzing the Hamiltonian in the oscillator representation (or Fock space) so as to understand its workings and simplify its form. In Sec. II.A we sketch the theory of effective interactions. In Sec. II.B we explain how to construct from data a minimal \mathcal{H}_m , while Sec. II.C will be devoted to extracting from realistic forces the most important contributions to \mathcal{H}_M . The basic tools are symmetry and scaling arguments, the clean separation of bulk and shell effects, and the reduction of \mathcal{H} to sums of factorable terms (Dufour and Zuker, 1996).

A. Effective interactions

The Hamiltonian is written in an oscillator basis as

$$\begin{aligned} \mathcal{H} = \mathcal{K} + \sum_{r \leq s, t \leq u, \Gamma} \mathcal{V}_{rstu}^{\Gamma} Z_{rs\Gamma}^+ \cdot Z_{tu\Gamma} \\ + \sum_{r \leq s \leq t, u \leq v \leq w, \Gamma} \mathcal{V}_{rstuvw}^{\Gamma} Z_{rst\Gamma}^+ \cdot Z_{uvw\Gamma}, \end{aligned} \quad (3)$$

where \mathcal{K} is the kinetic energy, $\mathcal{V}_{rr'}^{\Gamma}$ the interaction matrix elements, $Z_{r\Gamma}^+$ ($Z_{r\Gamma}$) create (annihilate) pairs ($r \equiv rs$) or triples ($r \equiv rst$) of particles in orbits r , coupled to $\Gamma = JT$. Dots stand for scalar products. The basis and the matrix elements are large but never infinite.⁷

The aim of an effective interaction theory is to reduce the secular problem in the large space to a smaller model space by treating the coupling between them perturbatively, thereby transforming the full potential, and its repulsive short-distance behavior, into a smooth pseudopotential.

In what follows, if we have to distinguish between large ($N\hbar\omega$) and model spaces, we use \mathcal{H} , \mathcal{K} , and \mathcal{V} for the pseudopotential in the former and H , K , and V for the effective interaction in the latter.

The general procedure for describing an exact eigenstate in a restricted space was obtained independently by Suzuki and Lee (1980) and Poves and Zuker (1981a).⁸ It consists of dividing the full space into model ($|i\rangle$) and external ($|\alpha\rangle$) determinants and introducing a transformation that respects strict orthogonality between the spaces and decouples them exactly:

$$|\bar{i}\rangle = |i\rangle + \sum_{\alpha} A_{i\alpha} |\alpha\rangle, \quad |\bar{\alpha}\rangle = |\alpha\rangle - \sum_i A_{i\alpha} |i\rangle, \quad (4)$$

⁷Nowadays, the nonrelativistic potentials must be thought of as derived from an effective field theory that has a cutoff of about 1 GeV (Entem and Machleidt, 2002). Therefore truly hard cores are ruled out, and \mathcal{H} should be understood to act on a sufficiently large vector space, not over the whole Hilbert space.

⁸The notations in both papers are very different, but the perturbative expansions are probably identical because the Hermitian formulation of Suzuki (1982) is identical to that given by Poves and Zuker (1981a). This paper also deals extensively with the coupled-cluster formalism.

$$\langle \bar{i} | \bar{\alpha} \rangle = 0, \quad A_{i\alpha} \text{ is defined through } \langle \bar{i} | \mathcal{H} | \bar{\alpha} \rangle = 0. \quad (5)$$

The idea is that the model space can produce one or several starting wave functions that can evolve to exact eigenstates through perturbative or coupled-cluster evaluation of the amplitudes $A_{i\alpha}$, which can be viewed as matrix elements of a many-body operator A . In coupled-cluster theory (or $\exp S$; Coester and Kümmel, 1960; Kümmel *et al.*, 1978) one sets $A = \exp S$, where $S = S_1 + S_2 + \dots + S_k$ is a sum of k -body operators. The decoupling condition $\langle \bar{i} | \mathcal{H} | \bar{\alpha} \rangle = 0$ then leads to a set of coupled integral equations for the S_i amplitudes. When the model space reduces to a single determinant, setting $S_1 = 0$ leads to Hartree-Fock theory if all other amplitudes are neglected. The S_2 approximation contains both low-order Brueckner theory and the random-phase approximation (RPA). In the presence of hard-core potentials, the priority is to screen them through the low-order Brueckner theory and to discard matrix elements contributing to the RPA. An important implementation of the theory was due to Zabolitzky, whose calculations for ${}^4\text{He}$, ${}^{16}\text{O}$, and ${}^{40}\text{Ca}$ included S_3 (Bethe-Faddeev) and S_4 (Day-Yacoubovsky) amplitudes (Kümmel, Lührmann, and Zabolitzky, 1978). This ‘‘Bochum truncation scheme,’’ which retraces the history of nuclear-matter theory, has the drawback that at each level it neglects terms that one would like to keep.

The way out of this problem (Heisenberg and Mihaila, 1999; Mihaila and Heisenberg, 2000) consists of a new truncation scheme in which some approximations are made, but no terms are neglected, relying on the fact that the matrix elements are finite. The calculations of these authors for ${}^{16}\text{O}$ (up to S_3) can be ranked with the quasixact Green’s-function Monte Carlo and no-core shell models for lighter nuclei.

In the quasidegenerate regime (many model states), the coupled-cluster equations determine an effective interaction in the model space. The theory is much simplified if we enforce the decoupling condition for a *single* state whose exact wave function is written as

$$\begin{aligned} |\overline{\text{ref}}\rangle &= (1 + A_1 + A_2 + \dots)(1 + B_1 + B_2 + \dots)|\text{ref}\rangle \\ &= (1 + C_1 + C_2 + \dots)|\text{ref}\rangle, \end{aligned} \quad (6)$$

where $C = \exp S$ and $|\text{ref}\rangle$ is a model determinant. The internal amplitudes associated with the B operators are those of an eigenstate obtained by diagonalizing $H_{\text{eff}} = \mathcal{H}(1 + A)$ in the model space. As it is always possible to eliminate the A_1 amplitude, at the S_2 level there is no coupling i.e., the effective interaction is a state-independent G matrix (Zuker, 1984), which has the advantage of providing an initialization for H_{eff} . Going to the S_3 level would be very hard, and we examine what has become standard practice.

The power of the coupled-cluster theory is that it provides a unified framework for the two things we expect from decoupling: to smooth the repulsion and to incorporate long-range correlations. The former demands jumps of, say, $50\hbar\omega$, the latter much less. Therefore it is

convenient to treat them separately. Standard practice assumes that G -matrix elements can provide a smooth pseudopotential in some sufficiently large space and then accounts for long-range correlations through perturbation theory. The equation to be solved is

$$G_{ijkl} = \mathcal{V}_{ijkl} - \sum_{\alpha\beta} \frac{\mathcal{V}_{ij\alpha\beta} G_{\alpha\beta kl}}{\epsilon_\alpha + \epsilon_\beta - \epsilon_i - \epsilon_j + \Delta}, \quad (7)$$

where ij and kl now stand for orbits in the model space, while in the pair $\alpha\beta$ at least one orbit is outside the model space, ϵ_x is an unperturbed (usually kinetic) energy, and Δ a free parameter called the *starting energy*. Hjorth-Jensen, Kuo, and Osnes (1995) describe in detail a sophisticated partition that amounts to having two model spaces, one large and one small.

In no-core shell-model calculations an $N\hbar\omega$ model space is chosen with $N \approx 6-10$. When initiated by Zheng *et al.* (1993) the pseudopotential was a G matrix with starting energy. Then the Δ dependence was eliminated, either by arcane perturbative maneuvers or by direct decoupling of two-body elements from a very large space (Navrátil and Barrett, 1996), further implemented by Navrátil, Vary, and Barrett (2000a) and extended to three-body effective forces (Navrátil *et al.* 2000; Navrátil and Ormand, 2002). It would be of interest to compare the resulting effective interactions to the Brueckner and Bethe-Faddeev amplitudes obtained in a full $\exp S$ approach (which are also free of arbitrary starting energies).

A most valuable contribution of the no-core model is the proof that it is possible to work with a pseudopotential in $N\hbar\omega$ spaces. The method relies on exact diagonalizations, which soon become prohibitive; hence, in the future, coupled-cluster theory may become the standard approach. Going to S_3 for $N=50$ —as Heisenberg and Mihaila (1999) did—is hard. For $N=10$ it should be much easier. See in this respect Kowalski *et al.* (2004).

Another important contribution of the no-core method is that the excitation spectra converge well before the full energy, which formally validates the $0\hbar\omega$ diagonalizations with rudimentary potentials⁹ and second-order corrections.

The $0\hbar\omega$ results are very good for the spectra. However, having a good pseudopotential to describe energies is not enough. The transition operators also need dressing. For some of them, notably $E2$, the dressing mechanism (coupling to $2\hbar\omega$ quadrupole excitations) has been well understood for years (see Dufour and Zuker, 1996, for a detailed analysis), and it yields the abundantly tested and confirmed recipe of using effective charges of $\approx 1.5e$ for the protons and $\approx 0.5e$ for neutrons. For Gamow-Teller transitions, mediated by the spin-isospin $\sigma\tau_\pm$ operator, the renormalization mechanism involves an overall *quenching factor* of 0.7–0.8 whose origin is far subtler. This will be examined in Secs. V.C.1 and V.C.2.

⁹Even old potentials provide good fits to the low-energy NN phase shifts, the only ones that matter at $0\hbar\omega$.

B. The monopole Hamiltonian

A many-body theory usually starts by separating the Hamiltonian into an “unperturbed” and a “residual” part, $\mathcal{H} = \mathcal{H}_0 + \mathcal{H}_r$. The traditional approach consists in choosing for \mathcal{H}_0 a one-body single-particle field. Since \mathcal{H} contains two- and three-body components, the separation is not mathematically clean. Therefore we propose the following:

$$\mathcal{H} = \mathcal{H}_m + \mathcal{H}_M, \quad (8)$$

where \mathcal{H}_m , the monopole Hamiltonian, contains \mathcal{K} and all quadratic and cubic (two- and three-body) forms in the scalar products of fermion operators $a_{r_x}^\dagger \cdot a_{s_y}$,¹⁰ while the multipole \mathcal{H}_M contains all the rest. A thorough discussion of the monopole Hamiltonian is given in Appendix A, where full derivations can be found.

Our plan is to concentrate on the two-body part, and introduce three-body elements as the need arises.

\mathcal{H}_m has a *diagonal* part, \mathcal{H}_m^d , written in terms of number and isospin operators ($a_{r_x}^\dagger \cdot a_{r_y}$). It reproduces the average energies of configurations at a fixed number of particles and isospin in each orbit (jt representation) or, alternatively, at a fixed number of particles in each orbit and each fluid (neutron-proton, np , or j representation). In jt representation the centroids

$$\mathcal{V}_{st}^T = \frac{\sum_J \mathcal{V}_{st}^{JT} (2J+1) [1 - (-)^{J+T} \delta_{st}]}{\sum_J (2J+1) [1 - (-)^{J+T} \delta_{st}]}, \quad (9a)$$

$$a_{st} = \frac{1}{4} (3\mathcal{V}_{st}^1 + \mathcal{V}_{st}^0), \quad b_{st} = \mathcal{V}_{st}^1 - \mathcal{V}_{st}^0, \quad (9b)$$

are associated with the two-body quadratics in number (m_s) and isospin operators (T_s),

$$m_{st} = \frac{1}{1 + \delta_{st}} m_s (m_t - \delta_{st}), \quad (10a)$$

$$T_{st} = \frac{1}{1 + \delta_{st}} \left(T_s \cdot T_t - \frac{3}{4} m_{st} \delta_{st} \right), \quad (10b)$$

to define the diagonal two-body part of the monopole Hamiltonian (Bansal and French, 1964; French 1969),

$$\mathcal{H}_{mjt}^d = \mathcal{K}^d + \sum_{s \leq t} (a_{st} m_{st} + b_{st} T_{st}) + \mathcal{V}_m^{d_3}. \quad (11)$$

The two-body part is a standard result, easily extended to include the three-body term

$$\mathcal{V}_m^{d_3} = \sum_{stu} (a_{stu} m_{stu} + b_{stu} T_{stu}), \quad (12)$$

where $m_{stu} \equiv m_{st} m_u$, or $m_s(m_s-1)(m_s-2)/6$ and $T_{stu} \equiv m_s T_{tu}$ or $(m_s-2)T_{su}$. The extraction of the full \mathcal{H}_m is

¹⁰Here r and s are subshells of the same parity and angular momentum; x and y stand for neutrons or protons.

more complicated and is given in detail in Appendix B. Here we need only note that \mathcal{H}_m is closed under unitary transformations of the underlying fermion operators, and hence *under spherical Hartree-Fock (HF) variation*. This property explains the appeal of separating $\mathcal{H}_m + \mathcal{H}_M$.

1. Bulk properties. Factorable forms

\mathcal{H}_m must contain all the information necessary to produce the parameters of the Bethe-Weiszäcker mass formula, and we start by extracting the bulk energy. The key step involves reduction to a sum of factorable forms valid for any interaction (Dufour and Zuker, 1996). Its enormous power derives from the strong dominance of a single term in all the cases considered so far.

For clarity we restrict our attention to the full isoscalar centroids defined in Appendix B, Eqs. (B18a) and (B18c),¹¹

$$\mathcal{V}_{st} = a_{st} - \frac{3\delta_{st}b_{st}}{4(4j_s + 1)}. \quad (13)$$

We diagonalize \mathcal{V}_{st}

$$U^{-1}\mathcal{V}_m^d U = \mathcal{E} \Rightarrow \mathcal{V}_{st} = \sum_k U_{sk} U_{tk} \mathcal{E}_k, \quad \therefore \quad (14)$$

$$\mathcal{V}_m^d = \sum_k \mathcal{E}_k \sum_s U_{sk} m_s \sum_t U_{tk} m_t - \sum_s \mathcal{V}_{ss} m_s. \quad (15)$$

For the three-body interaction, the corresponding centroids \mathcal{V}_{stu} are treated as explained by Dufour and Zuker (1996) and Appendix B.1: The st pairs are replaced by a single index x . Let L and M be the dimensions of the x and s arrays, respectively. Construct and diagonalize an $(L+M) \times (L+M)$ matrix whose nonzero elements are the rectangular matrices \mathcal{V}_{xs} and \mathcal{V}_{sx} . Disregarding the contractions, the strictly three-body part $\mathcal{V}^{(3)}$ can then be written as a sum of factors,

$$\mathcal{V}_m^{d3} = \sum_k \mathcal{E}_k^{(3)} \sum_s U_{sk}^{(1)} m_s \sum_{x=tu} U_{tu,k}^{(2)} m_t m_u. \quad (16)$$

Full factorization follows by applying Eqs. (14) and (15) to the $U_{tu,k}^{(2)}$ matrices for each k .

In Eq. (15) a single term strongly dominates all others. For the Kahana-Lee-Scott interaction (Kahana *et al.*, 1969b) and including the first eight major shells, the result in Fig. 1 is roughly approximated by

$$U_s \approx \frac{4 - 0.5(l - \langle l \rangle) + (j - l)}{\sqrt{D_p}}, \quad (17)$$

where p is the principal quantum number of an oscillator shell with degeneracy $D_p = \sum_s (2j_s + 1) = (p+1)(p+2)$, $\langle l \rangle = \sum_l l(2l+1) / \sum_l (2l+1)$. The (unitary) U matrices have been affected by an arbitrary factor of 6 to have num-

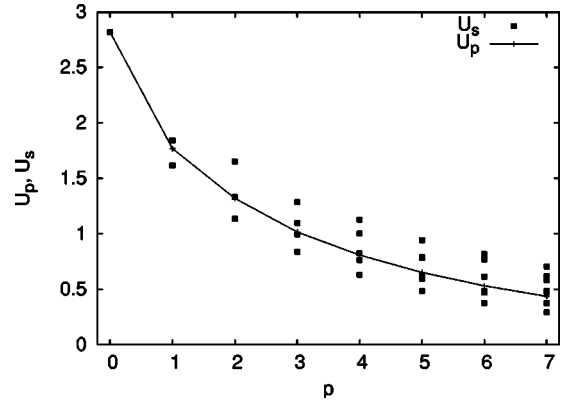


FIG. 1. The value of U_s as given by Eq. (17) for the different orbits of a major shell with principal quantum number p . Also shown is the $U_p (=4/\sqrt{D_p})$ term, with $D_p = (p+1)(p+2)$.

bers of order unity. Operators of the form ($D_s = 2j_s + 1$)

$$\hat{\Omega} = \sum_s m_s \Omega_s \quad \text{with} \quad \sum_s D_s \Omega_s = 0 \quad (18)$$

vanish at closed shells and are responsible for shell effects. As $l - \langle l \rangle$ and $j - l$ are of this type, only the U_p part contributes to the bulk energy.

To proceed it is necessary to know how interactions depend on the oscillator frequency ω of the basis, related to the observed square radius (and hence to the density) through the estimate [Bohr and Mottelson, 1969, Eq. (2-157)]

$$\frac{\hbar\omega}{(A)^{1/3}} = \frac{35.59}{\langle r^2 \rangle} \Rightarrow \hbar\omega \approx \frac{40}{A^{1/3}} \text{ MeV}. \quad (19)$$

A δ force scales as $(\hbar\omega)^{3/2}$. A two-body potential of short range is essentially linear in $\hbar\omega$; for a three-body one we shall tentatively assume an $(\hbar\omega)^2$ dependence while the Coulomb force goes exactly as $(\hbar\omega)^{1/2}$.

To calculate the bulk energy of nuclear matter we average out subshell effects through uniform filling $m_s \Rightarrow m_p D_s / D_p$. Though the Ω -type operators vanish, we have kept them for reference in Eqs. (21) and (22) below. The latter is an educated guess for the three-body contribution. The eigenvalue \mathcal{E}_0 for the dominant term in Eq. (15) is replaced by $\hbar\omega \mathcal{V}_0$ defined so as to have $U_p = 1$. The subindex m is dropped throughout. Then, using Boole's factorial powers, e.g., $p^{(3)} = p(p-1)(p-2)$, we obtain the following asymptotic estimates for the leading terms (i.e., disregarding contractions):

$$\mathcal{K}^d = \frac{\hbar\omega}{2} \sum_p m_p (p+3/2) \Rightarrow \frac{\hbar\omega}{4} (p_f+3)^{(3)} (p_f+2), \quad (20)$$

$$\mathcal{V}^d \approx \hbar\omega \mathcal{V}_0 \left(\sum_p \frac{m_p}{\sqrt{D_p}} + \hat{\Omega} \right)^2 \Rightarrow \hbar\omega \mathcal{V}_0 [p_f(p_f+4)]^2, \quad (21)$$

¹¹These ensure the right average energies for $T=0$ closed shells, which is not the case in Eq. (11) if one simply drops the b_{st} terms.

$$\begin{aligned} \mathcal{V}^{d3} &\approx (\hbar\omega)^2 \beta \mathcal{V}_0 \left(\sum_p \frac{m_p}{D_p} + \hat{\Omega}_1 \right) \left(\sum_p \frac{m_p}{\sqrt{D_p}} + \hat{\Omega}_2 \right)^2 \\ &\Rightarrow (\hbar\omega)^2 \beta \mathcal{V}_0 p_f^3 (p_f + 4)^2. \end{aligned} \quad (22)$$

Finally, we relate p_f to A :

$$\sum_p m_p = \sum_{p=0}^{p_f} 2(p+1)(p+2) \Rightarrow A = \frac{2(p_f)^3}{3}. \quad (23)$$

Note that in Eq. (22) we can replace $(\hbar\omega)^2$ with $(\hbar\omega)^{1+\kappa}$ and change the powers of D_p in the denominators accordingly.

Assuming that nondiagonal \mathcal{K}^d and \mathcal{V}^d terms cancel, we can vary with respect to $\hbar\omega$ to obtain the saturation energy

$$\begin{aligned} E_s &= \mathcal{K}^d + (1 - \beta\omega^\kappa p_f) \mathcal{V}^d, \\ \frac{\partial E}{\partial \omega} &= 0 \Rightarrow \beta\omega^\kappa p_f = \frac{\mathcal{K}^d + \mathcal{V}^d}{(\kappa + 1)\mathcal{V}^d} \\ \therefore E_s &= \frac{\kappa}{\kappa + 1} (\mathcal{K}^d + \mathcal{V}^d) = \frac{\hbar\omega_e}{4} \frac{\kappa}{\kappa + 1} (1 - 4\mathcal{V}_0) \left(\frac{3}{2} A \right)^{4/3}. \end{aligned} \quad (24)$$

The correct saturation properties are obtained by fixing \mathcal{V}_0 so that $E_s/A \approx 15.5$ MeV. The $\hbar\omega_e \approx 40A^{-1/3}$ choice ensures the correct density. It is worth noting that the same approach leads to $V_C \approx 3e^2 Z(Z-1)/5R^c$ (Duflo and Zuker, 2002).

It should be obvious that nuclear matter properties—derived from finite nuclei—can be calculated with techniques designed to treat finite nuclei. A successful theoretical mass table must necessarily extrapolate to the Bethe-Weiszäcker formula (Duflo and Zuker, 1995). What may be surprising, though, is that such calculations can be conducted so easily in the oscillator basis. This is due to the separation and factorization properties of the forces.

Clearly, Eq. (24) has no (or a trivial) solution for $\kappa = 0$, i.e., without a three-body term. Though two-body forces do saturate, they do it at the wrong place and at a heavy price because their short-distance repulsion prevents direct Hartree-Fock variation. The crucial question is now: Can we use realistic (2+3)-body potentials soft enough to do Hartree-Fock? Probably we can. The reason is that the nucleus is quite dilute, and nucleons only “see” the low-energy part of the two-body potential involving basically s -wave scattering, which has been traditionally well fitted by realistic potentials. This in turn explains why primitive versions of such potentials give results close to the modern interactions for G -matrix elements calculated at reasonable $\hbar\omega$ values.

Before we move on, we reiterate what we have learned so far: It may be possible to describe nuclear structure with soft (2+3)-body potentials consistent with the low-energy data coming from the $A=2$ and 3 systems.

2. The soft potential $V_{\text{low } k}$

At the time this review was written we were not aware that realistic soft potentials had actually been constructed by Bogner, Kuo, and Schwenk (2003). The idea is that the high-precision interactions are defined for arbitrary relative momentum k , but are constrained by nucleon-nucleon (NN) data available only for $k \lesssim 2.1 \text{ fm}^{-1}$. By integrating out the high-momentum components of a given potential, it is possible to construct a new one, $V_{\text{low } k}^\Lambda$, that has the same scattering properties for $k < \Lambda$ but vanishes for $k > \Lambda$. As the high-precision interactions give equivalent descriptions of the NN data, for $\Lambda \leq 2.1 \text{ fm}^{-1}$, $V_{\text{low } k}^\Lambda$ becomes a universal potential, independent of the one used in its construction. Furthermore effective-field theory provides arguments to associate it naturally with a three-body force (Bogner and Schwenk, 2004).

A comparison of $V_{\text{low } k}^\Lambda$ and G matrix elements—using the techniques described in Sec. II.D—reveals that they are essentially identical (Schwenk and Zuker, 2005). However, conceptually the difference is significant: G is an effective interaction that depends on an empirically defined starting energy [Eq. (7)], while $V_{\text{low } k}^\Lambda$ is a bare potential that depends on a sharply defined cutoff Λ and that is soft enough to allow a mean-field treatment (Coraggio *et al.*, 2003).

Historically, the “hard core” in the realistic forces has been thought to be dictated by the NN phase shifts and to be necessary to ensure proper saturation. The $V_{\text{low } k}$ approach respects the phase shifts and ignores the hard core, thus leading to a welcome simplification of the many-body problem. It remains to deal with the three-body force, which should ensure good saturation and shell formation properties.

3. Shell formation

In a first approximation, nuclear binding energies are given by the monopole Hamiltonian \mathcal{H}_m^d . When the large and smooth Bethe-Weiszäcker (liquid-drop) contributions are subtracted, one is left with energy patterns called *shell effects*. They are locally smooth but interrupted by spikes associated with closed-shell *magic nuclei*. These magic closures and the particle and hole states built on them, which we call $cs \pm 1$, are well represented by single determinants, and a good measure of “magicity” (or shell formation) is given by the differences in binding energies (BE) (gaps) $2\text{BE}(cs) - \text{BE}(cs + 1) - \text{BE}(cs - 1)$. A good test of the capacity of \mathcal{H}_m^d to ensure proper shell formation is provided by the evolution of the $cs \pm 1$ spectra between major closures, as illustrated in Fig. 2 for ^{40}Ca and ^{48}Ca .

It is found that the two-body realistic \mathcal{H}_m^d does quite well around ^{40}Ca , but around ^{48}Ca the $f_{7/2}$ and $d_{5/2}$ are severely underbound with respect to their neighbors in the pf and sd shells, respectively. The problem is quite general: when the largest orbit in a major shell fills, it binds itself and contributes to the binding of the largest

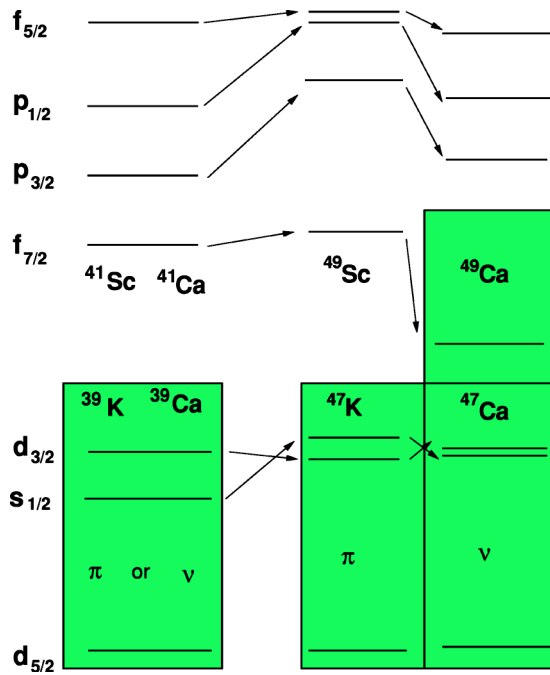


FIG. 2. (Color in online edition) Schematic view of the evolution of the spectra of the nuclei at closed shells plus or minus one particle going from ^{40}Ca to ^{48}Ca .

orbits in neighboring shells in a way that NN forces fail to reproduce (Schwenk and Zuker, 2005).

As the largest orbit in oscillator shell p is precisely the one that is expelled to become the intruder in shell $p-1$, the two-body realistic \mathcal{H}_m^d fails to produce the observed EI magicity at $N, Z=28, 50, 82$, and 126 . To correct this failure we must rely on three-body forces. Theoretical research on this field is quite active, but restricted to very light nuclei. Therefore it may be useful to examine what is involved in a phenomenological approach. To do so we retrace the steps in the construction of a minimal two-body $\tilde{\mathcal{H}}_m^d$, requiring that it reproduce all the observed $cs\pm 1$ states. With a half dozen parameters, a fit to the 90 available data leads to an rms deviation of some 220 keV. The gaps, not included in the fit, also come out quite well and provide a test of the reliability of the results (Duflo and Zuker, 1999).

The construction steps can be followed in Fig. 3. First we balance kinetic and potential contributions in Eqs. (20) and (21) through

$$W - 4K = \left(\sum_p \frac{m_p}{\sqrt{D_p}} \right)^2 - 2 \sum_p m_p (p + 3/2), \quad (25)$$

which has the advantage of canceling exactly to orders A and $A^{2/3}$. It can be seen in Fig. 3 that this term produces enormous spikes at the oscillator closures. The inclusion of three-body forces would not change this effect, but in yielding accurate total bindings it would eliminate the need for canceling bulk and surface terms through the $W-4K$ prescription that produces the unphysical drift in $A^{1/3}$ apparent in the figure. Next we add two one-body terms borrowed from the independent-particle model,

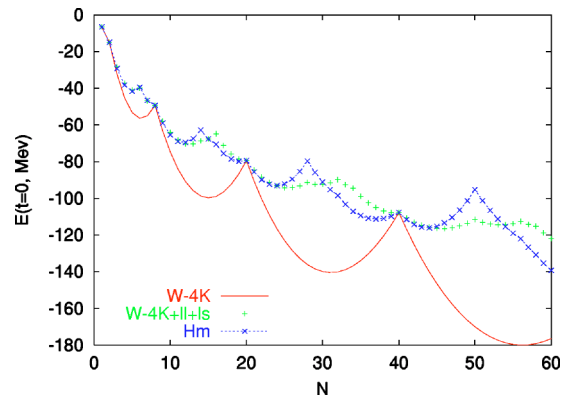


FIG. 3. (Color in online edition) The different contributions to $H_m = \tilde{\mathcal{H}}_m^d$ in Eq. (27) for $N=Z$ nuclei plotted as a function of neutron number N .

$$ls \equiv \alpha l \cdot s / A^{2/3}, \quad ll \equiv \beta [l(l+1) - p(p+3)/2] / A. \quad (26)$$

[In Duflo and Zuker (1999) these terms take a somewhat more sophisticated form.] It can be seen in Fig. 3 that these terms practically erase the spikes. The realistic \mathcal{H}_m^d does produce splittings between spin-orbit partners close to the phenomenological ones, but nothing close to term ll (Schwenk and Zuker, 2005). It will demand some ingenuity to construct a three-body contribution that does an equivalent job. The combination $W-4K+ls+ll$ describes basically the $cs\pm 1$ spectra around oscillator closures. The evolution to EI closures is mediated by terms we simply call Γ , and we finally obtain

$$H_m = \tilde{\mathcal{H}}_m^d = (W - 4K) + ls + ll + \Gamma \text{ terms.} \quad (27)$$

It can be seen in Fig. 3 that the Γ terms do produce the desired EI magicity, but as we shall see in Sec. V.A the proper mechanism must be three-body.

The task ahead is to start with the two-body realistic \mathcal{H}_m^d (which does some subtle things very well) and introduce the necessary corrective action. In principle this should be simpler than the construction we have outlined, which starts from scratch. The difficulty is that the corrections must necessarily be three-body. The end results should resemble—more often than not—those obtained with $\tilde{\mathcal{H}}_m^d$, of which we propose a sample. In Fig. 4 we show the situation for even $t=N-Z=0-18$. Plotting along lines of constant t has the advantage of detecting magicity for both fluids. In other words, spikes appear when either fluid is closed and are reinforced when both are closed. The spikes are invariably associated either with the harmonic-oscillator magic numbers (8,20,40) or the EI ones (14,28,50), but the latter always show magicity, while the former only do so at and above the double closures $(Z, N)(8,14)$, $(20,28)$, and $(40,50)$. For example, at $Z=20$ ^{40}Ca shows as a weak closure. $^{42,44,46}\text{Ca}$ are not closed (which agrees with experiment), ^{48}Ca is definitely magic, and spikes persist for the heavier isotopes. At $Z=40$, ^{80}Zr shows a nice spike, a bad prediction for a strongly rotational nucleus. However, there are no (or weak) spikes for the heavier isotopes except at ^{90}Zr and

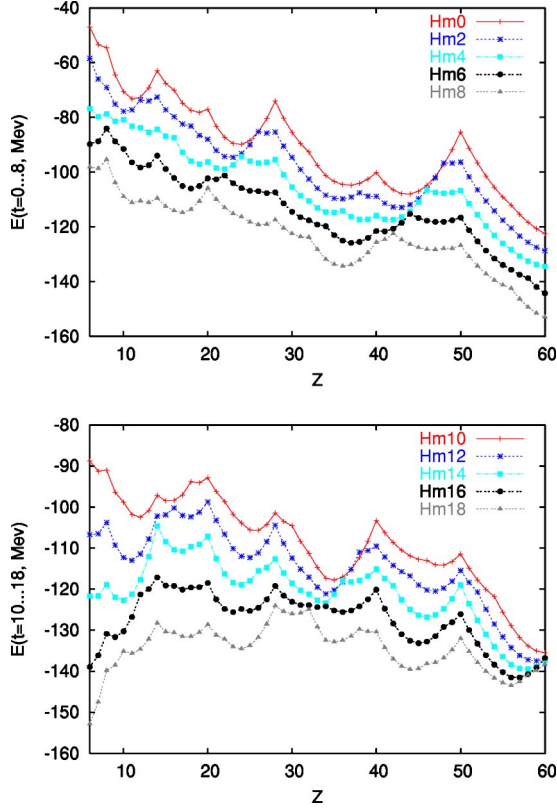


FIG. 4. (Color in online edition) Shell effects as a function of proton number Z . They are obtained through $H_m = \tilde{\mathcal{H}}_m^d$ in Eq. (27) by filling the lowest oscillator orbits for nuclei with even $t = N - Z = 0-8$ (upper panel), and $t = N - Z = 10-18$ (lower panel).

^{96}Zr , both definitely doubly magic. There are many other interesting cases, and the general trend is the following: No known closure fails to be detected. Conversely, not all predicted closures are real. They may be erased by pairing or deformation, as in the case of ^{80}Zr . Nonetheless, the predictive power for $\tilde{\mathcal{H}}_m^d$ is quite good. For further comments see Sec. V.A.

C. The multipole Hamiltonian

The multipole Hamiltonian is defined as $\mathcal{H}_M = \mathcal{H} - \mathcal{H}_m$. As we are no longer interested in the full \mathcal{H} , but its restriction to a finite space, \mathcal{H}_M will be more modestly called H_M , with monopole-free matrix elements given by

$$W_{rstu}^{JT} = V_{rstu}^{JT} - \delta_{rt} \delta_{su} V_{rs}^T. \quad (28)$$

We shall describe briefly the main results of Dufour and Zuker (1996), emphasizing points that were not stressed sufficiently in that paper and adding some new information (Sec. II.D).

There are two standard ways of writing H_M :

$$H_M = \sum_{r \leq s, t \leq u, \Gamma} W_{rstu}^{\Gamma} Z_{rs}^{\dagger} \cdot Z_{tu}^{\Gamma}, \quad \text{or} \quad (29)$$

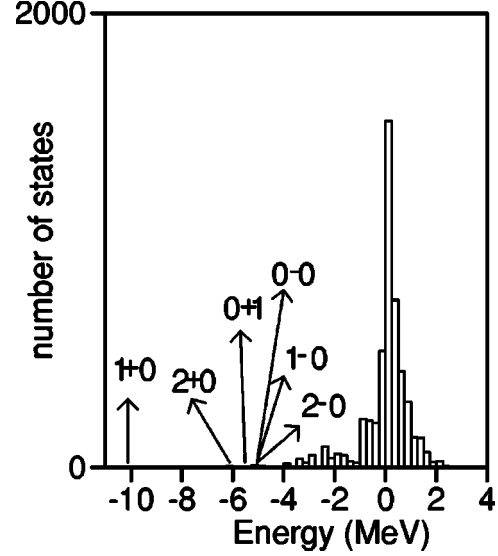


FIG. 5. e -eigenvalue density for the KLS interaction in the $pf+sdg$ major shells ($\hbar\omega=9$ MeV). Each eigenvalue has multiplicity $[\Gamma]$. The largest ones are shown by arrows. From Dufour and Zuker, 1996.

$$H_M = \sum_{rstu\Gamma} [\gamma]^{1/2} f_{rstu}^{\gamma} (S_{rt}^{\gamma} S_{su}^{\gamma})^0, \quad (30)$$

where $f_{rstu}^{\gamma} = \omega_{rstu}^{\gamma} \sqrt{(1 + \delta_{rs})(1 + \delta_{tu})}/4$. The matrix elements ω_{rstu}^{γ} and W_{rstu}^{Γ} are related through Eqs. (A9) and (A10), given in Appendix A.

Replacing pairs by single indices $rs \equiv x$, $tu \equiv y$ in Eq. (29) and $rt \equiv a$, $su \equiv b$ in Eq. (30), we proceed as in Eqs. (14) and (15) to bring the matrices $W_{xy}^{\Gamma} \equiv W_{rstu}^{\Gamma}$ and $f_{ab}^{\gamma} \equiv f_{rstu}^{\gamma}$ to diagonal form through unitary transformations $U_{xk}^{\Gamma}, u_{ak}^{\gamma}$. We obtain the factorable expressions

$$H_M = \sum_{k,\Gamma} E_k^{\Gamma} \sum_x U_{xk}^{\Gamma} Z_{x\Gamma}^{\dagger} \cdot \sum_y U_{yk}^{\Gamma} Z_{y\Gamma}, \quad (31)$$

$$H_M = \sum_{k,\gamma} e_k^{\gamma} \left(\sum_a u_{ak}^{\gamma} S_a^{\gamma} \sum_b u_{bk}^{\gamma} S_b^{\gamma} \right)^0 [\gamma]^{1/2}, \quad (32)$$

which we call the E (or normal, particle-particle, or pp) and e (or multipole, particle-hole, or ph) representations. As \mathcal{H}_m contains all the $\gamma=00$ and 01 terms, for \mathcal{H}_M , $\omega_{rstu}^{00} = \omega_{rstu}^{01} = 0$ [see Eq. (B11)]. There are no one-body contractions in the e representation because they are all proportional to $\omega_{rstu}^{0\tau}$.

The eigensolutions in Eqs. (31) and (32) using the Kahana-Lee-Scott interaction (Kahana *et al.*, 1969b; Lee, 1969), yield the density of eigenvalues (their number in a given interval) in the E representation that is shown in Fig. 5 for a typical two-shell case. It is skewed, with a tail at negative energies, which is what we expect from an attractive interaction.

The e eigenvalues are plotted in Fig. 6. They are very symmetrically distributed around a narrow central group, but a few of them are neatly detached. The strongest have $\gamma^{\pi} = 1^{-}0, 1^{+}1, 2^{+}0, 3^{-}0, 4^{+}0$. If the corresponding eigenvectors are eliminated from H in Eq. (32) and

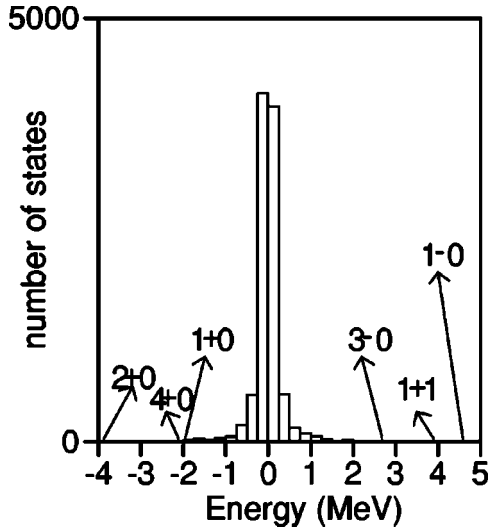


FIG. 6. e -eigenvalue density for the KLS interaction in the $pf+sdg$ major shells. Each eigenvalue has multiplicity $[\gamma]$. The largest ones are shown by arrows. From Dufour and Zuker, 1996.

the associated H in Eq. (31) is recalculated, the E distribution becomes quite symmetric, as expected for a random interaction.¹²

If the diagonalizations are restricted to one major shell, negative parity peaks are absent, but for the positive parity ones the results are practically identical to those of Figs. 5 and 6 except that the energies are halved. This point is crucial: *If u_{p_1} and u_{p_2} are the eigenvectors obtained in shells p_1 and p_2 , their eigenvalues are approximately equal, $e_{p_1} \approx e_{p_2} = e$. When diagonalizing in p_1+p_2 , the unnormalized eigenvector turns out to be $u_{p_1} + u_{p_2}$ with eigenvalue e .*

In the figures the eigenvalues for the two-shell case are doubled, because they are associated with normalized eigenvectors. To sum up, the contribution to H_M associated with the large $\Gamma=01$, and $\gamma=20$ terms,

$$H_{\bar{P}} = -\frac{\hbar\omega}{\hbar\omega_0} |E^{01}| (\bar{P}_p^\dagger + \bar{P}_{p+1}^\dagger) \cdot (\bar{P}_p + \bar{P}_{p+1}), \quad (33)$$

$$H_{\bar{q}} = -\frac{\hbar\omega}{\hbar\omega_0} |e^{20}| (\bar{q}_p + \bar{q}_{p+1}) \cdot (\bar{q}_p + \bar{q}_{p+1}), \quad (34)$$

turns out to be the usual pairing plus quadrupole Hamiltonians, except that the operators for each major shell of principal quantum number p are affected by a normalization. E^{01} and e^{20} are the one-shell values called generically e in the discussion above. To be precise,

$$\bar{P}_p^\dagger = \sum_{r \in p} Z_{rr01}^\dagger \Omega_r^{1/2} / \Omega_p^{1/2}, \quad (35)$$

¹²In the article of Dufour and Zuker (1996), the crucial phrase “if the corresponding eigenvectors are eliminated from H ” was omitted due to an erratum.

$$\bar{q}_p = \sum_{rs \in p} S_{rs}^{20} q_{rs} / \mathcal{N}_p, \quad (36)$$

where

$$\Omega_r = j_r + 1, \quad q_{rs} = \sqrt{\frac{1}{5}} \langle r || r^2 Y^2 || s \rangle \quad (37)$$

and

$$\Omega_p = \frac{1}{2} D_p, \quad \mathcal{N}_p^2 = \sum q_{rs}^2 \cong \frac{5}{32\pi} (p+3/2)^4. \quad (38)$$

The pairing plus quadrupole ($P+Q$) model has a long and glorious history (Baranger and Kumar, 1968; Bes and Sorensen, 1969) and one big problem: as more shells are added to a space, the energy grows, eventually leading to collapse. The only solution seemed to be to stay within limited spaces, but then the coupling constants had to be readjusted on a case-by-case basis. The normalized versions of the operators presented above are affected by universal coupling constants that do not change with the number of shells. Knowing that $\hbar\omega_0 = 9$ MeV, they are $|E^{01}|/\hbar\omega_0 = g' = 0.32$ and $|e^{20}|/\hbar\omega_0 = \kappa' = 0.216$ in Eqs. (33) and (34).

Introducing $A_{mf} \approx \frac{2}{3}(p_f+3/2)^3$, the total number of particles at the middle of the Fermi shell p_f , we find that the relationship between g' , κ' , and their conventional counterparts (Baranger and Kumar, 1968) is, for one shell,¹³

$$\frac{0.32\hbar\omega}{\Omega_p} \cong \frac{19.51}{A^{1/3} A_{mf}^{2/3}} = G \equiv G_0 A^{-1},$$

$$\frac{0.216\hbar\omega}{\mathcal{N}_p^2} \cong \frac{1}{2} \frac{216}{A^{1/3} A_{mf}^{4/3}} = \frac{\chi'}{2} \equiv \frac{\chi'_0}{2} A^{-5/3}. \quad (39)$$

To see how collapse occurs, let us assume $m = O(D_f) = O(A^{2/3})$ in the Fermi shell and promote them to a higher shell of degeneracy D . The corresponding pairing and quadrupole energies can be estimated as

$$E_P = -|G|4m(D-m+2) = -|G|O(mD), \quad (40)$$

and

$$E_q \approx -|\chi'|Q_0^2 = -|\chi'|O(m^2D), \quad (41)$$

respectively, which for the two possible scalings, become

$$E_{P(\text{old})} = O\left(\frac{mD}{A}\right) \Rightarrow E_{P(\text{new})} = O\left(\frac{m}{A^{1/3}}\right), \quad (42)$$

$$E_{q(\text{old})} = O\left(\frac{m^2D}{A^{5/3}}\right) \Rightarrow E_{q(\text{new})} = O\left(\frac{m^2}{A^{1/3}D}\right). \quad (43)$$

If the m particles stay at the Fermi shell, all energies go as $A^{1/3}$, as they should. If D grows, both energies grow in the old version. For sufficiently large D the gain will

¹³According to Dufour and Zuker (1996) the bare coupling constants should be renormalized to $0.32(1+0.48)$ and $0.216(1+0.3)$.

TABLE I. The overlaps between the KLS (A) and Bonn (B) interactions for the first ten oscillator shells (2308 matrix elements), followed by those for the pf shell (195 matrix elements) for the BonnC (C) and KB (K) interactions.

$O_{AA}^0=17.56$	$O_{AA}^1=2.61$	$O_{AA}=6.49$
$O_{BB}^0=11.84$	$O_{BB}^1=2.31$	$O_{BB}=4.78$
$\bar{O}_{AB}^0=0.98$	$\bar{O}_{AB}^1=0.99$	$\bar{O}_{AB}=0.98$
$O_{CC}^0=3.71$	$O_{CC}^1=0.56$	$O_{CC}=1.41$
$O_{KK}^0=3.02$	$O_{KK}^1=0.46$	$O_{KK}=1.15$
$\bar{O}_{CK}^0=0.99$	$\bar{O}_{CK}^1=0.97$	$\bar{O}_{CK}=0.99$

become larger than the monopole loss $O(mD^{1/2}\hbar\omega) = O(D^{1/2}A^{1/3})$. Therefore the traditional forces lead the system to collapse. In the new form there is no collapse: E_p stays constant, E_q decreases, and the monopole term provides the restoring force that guarantees that particles will remain predominantly in the Fermi shell.

As a model for \mathcal{H}_M , $P+Q$ is likely to be a reasonable first approximation for many studies, provided it is supplemented by a reasonable \mathcal{H}_m , to produce the $P+Q+m$ model.

D. Universality of the realistic interactions

To compare sets of matrix elements we define the overlaps

$$O_{AB} = d_2^{-1} \sum_{rstu\Gamma} V_{rstuA}^\Gamma V_{rstuB}^\Gamma[\Gamma], \quad (44)$$

$$\bar{O}_{AB} = \frac{O_{AB}}{\sqrt{O_{AA}O_{BB}}}, \quad (45)$$

where d_2 is the dimensionality of the two-particle space, each state being counted $[\Gamma]=(2J+1)(2T+1)$ times. Similarly, O_{AB}^T is the overlap for matrix elements with the same T . The upper set of numbers in Table I contains what is probably the most important single result concerning the interactions: a 1969 realistic potential (Kahana *et al.*, 1969b; Lee, 1969) and a modern Bonn one (Hjorth-Jensen, 1996). These differ in total

strength(s) O_{AA} but the normalized cross overlaps \bar{O}_{AB} are very close to unity.

Now all the modern realistic potentials agree closely with one another in their predictions except for the binding energies. For nuclear matter the differences are substantial (Pieper *et al.*, 2001), and for the Bonn A, Bonn B, and Bonn C potentials, all earlier versions of the CD-Bonn potential studied by Hjorth-Jensen *et al.* (1995) they become enormous. However, the matrix elements given in this reference for the pf shell have normalized cross overlaps of better than 0.998. At the moment, the overall strengths must be viewed as free parameters.

At a fundamental level the discrepancies in total strength stem from the degree of nonlocality in the potentials and the treatment of the tensor force. In the old interactions, uncertainties were also due to the starting energies and the renormalization processes, which again affected mainly the total strength(s), as can be gathered from the bottom part of Table I.

The dominant terms of H_M are central and Table II collects their strengths (in MeV) for effective interactions in the pf shell. These include the results of Kuo and Brown (1968; KB), the potential fit of Richter *et al.* (1991; FPD6), the Gogny force—successfully used in countless mean-field studies—(Dechargé and Gogny, 1980), and BonnC (Hjorth-Jensen *et al.*, 1995).

There is not much to choose between the different forces, which is a nice indication that overall nuclear

TABLE II. Leading terms of the multipole Hamiltonian. For the GXPF1 force see Sec. V.A.1.

Interaction	Particle-particle		Particle-hole		
	$JT=01$	$JT=10$	$\lambda\tau=20$	$\lambda\tau=40$	$\lambda\tau=11$
KB ^a	-4.75	-4.46	-2.79	-1.39	+2.46
FPD6 ^b	-5.06	-5.08	-3.11	-1.67	+3.17
GOGNY ^c	-4.07	-5.74	-3.23	-1.77	+2.46
BonnC ^d	-4.20	-5.60	-3.33	-1.29	+2.70
GXPF1 ^e	-4.18	-5.07	-2.92	-1.39	+2.47

^aKuo and Brown (1968).

^bRichter *et al.* (1991).

^cDechargé and Gogny (1980).

^dHjorth-Jensen *et al.* (1995).

^eHonma *et al.* (2004).

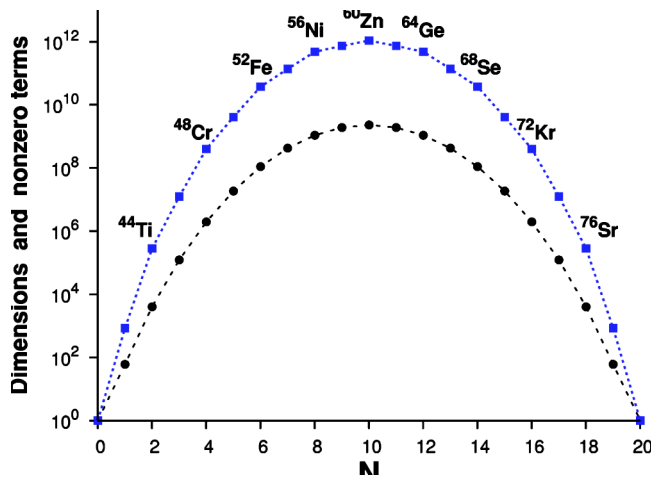


FIG. 7. (Color in online edition) m -scheme dimensions (circles) and total number of nonzero matrix elements (squares) in the pf shell for nuclei with $M=T_z=0$ as a function of neutron number N . The dotted and dashed lines serve as guides for the eye.

data (used in the FPD6 and Gogny fits) are consistent with the NN data used in the realistic Kuo-Brown and BonnC G matrices. The splendid performance of Gogny deserves further study. The only qualm is with the weak quadrupole strength of the Kuo-Brown interaction, which can be understood by looking again at the bottom part of Table I. In assessing the $JT=01$ and $JT=10$ pairing terms, it should be borne in mind that their renormalization remains an open question (Dufour and Zuker, 1996).

We conclude that some fine tuning may be in order and three-body forces may (one day) bring some multipole news, but as of now the problem is \mathcal{H}_m , not \mathcal{H}_M .

III. THE SOLUTION OF THE SECULAR PROBLEM IN A FINITE SPACE

Once the interaction and the valence space are ready, it is time to construct and diagonalize the many-body secular matrix of the Hamiltonian describing the (effective) interaction between valence particles in the valence space. Two questions now need to be considered: which basis to take to calculate the nonzero many-body matrix elements and which method to use for diagonalization of the matrix.

A. The Lanczos method

In the standard diagonalization methods (Wilkinson, 1965) the CPU time increases as N^3 , N being the dimension of the matrix. Therefore these methods cannot be used in large-scale shell-model calculations. Nuclear shell-model calculations have two specific features. The first is that, in the vast majority of cases, only a few (and very often only one) eigenstates of a given angular momentum (J) and isospin (T) are needed. Second, the matrices are very sparse. As can be seen in Fig. 7, the num-

ber of matrix elements varies linearly instead of quadratically with the size of the matrices. For these reasons, iterative methods are of general use, in particular the Lanczos method (Lanczos, 1950). As an alternative, the Davidson method (Davidson, 1975) has the advantage of avoiding the storage of a large number of vectors; however, the large increase in storage capacity of modern computers has somewhat minimized these advantages.

The Lanczos method consists in the construction of an orthogonal basis in which the Hamiltonian matrix (H) is tridiagonal. A normalized starting vector (the *pivot state*) $|1\rangle$ is chosen. The vector $|a_1\rangle=H|1\rangle$ has necessarily the form

$$|a_1\rangle = H_{11}|1\rangle + |2'\rangle, \quad \text{with } \langle 1|2'\rangle = 0. \quad (46)$$

One calculates $H_{11}=\langle 1|H|1\rangle$ through $\langle 1|a_1\rangle=H_{11}$ and normalizes $|2\rangle=|2'\rangle/\langle 2'|2'\rangle^{1/2}$ to find $H_{12}=\langle 1|H|2\rangle=\langle 2'|2'\rangle^{1/2}$. Then one iterates until state $|k\rangle$ has been found. The vector $|a_k\rangle=H|k\rangle$ has necessarily the form

$$|a_k\rangle = H_{kk-1}|k-1\rangle + H_{kk}|k\rangle + |(k+1)'\rangle. \quad (47)$$

One calculates $\langle k|a_k\rangle=H_{kk}$, thereby finding $|(k+1)'\rangle$. Normalizing this, one finds $H_{kk+1}=\langle (k+1)'|(k+1)'\rangle^{1/2}$.

The (real symmetric) matrix is diagonalized at each iteration, and the iterative process continues until all the required eigenvalues are converged according to some criterion. The number of iterations depends little on the dimension of the matrix. Besides, the computing time is directly proportional to the number of matrix elements and for this reason it is nearly linear (in the dimension of the matrix, instead of cubic as in the standard methods). It depends on the number of iterations, which in turn depends on the number of converged states needed, as well as on the choice of starting vector.

The Lanczos method can also be used as a projection method. For example, in the m -scheme basis, a Lanczos calculation with the operator J^2 will generate states with well-defined J . Taking these states as starting vectors, the Lanczos procedure (with H) will remain inside a fixed J subspace and therefore will improve the convergence properties. When only one converged state is required, it is convenient to use as the pivot state the solution obtained in a previous truncated calculation. For instance, starting with a random pivot, the calculation of the ground state of ^{50}Cr in the full pf space (dimension in m scheme 14 625 540 Slater determinants) requires twice as many iterations as if we started with the pivot obtained as a solution in a model space in which only four particles were allowed outside the $1f_{7/2}$ shell (dimension 1 856 720). The overlap between these two 0^+ states is 0.985. When more eigenstates are needed ($n_c > 1$), the best choice for the pivot is a linear combination of the n_c lower states in the truncated space.

Even though the Lanczos method is very efficient in the shell-model framework, numerical problems can sometimes appear. Mathematically the Lanczos vectors are orthogonal, but numerically this is not strictly true due to the limited floating-point machine precision.

TABLE III. Some dimensions in the pf shell.

$A-40$	4	8	12	16	20
$M=T_z=0$	4000	2×10^6	1.10×10^8	1.09×10^9	2.29×10^9
$J=T_z=0$	156	41355	1.78×10^6	1.54×10^7	3.13×10^7
$J=T=0$	66	9741	3.32×10^5	2.58×10^6	5.05×10^6

Hence small numerical errors in precision can, after many iterations, produce catastrophes. In particular, the states of lowest energy may reappear many times, rendering the method inefficient. To solve this problem it is necessary to orthogonalize each new Lanczos vector to all the preceding ones. The same defects in precision can cause the appearance of unexpected states. For example, in an m -scheme calculation with a $J=4$, $M=0$ pivot, when many iteration are performed, a $J=0$ or even a $J=2$ state may suddenly appear. This specific problem can be solved by projecting each new Lanczos vector onto good J .

B. The choice of the basis

Given a valence space, the optimal choice of the basis is related to the physics of the particular problem to be solved. As we discuss later, depending on what states or properties we want to describe (ground state, yrast band, strength function,...) and depending on the type of nucleus (deformed, spherical,...) different choices of the basis are favored. There are essentially three possibilities depending on the underlying symmetries: the m scheme, the J coupled scheme, and the JT coupled scheme.

As the m -scheme basis consists of Slater determinants, the calculation of the many-body matrix elements is trivial, since they are equal to the decoupled two-body matrix elements up to a phase. This means that, independently of the size of the matrix, the number of possible values of matrix elements is relatively limited. However, the simplicity of the m scheme is counterbalanced by the fact that only J_z and T_z are good quantum numbers. Therefore all the possible (J, T) states are contained in the basis, and as a consequence the dimensions of the matrices are maximal. For a given number of valence neutrons n_v and protons z_v the number of different Slater determinants that can be built in the valence space is

$$d = \binom{D_n}{n_v} \cdot \binom{D_p}{z_v}, \quad (48)$$

where D_n and D_p are the degeneracies of the neutron and proton valence spaces. Working at fixed M and T_z the bases are smaller [$d = \sum_{M, T_z} d(M, T_z)$]. The J or JT coupled bases divide the full m -scheme matrix into blocks whose dimensions are much smaller. This is especially striking for the $J=T=0$ states (see Table III).

It is often convenient to truncate the space. In the particular case of the pf shell, calling f the largest sub-

shell ($f_{7/2}$), and r , generically, any or all of the other subshells of the $p=3$ shell, the possible t truncations involve the spaces

$$f^{n-m_0} r^{m_0} + f^{n-m_0-1} r^{m_0+1} + \dots + f^{n-m_0-t} r^{m_0+t}, \quad (49)$$

where $m_0 \neq 0$ if more than eight neutrons (or protons) are present. For $t=m-m_0$ we have the full space $(pf)^m$ for $A=40+m$. However, low-order truncations ($t < 3$) must be avoided, because different configurations are affected in different ways, and they can lead to unphysical results.

In the late 1960s, the Rochester group developed the algorithms needed for efficient work in the (J, T) coupled basis and implemented them in the Oak-Ridge Rochester Multi-Shell code (French *et al.*, 1969). The calculation proceeds as follows: First, the states of n_i particles in a given j_i shell are defined: $|\gamma_i\rangle = |(j_i)^{n_i} \nu_i J_i x_i\rangle$, where ν_i is the seniority and x_i any extra quantum number. Next, the states of N particles distributed in several shells are obtained by successive angular momentum couplings of the one-shell basic states:

$$(\{[|\gamma_1\rangle|\gamma_2\rangle]^{F_2}|\gamma_3\rangle\}^{F_3} \dots |\gamma_k\rangle)^{F_k}. \quad (50)$$

Compared to the simplicity of the m scheme, the calculation of nonzero many-body matrix elements is much more complicated. It involves products of $9j$ symbols and coefficients of fractional parentage (cfp), i.e., the single-shell reduced matrix elements of operators of the form

$$(a_{j_1}^\dagger a_{j_2}^\dagger)^\lambda, (a_{j_1}^\dagger a_{j_2})^\lambda, a_{j_1}^\dagger, [(a_{j_1}^\dagger a_{j_2}^\dagger)^\lambda a_{j_3}]^{j_4}. \quad (51)$$

This complexity explains why, in the OXBASH code (Brown *et al.*, 1985) the JT coupled basis states are written in the m -scheme basis to calculate the nonzero many-body matrix elements. The Oxford-Buenos Aires shell-model code, widely distributed and used, has proven to be an invaluable tool in many calculations. Another recent code that works in JT coupled formalisms, though it has had much less use, is the Drexel University DUPSM (Novoselsky and Vallières, 1997).

In the case of only J (without T) coupling, a strong simplification in the calculation of nonzero many-body matrix elements can be achieved using the *quasispin formalism* (Kawarada and Arima, 1964; Lawson and Macfarlane, 1965; Ichimura and Arima, 1966), as in the code NATHAN described below. The advantages of the coupled scheme decrease when J and T increase. As an example, in ^{56}Ni the ratio $\dim(M=J)/\dim(J)$ is 70 for $J=0$ but only 5.7 for $J=6$. The coupled scheme has another disadvantage compared to the m scheme. This

concerns the percentage of nonzero matrix elements. Consider, for example, the state 4^+ in ^{50}Ti (full pf space); the percentages of nonzero many-body matrix elements are, respectively, 14% in the JT basis (see Novoselsky *et al.*, 1997), 5% in the J basis, and only 0.05% in m scheme. For all these reasons and with the present computing facilities, we conclude that the m scheme is the most efficient choice for ordinary shell-model calculations, albeit with some notable exceptions that we shall mention below.

C. The Glasgow m -scheme code

The steady and rapid increase of computer power in recent years has resulted in a dramatic increase in the dimensionality of shell-model calculations. Today it is crucial to know the limits of a given computer code, their origin, and their evolution. As far as the nonzero many-body matrix elements can be calculated and stored, diagonalization with the Lanczos method is trivial. This means that the fundamental limitation of standard shell-model calculations is the capacity to store the nonzero many-body matrix elements. This is the origin of the term “giant” matrices, which we apply to those for which it is necessary to recalculate the matrix elements during the diagonalization process. The first breakthrough in the treatment of giant matrices was the shell-model code developed by the Glasgow group (Whitehead *et al.*, 1977). Let us recall its basic ideas: It works in the m scheme and each Slater determinant is represented in the computer by an integer word. Each bit of the word is associated with a given individual state $|nljm\tau\rangle$. Each bit has the value 1 or 0, depending on whether the state is occupied or empty. A two-body operator $a_l^\dagger a_j^\dagger a_k a_l$ will select words having the bits i, j, k, l in the configuration 0011, say, and change them to 1100, generating a new word, which has to be located in the list of all the words using the bisection method.

D. The m -scheme code ANTOINE

The shell-model code ANTOINE¹⁴ (Caurier and Nowacki, 1999) has retained many of these ideas, while improving upon the Glasgow code in several respects. To start with, it takes advantage of the fact that the dimension of the proton and neutron spaces is small compared with the full space dimension, with the obvious exception of semimagic nuclei. For example, the 1 963 461 Slater determinants with $M=0$ in ^{48}Cr are generated with only the 4865 Slater determinants (corresponding to all the possible M values) in ^{44}Ca . The states of the basis are written as the product of two Slater determinants, one for protons and one for neutrons: $|I\rangle = |i, \alpha\rangle$. We use I, J , capital letters for states in the full space, i, j , lower-case letters for states of the first sub-

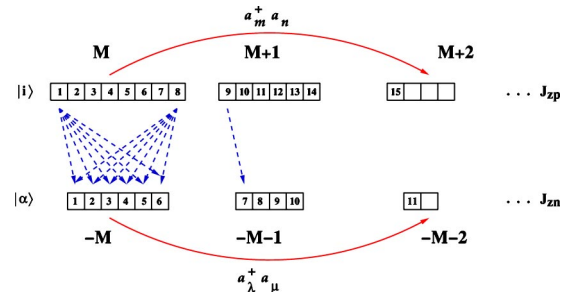


FIG. 8. (Color in online edition) Schematic representation of the shell-model basis. Any shell-model basis state $|I\rangle$ is a product of two Slater determinants, one for protons $|i\rangle$ and another for neutrons $|\alpha\rangle$. In the upper row each box represents a proton Slater determinant, while in the lower row each box represents a neutron Slater determinant. They are grouped in blocks with the same J_z value. Shell-model basis states $|I\rangle$ with total $J_z=0$ are built taking Slater determinants for protons and neutrons with the same absolute value of M but different signs (dashed arrows). Any two-body proton-neutron operator ($a_m^\dagger a_n a_\lambda^\dagger a_\mu$) conserves the total value of M , hence an increase of the M value of the protons must be accompanied by an equivalent decrease of the M value of the neutrons (upper and lower curved arrows).

space (protons or neutrons), and α, β , lower-case greek letters for states of the second subspace (neutrons or protons). The Slater determinants i and α can be classified by their M values, M_1 and M_2 . The total M being fixed, the Slater determinants of the two subspaces will be associated only if $M_1 + M_2 = M$. A pictorial example is given in Fig. 8.

It is clear that for each $|i\rangle$ state the allowed $|\alpha\rangle$ states run, without discontinuity, between a minimum and a maximum value. Building the basis in the total space by means of an i loop and a nested α loop, it is possible to construct numerically an array $R(i)$ that points to the $|I\rangle$ state:¹⁵

$$I = R(i) + \alpha. \quad (52)$$

For example, according to Fig. 8, the numerical values of R are $R(1)=0, R(2)=6, R(3)=12, \dots$. Equation (52) holds even in the case of truncated spaces, provided we define subblocks labeled with M and t [the truncation index defined in Eq. (48)]. Before the diagonalization, all calculations that involve only the proton or the neutron spaces separately are carried out and the results stored. For the proton-proton and neutron-neutron matrix elements the numerical values of $R(i), R(j), W_{ij}$, and $\alpha, \beta, W_{\alpha\beta}$, where $\langle i|H|j\rangle = W_{ij}$ and $\langle \alpha|H|\beta\rangle = W_{\alpha\beta}$, are precalculated and stored. Therefore in the Lanczos procedure a simple loop on α and i generates all the proton-proton and neutron-neutron matrix elements, $W_{IJ} = \langle I|H|J\rangle$. For proton-neutron matrix elements the situation is slightly more complicated. Let us assume that the $|i\rangle$ and $|j\rangle$ Slater determinants are connected by the one-body op-

¹⁴A version of the code can be downloaded from the URL <http://sbgat194.in2p3.fr/theory/antoine/main.html>

¹⁵We use Dirac's notation for the quantum-mechanical state $|i\rangle$. The position of this state in the basis is denoted by i .

erator $a_q^\dagger a_r$ (where, in the list of all possible one-body operators, appears at position p), with $q=nljm$ and $r=n'l'j'm'$ and $m'-m=\Delta m$. Equivalently, the $|\alpha\rangle$ and $|\beta\rangle$ Slater determinants are connected by a one-body operator whose position is denoted by μ . We precalculate the numerical values of $R(i)$, $R(j)$, p , and α , β , μ . Conservation of the total M implies that proton operators with Δm must be associated with neutron operators with $-\Delta m$. Thus we could draw the equivalent to Fig. 8 for the proton and neutron one-body operators. In the same way as we did before for $I=R(i)+\alpha$, we can now define an index $K=Q(p)+\mu$ that labels the different two-body matrix elements. Then, we denote $V(K)$ the numerical value of the proton-neutron two-body matrix element that connects the states $|i,\alpha\rangle$ and $|j,\beta\rangle$. Once $R(i)$, $R(j)$, $Q(p)$, and α , β , μ are known, the nonzero elements of the matrix in the full space are generated with three integer additions:

$$I=R(i)+\alpha, \quad J=R(j)+\beta, \quad K=Q(p)+\mu. \quad (53)$$

The nonzero many-body matrix element of the Hamiltonian between states $|I\rangle$ and $|J\rangle$ is then

$$\langle I|H|J\rangle = \langle J|H|I\rangle = V(K). \quad (54)$$

The performance of the code is optimal when the two subspaces have comparable dimensions. It becomes less efficient for asymmetric nuclei (for semimagic nuclei all the matrix elements must be stored) and for large truncated spaces. No-core calculations are typical in this case. If we consider an $N=Z$ nucleus like ${}^6\text{Li}$, in a valence space that comprises up to $14\hbar\omega$ configurations, there are 50 000 Slater determinants for protons and neutrons with $M=1/2$ and $t=14$. Their respective counterparts can only have $M=-1/2$ and $t=0$, and they have dimensionality 1. This situation is the same as in semimagic nuclei.

As long as two Lanczos vectors can be stored in the RAM of the computer, the calculations are straightforward. Until recently this was the fundamental limitation of the shell-model code ANTOINE. It is now possible to overcome it by dividing the Lanczos vectors into segments:

$$\Psi_f = \sum_k \Psi_f^{(k)}. \quad (55)$$

The Hamiltonian matrix is also divided into blocks so that the action of the Hamiltonian during a Lanczos iteration can be expressed as

$$\Psi_f^{(k)} = \sum_q H^{(q,k)} \Psi_i^{(q)}. \quad (56)$$

The k segments correspond to specific values of M (and occasionally t) of the first subspace. The price to pay for the increase in size is a strong reduction in performance of the code. Now, $\langle I|H|J\rangle$ and $\langle J|H|I\rangle$ are not generated simultaneously when $|I\rangle$ and $|J\rangle$ do not belong at the same k segment of the vector, and longer computing time is needed. As compensation, ANTOINE gives a natural way to parallelize the code, each processor calculat-

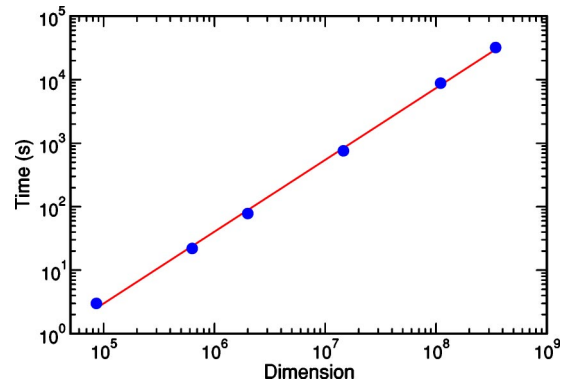


FIG. 9. (Color in online edition) Time needed to compute 15 Lanczos iterations in a Pentium 4 processor at 2.6 GHz as a function of the m -scheme dimension of the basis. The points correspond to calculations with the code ANTOINE for ${}^{46}\text{Ti}$, ${}^{48}\text{Ti}$, ${}^{48}\text{Cr}$, ${}^{50}\text{Cr}$, ${}^{52}\text{Fe}$, and ${}^{54}\text{Fe}$. The line represents a fit to the points with slope 1.1 in the log-log plot.

ing some specific $\Psi_f^{(k)}$, although it would never do it as efficiently as the NATHAN code described below. This technique allows the diagonalization of matrices with dimensions in the billion range, without parallelization. All the nuclei of the pf shell can now be calculated without truncation.

ANTOINE's performance can be seen in Fig. 9, where we have plotted the computing time it takes to make 15 Lanczos iterations in a Pentium 4 processor at 2.6 GHz, as a function of the size of the basis. The line is fitted to the points and corresponds to a slope of 1.1 in the log-log plot. In this range of dimensions (and a few orders of magnitude beyond) an $N \log N$ dependence works equally well. Therefore the computing time varies almost linearly with the dimension of the basis.

Other m -scheme codes have recently joined ANTOINE in the run, incorporating some of its algorithmic findings. These include MSHELL (Mizusaki, 2000) and REDSTICK (Ormand and Johnson, 2002).

E. The coupled code NATHAN

As the mass of the nucleus increases, the possibilities for performing shell-model calculations become more and more limited. To give an order of magnitude, the dimension of the matrix of ${}^{52}\text{Fe}$ with six protons and six neutrons in the pf shell is 10^8 . On the other hand, for ${}^{132}\text{Ba}$, which also has six protons and six neutron holes in a valence space of five shells, four of them equivalent to the pf shell plus the $1h_{11/2}$ orbit, the dimension reaches 2×10^{10} . Furthermore, when many protons and neutrons are active, nuclei tend to get deformed and their description requires even larger valence spaces. For instance, to calculate the deformed nuclei in the vicinity of ${}^{80}\text{Zr}$, the “normal” valence space, $2p_{3/2}$, $1f_{5/2}$, $2p_{1/2}$, $1g_{9/2}$, must be complemented with, at least, the orbit $1d_{5/2}$. This means that we will have to restrict our study to nuclei that are close to magic (${}^{130}\text{Xe}$ remains an easy calculation) or semimagic (for instance, the tellu-

rium isotopes) configurations. These nuclei are spherical, so the seniority can provide a good truncation scheme. This explains the appeal of a shell-model code in a coupled basis and quasispin formalism.

In the shell-model code NATHAN (Caurier and Nowacki, 1999) the fundamental idea of the code ANTOINE is kept, i.e., splitting the valence space into two parts and writing the full space basis as the product of states belonging to these two parts. Now, $|i\rangle$ and $|\alpha\rangle$ are states with good angular momentum. They are built with the usual techniques of the Oak-Ridge/Rochester group (French *et al.*, 1969). Each subspace is now partitioned with the labels J_1 and J_2 . The only difference from the m scheme is that, instead of having a one-to-one association ($M_1 + M_2 = M$) for a given J_1 , we now have all the possible J_2 , $J_{min} \leq J_2 \leq J_{max}$, with $J_{min} = |J_0 - J_1|$ and $J_{max} = J_0 + J_1$. The continuity between the first state with J_{min} and the last with J_{max} is maintained, and consequently the fundamental relation $I = R(i) + \alpha$ still holds. The generation of proton-proton and neutron-neutron nonzero many-body matrix elements proceeds exactly as in the m scheme. For proton-neutron matrix elements the one-body operators in each space can be written as $O_p^\lambda = (a_{i_1}^\dagger a_{i_2})^\lambda$. There exists a strict analogy between Δm in the m scheme and λ in the coupled scheme. Hence we can still establish a relation $K = Q(p) + \omega$. The nonzero many-body matrix element now read

$$\langle I | H | J \rangle = \langle J | H | I \rangle = h_{ij} \cdot h_{\alpha\beta} \cdot W(K), \quad (57)$$

with $h_{ij} = \langle i | O_p^\lambda | j \rangle$, $h_{\alpha\beta} = \langle \alpha | O_n^\lambda | \beta \rangle$, and

$$W(K) \propto V(K) \cdot \begin{Bmatrix} i & \alpha & J \\ j & \beta & J \\ \lambda & \lambda & 0 \end{Bmatrix}, \quad (58)$$

where $V(K)$ is a two-body matrix element. We need to perform—as in the m scheme code—the three integer additions which generate I , J , and K , but, in addition, there are two floating-point multiplications to be done, since h_{ij} and $h_{\alpha\beta}$, which in the m scheme were just phases, are now a product of cfp's and $9j$ symbols [see Eq. (3.10) in French *et al.*, 1969]. Within this formalism we can introduce seniority truncations, but the problem of semimagic nuclei and the asymmetry between proton and neutron spaces remain. To overcome this difficulty in equalizing the dimension of the two subspaces we have generalized the code to allow one of the two subspaces to contain a mixture of proton and neutron orbits. For example, for heavy scandium or titanium isotopes, we can include the neutron $1f_{7/2}$ orbit in the proton space. For the $N=126$ isotones we have only proton shells. We then take the $1i_{13/2}$ and $1h_{9/2}$ orbits as the first subspace, while the $2f_{7/2}$, $2f_{5/2}$, $3p_{3/2}$, and $3p_{1/2}$ form the second one. The states previously defined with J_p and J_n are now labeled A_1 , J_1 and A_2 , J_2 , respectively, where A_1 and A_2 are the number of particles in each subspace. In h_{ij} and $h_{\alpha\beta}$ mean values of all the operators now appear in Eq. (51).

The fact that in the coupled scheme the dimensions are smaller and that angular momentum is explicitly enforced makes it possible to perform a very large number of Lanczos iterations without storage or precision problems. This can be essential for the calculation of strength functions or when many converged states are needed, for example, to describe non-yrast-deformed bands. The coupled code has another important advantage; it can be easily parallelized. Our tests using up to 16 processors show that the speedup of the parallel version is optimal. The typical working dimension for large matrices in NATHAN is 10^7 (10^9 with ANTOINE). This means that there is no problem in defining as many final vectors as processors are available. The calculation of the nonzero many-body matrix elements is shared between the different processors (each processor taking a piece of the Hamiltonian, $H = \sum_k H^{(k)}$), leading to different vectors that are added to obtain the full one:

$$\Psi_f^{(k)} = H^{(k)} \Psi_i, \quad \Psi_f = \sum_k \Psi_i^{(k)}. \quad (59)$$

F. No-core shell model

The *ab initio* no-core shell model (Navrátil *et al.*, 2000a, 2000b) is a method of solving the nuclear many-body problem for light nuclei using realistic internucleon forces. The calculations are performed using a large but finite harmonic-oscillator basis. Due to the basis truncation, it is necessary to derive an effective interaction from the underlying internucleon interaction that is appropriate for the basis size employed. The effective interaction contains, in general, up to A -body components even if the underlying interaction had, e.g., only two-body terms. In practice, the effective interaction is derived in a subcluster approximation retaining just two- or three-body terms. A crucial feature of the method is that it converges to the exact solution when the basis size increases and/or the effective interaction clustering increases (Navrátil *et al.*, 2000b).

At first, applications of this model were limited to realistic two-nucleon interactions, either G -matrix-based two-body interactions (Zheng *et al.*, 1994), or interactions derived by the Lee-Suzuki procedure (Suzuki and Lee, 1980) for the no-core shell model (Navrátil and Barrett, 1996). This resulted in the elimination of the purely phenomenological parameter Δ used to define the G -matrix starting energy. A truly *ab initio* formulation was presented by Navrátil and Barrett (1998), in which convergence to the exact solutions was demonstrated for the $A=3$ system. The same was later accomplished for the $A=4$ system (Navrátil and Barrett, 1999), where it was also shown that a three-body effective interaction could be introduced to improve the convergence of the method. The ability of the no-core shell-model approach to derive a three-body effective interaction and apply it in either a relative-coordinate (Navrátil *et al.*, 2000) or a Cartesian-coordinate formalism (Navrátil and Ormand, 2002), together with its abil-

ity to solve a three-nucleon system with a genuine three-nucleon force (Marsden *et al.*, 2002), now opens up the possibility of including a realistic three-nucleon force in the Hamiltonian and performing calculations using two- and three-nucleon forces for the p -shell nuclei. The successes of the no-core approach include the first published result of the binding energy of ${}^4\text{He}$ with the CD-Bonn nucleon-nucleon potential (Navrátil and Barrett, 1999), the near-converged results for $A=6$ using a non-local Hamiltonian (Navrátil *et al.*, 2001), and the first observation of the incorrect ground-state spin in ${}^{10}\text{B}$ predicted by the realistic two-body nucleon-nucleon interactions (Caurier *et al.*, 2002). This last result, together with the already known problems of underbinding, confirms the need for realistic three-nucleon forces, a need also indicated by the Green's function Monte Carlo calculations of Wiringa and Pieper (2002; see also Pieper and Wiringa, 2001, for a review of the result of the Urbana-Argonne collaboration for nuclei $A \leq 10$).

Recently, a new version of the shell model code ANTOINE has been developed for no-core shell-model applications (Caurier, Navratil, *et al.*, 2001). This new code allows one to perform calculations in significantly larger basis spaces and makes it possible to reach full convergence for the $A=6$ nuclei. In addition, it shows promise for the investigation of slowly converging intruder states and states with unnatural parity. The largest bases reached with this code so far are, according to the number of harmonic-oscillator excitations, the $14\hbar\omega$ space for ${}^6\text{Li}$ and, according the matrix dimension, the $10\hbar\omega$ calculations for ${}^{10}\text{C}$. In the latter case, the m -scheme matrix dimension exceeds 800 million.

G. Present possibilities

The combination of advances in computer technology and in algorithms has enlarged the scope of possible shell-model studies. The rotational band of ${}^{238}\text{U}$ seems still to be beyond the reach of shell-model calculations, but predictions for ${}^{218}\text{U}$ are already available. Let us list some of the present opportunities.

- (i) No-core calculations. One of the major problems of the no-core shell model is the convergence of the results with the size of the valence space. For ${}^6\text{Li}$ we can handle excitations up to $14\hbar\omega$ and at least $8\hbar\omega$ for all p -shell nuclei.
- (ii) The pf shell. This is where the shell model has been most successful, and exact diagonalizations are now possible throughout the region. Beyond ${}^{56}\text{Ni}$, as the $1f_{7/2}$ orbit becomes more and more bound, truncated calculations are close to exact. For instance, in ${}^{60}\text{Zn}$ (Mazzocchi *et al.*, 2001) the wave functions are fully converged when $6p-6h$ excitations are included.
- (iii) The $r_3 g$ -valence space. We use the notation r_p for the set of nlj orbits with $2(n-1)+l=p$, excluding the orbit with maximum total angular momentum $j=p+1/2$. This space describes nuclei in the region $28 < N, Z < 50$; ${}^{56}\text{Ni}$ is taken to be the inert core. Most of these nuclei are nearly spherical and can be treated without truncations. The $\beta\beta$ decay (with and without neutrinos) of ${}^{76}\text{Ge}$ and ${}^{82}\text{Se}$ is a prime example. The deformed nuclei ($N \sim Z \sim 40$) are more difficult because they demand the inclusion of the $2d_{5/2}$ orbit to describe prolate states and oblate-prolate shape coexistence.
- (iv) The $pf g$ space. An extension of the pf valence space by the addition of the $1g_{9/2}$ orbitals is still beyond present computing power. Furthermore, serious center-of-mass spuriousness is expected in the $1f_{7/2}^{-k} 1g_{9/2}^k$ configurations (see Appendix C). However, a restricted option, based on a reasonable approximation, is available. For neutron-rich nuclei in the nickel region, a tractable valence space that avoids the center-of-mass problem can be defined as a ${}^{48}\text{Ca}$ core on top of which pf protons and $r_3 g$ neutrons are active.
- (v) Heavy nuclei. All the semimagic nuclei, for instance, the $N=126$ isotones, can be easily studied, and the addition of a few particles or holes remains tractable. Some long chains of tellurium and bismuth isotopes have been recently studied (Caurier *et al.*, 2003).

IV. THE LANCZOS BASIS

There is a strong connection between the Lanczos algorithm, the partition function, $Z(\beta) = \sum_i \langle i | \exp(-\beta\mathcal{H}) | i \rangle$, and the evolution operator $\exp(i\mathcal{H}t)$. In these three cases, powers of the Hamiltonian determine the properties of the systems. The partition function can be written as $Z(\beta) = \sum_E \rho(E) \exp(-\beta E)$, i.e., the Laplace transform of the density of states, a quantity readily accessible once the Hamiltonian has been fully diagonalized. The evolution operator addresses more specifically the problem of evolving from a starting vector into the exact ground state. We shall discuss both questions in turn.

A. Level densities

For many, the shell model is still synonymous with diagonalizations, in turn synonymous with a black box. One still hears questions such as: Who is interested in diagonalizing a large matrix? As an answer we propose to examine Fig. 10 showing the two point functions that define the diagonal, H_{ii} , and off-diagonal elements, H_{ii+1} , in a typical Lanczos construction. The continuous lines are calculated knowing the first four moments of the matrix (i.e., of the $1+2$ -body Hamiltonian \mathcal{H} it represents). These results hold at fixed quantum numbers, i.e., when the matrix admits no block decomposition.

When the matrix is diagonalized the level density is well reproduced by a continuous binomial,

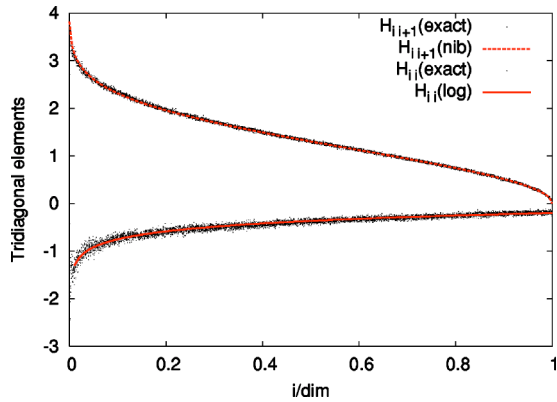


FIG. 10. (Color in online edition) Tridiagonal matrix elements for a 6579-dimensional matrix, and the logarithmic and inverse binomial (nib) approximations. The x axis represents the index of the matrix element normalized to the total dimension of the matrix. From Zuker *et al.*, 2001.

$$\rho_b(x, N, p, S) = p^{xN} q^{\bar{x}N} d \frac{\Gamma(N+1)}{\Gamma(xN+1)\Gamma(\bar{x}N+1)} \frac{N}{S}, \quad (60)$$

where x is an adimensional energy, $\bar{x}=1-x$, N the number of valence particles, p an asymmetry parameter, $p+q=1$, and S the span of the spectrum (distance between lowest and highest eigenstates). Introducing the energy scale ε , S , the centroid E_c , the variance σ^2 , and x are given by

$$S = N\varepsilon, \quad E_c = Np\varepsilon, \quad \sigma^2 = Np(1-p)\varepsilon^2, \quad x = \frac{E}{S}. \quad (61)$$

Note that $\rho_b(x, N, p, S)$ reduces to a discrete binomial, $\binom{N}{n}$, if $x = n/N = n\varepsilon/S$, with integer n .

N , p , and S are calculated using the moments of the Hamiltonian \mathcal{H} , i.e., averages given by the traces of \mathcal{H}^K , to be equated to the corresponding moments of $\rho_b(x, N, p, S)$, which for low K are the same as those of a discrete binomial. The necessary definitions and equalities follow:

$$\begin{aligned} d^{-1} \text{tr}(\mathcal{H}^K) &= \langle \mathcal{H}^K \rangle, \quad E_c = \langle \mathcal{H} \rangle, \quad \mathcal{M}_K = \langle (\mathcal{H} - E_c)^K \rangle, \\ \sigma^2 &= \mathcal{M}^2, \quad \bar{\mathcal{M}}_K = \frac{\mathcal{M}K}{\sigma^K}, \quad \gamma_1 = \bar{\mathcal{M}}_3 = \frac{q-p}{\sqrt{Npq}}, \\ \gamma_2 &= \mathcal{M}_4 - 3 = \frac{1-6pq}{Npq}, \quad d = d_0(1+p/q)^N. \end{aligned} \quad (62)$$

These quantities also define the logarithmic and inverse binomial forms of H_{ii} and H_{ii+1} in Fig. 10. Note that the corresponding lines are almost impossible to distinguish from those of the exact matrix. The associated level densities are found in Fig. 11.

The mathematical status of these results is somewhat mixed. Mon and French (1975) proved that the total density of a Hamiltonian system is, to a first approximation, a Gaussian. Zuker (2001) extended the approxima-

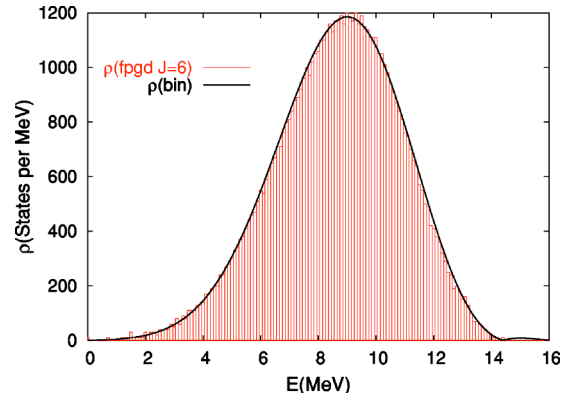


FIG. 11. (Color in online edition) Exact (bins) and binomial (solid curve) level densities for the matrix in Fig. 10.

tion to a binomial, but the result remains valid only in the neighborhood of the centroid. Furthermore, one does not expect it to hold generally because binomial thermodynamics is trivial and precludes the existence of phase transitions. In the example given above, we do not deal with the total density, which involves all states, $\rho = \sum_{JT} (2J+1)(2T+1)\rho_{JT}$, but with a partial ρ_{JT} at fixed quantum numbers. In this case Zuker *et al.* (2001) conjectured that the tridiagonal elements given by the logarithmic and inverse binomial forms are valid, and hence describe the full spectrum. The conjecture breaks down if a dynamical symmetry is so strong as to define new (approximately) conserved quantum numbers.

Granted that a single binomial cannot cover all situations, we may nonetheless explore its validity in nuclear physics, where the observed level densities are extremely well approximated by the classical formula of Bethe (1936) with a shift Δ ,

$$\rho_B(E, a, \Delta) = \frac{\sqrt{2\pi}}{12} \frac{e^{\sqrt{4a(E+\Delta)}}}{(4a)^{1/4} (E+\Delta)^{5/4}}. \quad (63)$$

Obviously, if binomials are to be useful, they must reproduce—for some range of energies—Eq. (63). They do indeed, as shown in Fig. 12, where the experimental

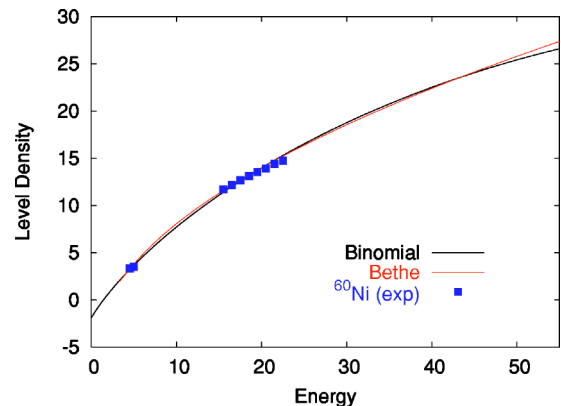


FIG. 12. (Color in online edition) The experimental level density for ^{60}Ni compared with the predictions of the Bethe and the binomial formulas.

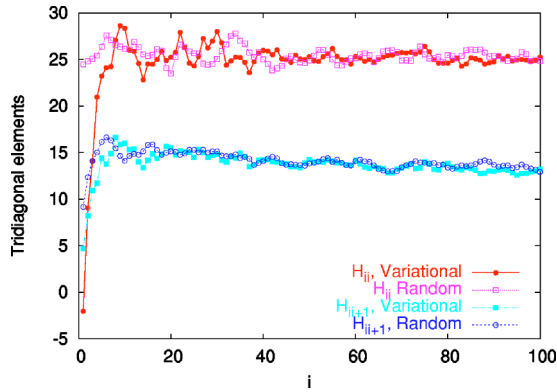


FIG. 13. (Color in online edition) Tridiagonal matrix elements after 100 Lanczos iterations for a random and a variational pivot. H_{ii} denotes the diagonal matrix element and H_{ii+1} the nondiagonal.

points for ^{60}Ni (Iljinov *et al.*, 1992) are also given. Though the Bethe and binomial forms are seen to be equivalent, the latter has the advantage that the necessary parameters are well defined and can be calculated, while in the former, the precise meaning of the a parameter is elusive. The shift Δ is necessary to adjust the ground-state position. The problem also exists for the binomial,¹⁶ and the result in the figure (Zuker, 2001) solves it phenomenologically. The shell-model Monte Carlo method provides the only parameter-free approach to level densities (Dean *et al.*, 1995; Nakada and Alhassid, 1997; Langanke, 1998), whose reliability is now established (Alhassid *et al.*, 1999). The problem is that the calculations are hard.

As the shape of the level density is well reproduced by a binomial *except* in the neighborhood of the ground state, to reconcile simplicity with full rigor we have to examine the tridiagonal matrix at the origin.

B. The ground state

Obviously, when performing a Lanczos calculation, some dependence on the pivot should exist. We examine it through the $J=1T=3$ pf states in ^{48}Sc .¹⁷ The matrix is 8590 dimensional, and we calculate the ground state with two pivots, one random (homogeneous sum of all basic states), the other variational (lowest eigenstate in $f_{7/2}^8$ space). A zoom on the first matrix elements in Fig. 13 reveals that they are very different for the first few iterations, but soon they merge into the canonical patterns discussed in the preceding section. The ground-state wave function is unique, of course, but it takes the different aspects shown in Fig. 14. In both cases the convergence is very fast, and it is not difficult to show in general that it occurs for a number of iterations of order

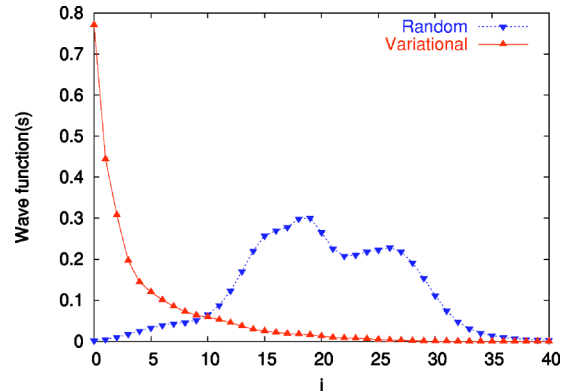


FIG. 14. (Color in online edition) The ground-state wave function in the Lanczos basis for a random and a variational pivot. The plotted values are the squared overlaps of the successive Lanczos vectors with the final wave function.

$N \log N$ for dimensionality $d=2^N$. However, the variational pivot is clearly better if we are interested in the ground state. If its overlap with the exact solution exceeds 50%, all other contributions are bound to be smaller and in general they will decrease uniformly.¹⁸ We shall see how to exploit this property of good pivots to simplify the calculations.

1. The $\exp(\mathbf{S})$ method

In Sec. II.A we sketched the coupled-cluster [or $\exp(\mathbf{S})$] formalism. The formulation in the Lanczos basis cannot do justice to the general theory, but it is a good introduction to the underlying ideas. Furthermore, it turns out to be quite useful.

The construction is as in Eqs. (46) and (47), but the succeeding vectors—except for the pivot—are not normalized. Then, the full wave function takes the form

$$|\bar{0}\rangle = (1 + c_1 P_1 + c_2 P_2 + \cdots + c_I P_I)|0\rangle, \quad (64)$$

where P_m is a polynomial in H that, acting on the pivot, produces orthogonal unnormalized vectors in the Lanczos basis: $P_m|0\rangle = |m\rangle$. Equation (47) becomes

$$\mathcal{H}|m\rangle = V_m|m-1\rangle + E_m|m\rangle + |m+1\rangle. \quad (65)$$

To relate this to the normalized version ($m \Rightarrow \bar{m}$), we divide by $\langle m|m\rangle^{1/2}$, then multiply and divide $|m-1\rangle$ and $|m+1\rangle$ by their norms to recover Eq. (47), and obtain $E_m = H_{\bar{m}\bar{m}}$, $V_m = \langle m|m\rangle / \langle m-1|m-1\rangle = H_{\bar{m}\bar{m}-1}^2$. The secular equation $(\mathcal{H} - E)|\bar{0}\rangle = 0$ leads to the recursion

$$c_{m-1} + (E_m - E)c_m + V_{m+1}c_{m+1} = 0, \quad (66)$$

whose solution is equivalent to diagonalizing a matrix with V_{m+1} in the upper diagonal and 1 in the lower one, which is of course equivalent to the symmetric problem. However, here we shall solve the recursion by transforming it into a set of nonlinear coupled equations for

¹⁶The energies refer to the mean (centroid) of the distribution, while they are measured with respect to the ground state.

¹⁷They are reached in the $^{48}\text{Ca}(p,n)^{48}\text{Sc}$ reaction, which will be our standard example of a Gamow-Teller transition.

¹⁸There are some very interesting counterexamples. One is found in Fig. 24, where the natural pivot is heavily fragmented.

the c_m amplitudes. The profound reason for using an unnormalized basis is that the first term in Eq. (66), $E = E_0 + V_1 c_1$, implies that once c_1 is known the problem is solved. Calling $\varepsilon_m = E_m - E_0$ and replacing $E = E_0 + V_1 c_1$ in Eq (66) leads to

$$c_{m-1} + (\varepsilon_m - V_1 c_1) c_m + V_{m+1} c_{m+1} = 0. \quad (67)$$

Now we introduce

$$\sum c_m P_m = \exp\left(\sum S_m P_m\right). \quad (68)$$

Expanding the exponential and equating terms, we have

$$c_1 = S_1, \quad c_2 = S_2 + \frac{1}{2} S_1^2, \quad (69)$$

$$c_3 = S_3 + S_1 S_2 + \frac{1}{3!} S_1^3, \quad \text{etc.} \quad (70)$$

Note that we have used the formal identification $P_m P_n = P_{n+m}$ as a heuristic way of suggesting Eqs. (69). Inserting these in Eq. (67) and regrouping gives a system of coupled equations. The first two are

$$0 = S_2 V_2 + S_1^2 \left(\frac{1}{2} V_2 - V_1 \right) + S_1 \varepsilon_1 + 1, \quad (71)$$

$$0 = S_3 V_3 + S_2 \varepsilon_2 + S_1 S_2 (V_3 - V_1) + \frac{1}{2} S_1^2 \varepsilon_2 + S_1^3 \left(\frac{1}{3!} V_3 - \frac{1}{2} V_1 \right) + S_1. \quad (72)$$

Hence, instead of the usual c_m truncations, we can use S_m truncations, which have the advantage of providing a model for the wave function over the full basis. At the first iteration Eq. (71) is solved neglecting S_2 . The resulting value for S_1 is inserted into Eq. (72), which is solved by neglecting S_3 . The resulting value for S_2 is reinserted into Eq. (71) and the process is repeated. Once S_1 and S_2 are known, the equation for S_3 (not shown) may be incorporated, and so on. Since the energy depends only on S_1 , convergence is reached when its value remains constant from step to step. With a very good pivot, Eq. (71) should give a fair approximation, improved by incorporating Eq. (72) and checked by the equation for S_3 .

If all amplitudes except S_1 are neglected, the difference scheme [Eq. (66)] is the same as would be obtained for a harmonic $\mathcal{H} \equiv \varepsilon S^0 + V(S^+ + S^-)$. Successive approximations amount to introducing anharmonicities. An equivalent approach—numerically expedient—consists of diagonalizing the matrices at each c_m truncation level. Then, after some iteration, the energies converge exponentially. We introduce

$$\text{conv}(i, a, e_0, i_0) = e_0 \frac{\exp(-ai) - 1}{\exp(-ai_0) - 1}, \quad (73)$$

which equals e_0 at point $i=i_0$. We choose a so as to yield $\text{conv}(i=i_0+1) = e(i_0+1)$, i.e., the correct energy at the next point. Then we check that $e(i_0+2)$ is well reproduced. Figure 15 provides an example, showing the effi-

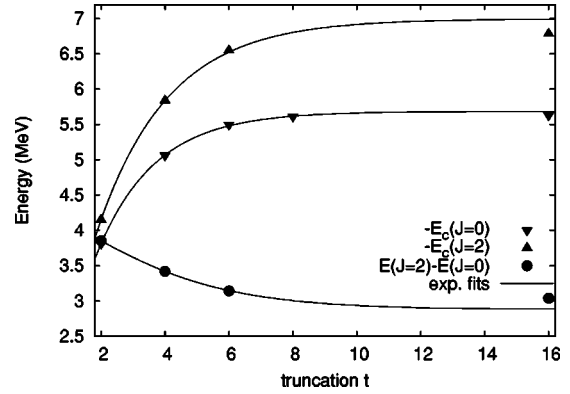


FIG. 15. Energy gain of the ground state relative to the closed shell and of the first excited state relative to the $t=1$ calculation in ^{56}Ni as a function of the truncation level t . From Caurier, Martinez-Pinedo, *et al.*, 1999b.

ciency of the method for the ground state of ^{56}Ni . The index i is replaced by the truncation level $i \equiv t/2$ [Eq. (49) with $m=16, m_0=0$]. We set $i_0=1$, fix a so as to reproduce the energy at the second iteration, and check that the curve indeed gives the correct value at the third point. The results reproduce those of the S_2 truncation, confirming that “exponential convergence” and $\exp(S)$ are very closely related. In this example, the closed-shell pivot is particularly good, and the exponential regime sets in at the first iteration. For the first excited state the pivot is not so good, and the prediction has an error of some 200 keV, which remains acceptable for practical purposes. In general, the exponential regime sets in for some value of i_0 that may be quite large (Fig. 14 suggests $i_0 \approx 25$ for the random pivot). Fortunately, it is often possible to find good pivots, and this subject deserves comment.

In the case of ^{56}Ni the good pivot state is a closed shell. As a consequence, the first iterations are associated with truncated spaces of much smaller dimensionalities than the total one ($d_m \approx 10^9$). This also happens for lighter pf shell nuclei, for which the $f_{7/2}^m$ [or eventually $(f_{7/2} p_{3/2})^m$] subspaces provide a good pivot. The same argument applies for other regions. For well-deformed nuclei Hartree-Fock calculations should provide good determinantal pivots, and hence enormous gains in dimensionality, once projection to good angular momentum can be tackled efficiently.

As we shall see next, the Lanczos and $\exp S$ procedures provide a convenient framework in which to analyze other approaches.

2. Other numerical approximation methods

The exponential convergence method introduced in the previous section was first described by Horoi *et al.* (1999), under a different but equivalent guise. In later work, a hierarchy of configurations determined by their average energy and width was proposed. Successive diagonalizations make it possible to reach the exact energy by exponential extrapolation. The method has been

successfully applied to the calculation of the binding energies of the *pf*-shell nuclei (Horoi *et al.*, 2002) and to calculation of the excitation energies of the deformed 0^+ states of ^{56}Ni and ^{52}Cr (Horoi *et al.*, 2003).

The work of Mizusaki and Imada (2002, 2003) is based on the fact that the width of the total Hamiltonian in a truncated space tends to zero as the solution approaches the exact one. They have devised different extrapolation methods and applied them to some *pf*-shell nuclei.

Andreozzi, Lo Iudice, and Porrino (2003) have recently proposed a factorization method that allows for importance sampling to approximate the exact eigenvalues and transition matrix elements.

A totally different approach that has proven its power in other fields, the density-matrix renormalization group, has been proposed (Dukelsky and Pittel, 2001; Dukelsky *et al.*, 2002), and Papenbrock and Dean (2003) have developed a method based on the optimization of product wave functions of protons and neutrons that seems very promising.

Still, to our knowledge, the only prediction for a truly large matrix that has preceded the exact calculation remains that of ^{56}Ni , $J=2$ in Fig. 15. It was borne out when the diagonalization became feasible two years later.

3. Monte Carlo methods

Monte Carlo methods rely on the imaginary-time evolution operator's acting on some trial wave function $\exp(-\beta\mathcal{H})|0\rangle$, which tends to the exact ground state $|\bar{0}\rangle$ as $\beta \Rightarrow \infty$. This is very much what the Lanczos algorithm does, but no basis is constructed. Instead, the energy (or some observable $\hat{\Omega}$) is calculated through

$$\frac{\langle 0|e^{-\beta\mathcal{H}/2}\hat{\Omega}e^{-\beta\mathcal{H}/2}|0\rangle^{\beta \rightarrow \infty}}{\langle 0|e^{-\beta\mathcal{H}}|0\rangle} \Rightarrow \frac{\langle \bar{0}|\hat{\Omega}|\bar{0}\rangle}{\langle \bar{0}|\bar{0}\rangle}, \quad (74)$$

which is transformed into a quotient of multidimensional integrals evaluated through Metropolis Monte Carlo methods with importance sampling. A *sign problem* arises because the integrands are not positive definite, leading to enormous precision problems. The Green's-function Monte Carlo studies mentioned at the beginning of Sec. II are conducted in coordinate space. The shell-model Monte Carlo variant is formulated in Fock space and hence directly amenable to comparisons with standard shell-model results (see Koonin, Dean, and Langanke, 1997a, for a review). The approach relies on the Hubbard-Stratonovich transformation, and the sign problem is circumvented either by an extrapolation method or by choosing Hamiltonians that are free of it while remaining quite realistic (e.g., pairing plus quadrupole). At present the shell-model Monte Carlo approach remains the only approach that can deal with much larger valence spaces than the standard shell model. It should be understood that this approach does not lead to detailed spectroscopy, as it only produces ground-state averages, but it is very well suited for finite-temperature calculations. The introduction of Monte

Carlo techniques in the Lanczos construction is certainly a tempting project.

The quantum Monte Carlo diagonalization method of Otsuka, Honma, and Mizusaki (1998) consists in exploring the mean-field structure of the valence space by means of Hartree-Fock calculations that break the symmetries of the Hamiltonian. Good quantum numbers are enforced by projection techniques (Peierls and Yoccoz, 1957). Then the authors borrow from the shell-model Monte Carlo approach to select an optimal set of basis states, and the full Hamiltonian is explicitly diagonalized on this basis. More basis states are iteratively added until convergence is achieved. For a very recent review of the applications of this method see Otsuka, Honma, *et al.* (2001). A strong connection between mean-field and shell-model techniques is also at the heart of the Vampir approach (Petrovici *et al.*, 1999; Schmid, 2001) and of the projected shell model (Hara and Sun, 1995).

C. Lanczos strength functions

The choice of pivot in the Lanczos tridiagonal construction is arbitrary and it can be adapted to special problems. One of the most interesting is the calculation of strength functions (Whitehead, 1980; Bloom, 1984): If U_{ij} is the unitary matrix that achieves diagonal form, its first column U_{i0} gives the amplitudes of the ground-state wave function in the tridiagonal basis, while the first row U_{0j} determines the amplitude of the pivot in the j th eigenstate. U_{0j}^2 plotted against the eigenenergies E_j is called the *strength function* for that pivot.

In practice, given a transition operator \mathcal{T} , we use it to act on a target state $|t\rangle$ to define a pivot $|0'\rangle = \mathcal{T}|t\rangle$ that exhausts the sum rule $\langle 0'|0'\rangle$ for \mathcal{T} . Once it is normalized it follows, by definition, that

$$|0\rangle = \frac{\mathcal{T}|t\rangle}{\sqrt{\langle 0'|0'\rangle}} = \sum_j U_{0j}|j\rangle, \quad (75)$$

whose moments,

$$\langle 0|\mathcal{H}^k|0\rangle = \sum_j U_{0j}^2 E_j^k, \quad (76)$$

are those of the strength function

$$S(E) = \sum_j \delta(E - E_j) U_{0j}^2, \quad (77)$$

As the Lanczos vector $|I\rangle$ is obtained by orthogonalizing $\mathcal{H}^I|0\rangle$ to all previous Lanczos vectors $|i\rangle$, $i < I$, the tridiagonal matrix elements are linear combinations of the moments of the strength distribution. Therefore the eigensolutions of the $I \times I$ matrix define an approximate strength function $S_I(E) = \sum_{i=1, I} \delta(E - E_i) \langle i|\mathcal{T}|0\rangle^2$, whose first $2I - 1$ moments are the exact ones. The eigenstates act as *doorways*, whose strength will be split until they become exact solutions when I is large enough. This is illustrated in Fig. 16, which retraces the fragmentation process of the sum-rule pivot. In this case, a ^{48}Sc doorway is obtained by applying the Gamow-Teller operator to the ^{48}Ca ground state. The term doorway applies to

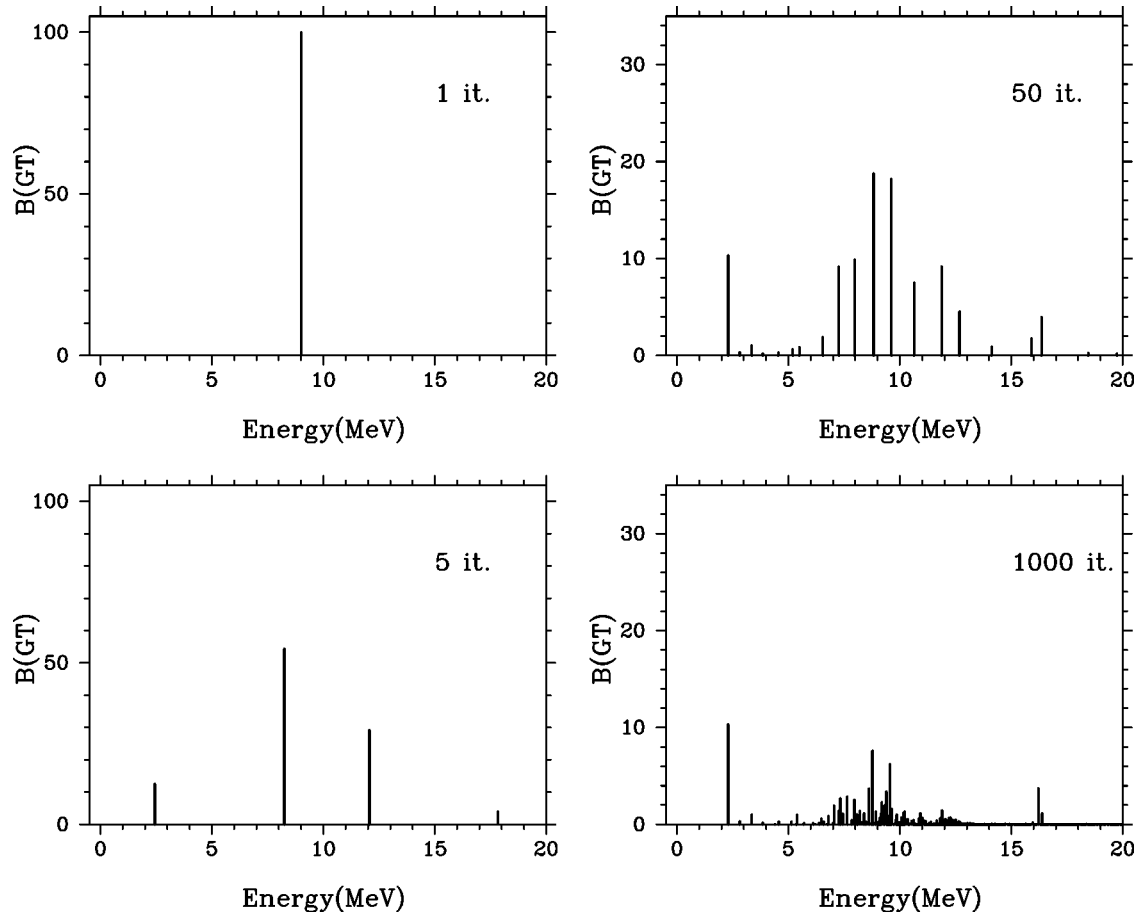


FIG. 16. Evolution of the Gamow-Teller strength function of ^{48}Ca as the number of Lanczos iterations on the doorway state increases.

vectors that have a physical meaning but are not eigenstates. After full convergence is achieved for all states in the resonance region, the strength function has the aspect shown at the bottom of the figure. In practice, all the spikes are affected by experimental width, and assuming a perfect calculation, the observed profile would have the aspect shown at the bottom of Fig. 17, after convoluting with Gaussians of 150-keV width. The upper panel shows the result for 50 iterations and 250-keV widths for the nonconverged states. The profiles become almost identical.

V. THE $0\hbar\omega$ CALCULATIONS

In this section we first revisit the p , sd , and pf shells to explain how a three-body monopole mechanism solves hitherto intractable problems. Then we propose a sample of pf -shell results that will not be discussed elsewhere. Finally Gamow-Teller transitions and strength functions are examined in some detail.

A. The monopole problem and the three-body interaction

The importance of the monopole interaction was first established by Bansal and French (1964). Its efficiency in cross-shell calculations was further confirmed by Zamick

(1965), and the success of the model of Zuker, Buck, and McGrory (1968) is implicitly due to a monopole correction to a realistic force. Zuker (1969) identified the main shortcoming of the model as due to what must be now accepted as a three-body effect.¹⁹ The associated trouble showed up in $0\hbar\omega$ calculations somewhat later simply because it takes larger matrices to detect it in the sd shell than in the Zuker-Buck-McGrory space (dimensionalities of 600 as compared to 100 for six particles). For up to five particles the results of Halbert *et al.* (1971) with a realistic interaction were quite good, but at ^{22}Na they were so bad that they became the standard example of the unreliability of the realistic forces (Brown and Wildenthal, 1988) and led to the titanic²⁰ universal sd (USD) fit of the 63 matrix elements in the shell by Wildenthal (1984).

Though the pf shell demands much larger dimensionalities, it has the advantage of containing two doubly

¹⁹The Zuker-Buck-McGrory model describes the region around ^{16}O through a $p_{1/2}s_{1/2}d_{5/2}$ space. The French-Bansal parameters b_{pd} and b_{ps} [see Eq. (9b)] must change when going from ^{14}N to ^{16}O , which requires a three-body mechanism.

²⁰It took two years on a Vax. Nowadays it would take an afternoon on a laptop.

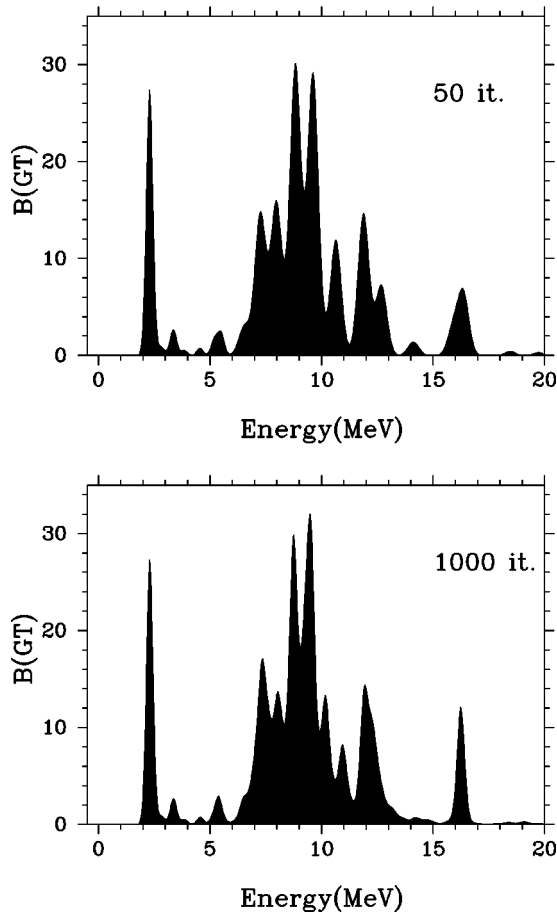


FIG. 17. The strength functions of Fig. 16 convoluted with Gaussians of 150 keV width: upper panel, 50 iterations; bottom panel, 1000 iterations.

magic nuclei, ^{48}Ca and ^{56}Ni , for which truncated calculations proved sufficient to identify very early the heart of the monopole problem: the failure to produce extruded-intruded (EI) closures.

Figure 18 gives an idea of what happens in ^{49}Ca with the Kuo-Brown interaction (Kuo and Brown, 1968):

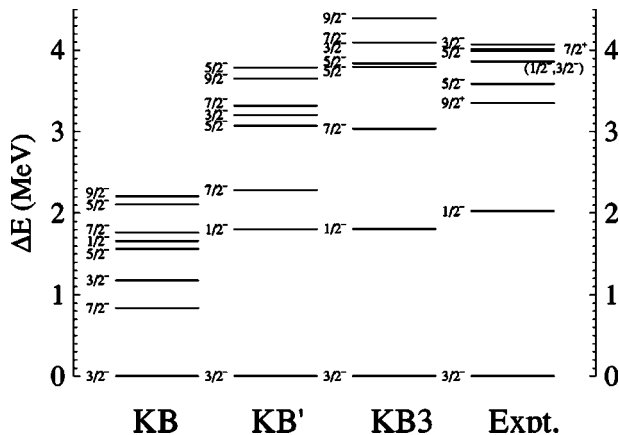


FIG. 18. The level scheme of ^{49}Ca obtained with the interactions KB, KB', and KB3, compared to the experimental result. From Martínez-Pinedo, Zuker, *et al.*, 1997.

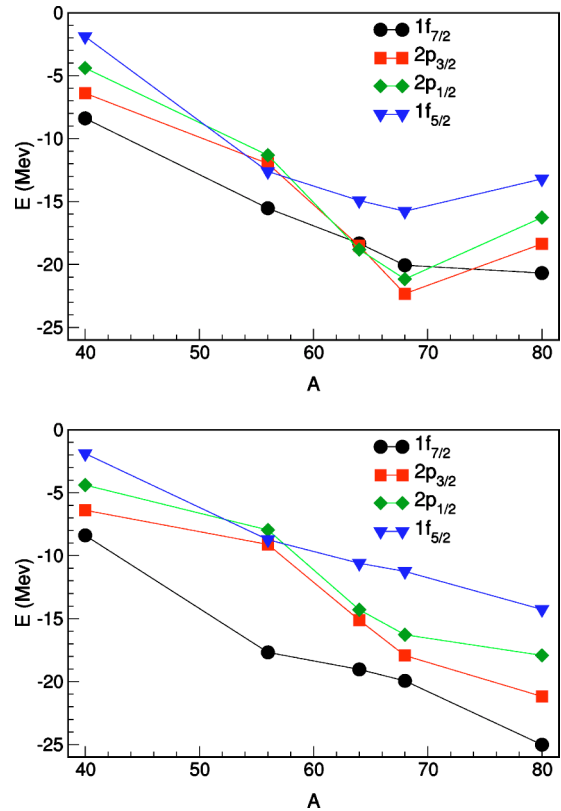


FIG. 19. (Color in online edition) Effective single-particle energies in the pf shell along the $N=Z$ line, computed with the BonnC (upper panel) and KB3 (lower panel) interactions.

there are six states below 3 MeV, where only one exists. In Pasquini (1976) and Pasquini and Zuker (1978) the following modifications were proposed ($f \equiv f_{7/2}, r \equiv f_{5/2}, p_{3/2}, p_{1/2}$):

$$V_{fr}^T(\text{KB1}) = V_{fr}^T(\text{KB}) - (-)^T 300 \text{ keV},$$

$$V_{ff}^0(\text{KB1}) = V_{ff}^0(\text{KB}) - 350 \text{ keV},$$

$$V_{ff}^1(\text{KB1}) = V_{ff}^1(\text{KB}) - 110 \text{ keV}. \quad (78)$$

The first line defines KB' in Fig. 18. The variants KB2 and KB3 in Poves and Zuker (1981b) keep the KB1 centroids and introduce very minor multipole modifications. KB3 was adopted as standard²¹ in successful calculations in $A=47-50$ that will be described in the next sections (Courier *et al.*, 1994; Martínez-Pinedo, Poves, Robledo, *et al.*, 1996; Martínez-Pinedo, Zuker, *et al.*, 1997).

For higher masses, there are some problems, but nothing comparable to the serious ones encountered in the sd shell, where modifications like those in Eq. (78) are beneficial but (apparently) insufficient. The effective single-particle energies in Fig. 19 are just the monopole values of the particle and hole states at the subshell closures. They give an idea of what happens in a two-body

²¹The multipole changes—which were beneficial in the perturbative treatment of Poves and Zuker (1981b)—had much less influence in the exact diagonalizations.

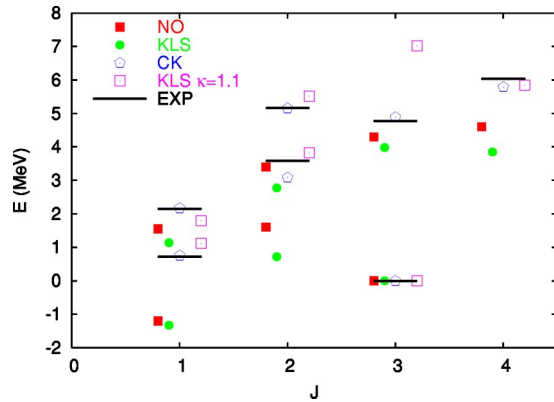


FIG. 20. (Color in online edition) The excitation spectrum of ^{10}B for different interactions described in the text: NO, Navrátil and Ormand; KLS, Kahana-Lee-Scott; CK, Cohen-Kurath. Adapted from Zuker, 2003.

description. At the origin, in ^{41}Ca , the spectrum is the experimental one. At ^{57}Ni there is a bunching of the upper orbits, which realistic BonnC and Kuo-Brown models describe reasonably well, but they fail to produce a substantial gap. Hence the need of KB1-type corrections. At the end of the shell, the BonnC and Kuo-Brown interactions reproduce an expanded version of the ^{41}Ca spectrum that is most certainly incorrect. The indication from $\tilde{\mathcal{H}}_m^d$ in Eq. (27) is that the bunching of the upper orbits should persist. By incorporating this hint—which involves the $V_{rr'}$ centroids—and fine-tuning the V_{fr} ones Poves *et al.* (2001) defined a KB3G (G comes from improved gaps) interaction, which offers interesting improvements over KB3 in $A=50-52$. Around ^{56}Ni there are still some problems, though not as severe as those encountered in the sd and p shells. Compared to KB3, the interaction FPD6 (Richter *et al.*, 1991) has a better gap in ^{56}Ni , but the orbit $1f_{5/2}$ is definitely too low in ^{57}Ni . This produces problems with the description of Gamow-Teller processes (see Borcea *et al.*, 2001, for a recent experimental check on the beta decay of ^{56}Cu).

The classic fits of Cohen and Kurath (1965) defined the state of the art in the p shell for a long time. The first realistic G -matrix elements (Kuo and Brown, 1966) dealt with the sd shell, a subject of very active research at the time. As the p shell problem was assumed to be solved, nobody seems to have noticed that G matrices produce in ^{10}B a catastrophe parallel to the one in ^{22}Na . The work of Navrátil and Ormand (2002), and Pieper, Varga, and Wiringa (2002) acted as a powerful reminder that brought to the fore the three-body nature of the discrepancies.

Once this is understood, the solution follows: Eq. (78) is assumed to be basically sound but the corrections are taken to be linear in the total number of valence particles m (the simplest form that a three-body term can take).

Using $f \equiv (p_{3/2}, d_{5/2}, f_{7/2})$ generically in the (p, sd, pf) shells, respectively, and $r = p_{1/2}$ and $r \equiv d_{3/2}, s_{1/2}$ for the p

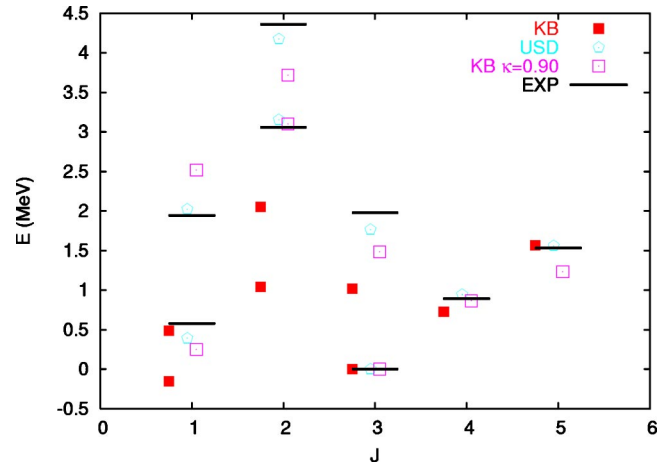


FIG. 21. (Color in online edition) The excitation spectrum of ^{22}Na for different interactions: KB, Kuo-Brown; USD, universal sd . Adapted from Zuker, 2003.

and sd shells, Zuker (2003) proposes $[\kappa = \kappa_0 + (m - m_0)\kappa_1]$

$$V_{fr}^T(R) \Rightarrow V_{fr}^T(R) - (-)^T \kappa,$$

$$V_{ff}^T(R) \Rightarrow V_{ff}^T(R) - 1.5\kappa\delta_{T_0}, \quad (79)$$

where R stands for any realistic two-body potential. The results for ^{10}B are shown in Fig. 20. The black squares (NO) are from Navrátil and Ormand (2002, Fig. 4, $6\hbar\Omega$).

The solid circles correspond to the bare Kahana-Lee-Scott G matrix ($\hbar\omega=17$ MeV), the open squares to the same with $\kappa=1.1$, and the pentagons to the Cohen-Kurath fit. Navrátil-Ormand and Kahana-Lee-Scott give quite similar spectra, as expected from the discussion in Secs. II.A and II.D. The κ correction eliminates the severe discrepancies with experiment and give values close to those of Cohen and Kurath.

In ^{22}Na the story repeats itself, as shown in Fig. 21: BonnC and KB are very close to one another, the ground-state spin is again $J=1$ instead of $J=3$, and the whole spectrum is awful. The κ correction restores the levels to nearly correct positions, though the universal sd model (USD) still gives a better fit. This simple cure was not discovered earlier because κ is not a constant. In ^{24}Mg we could still use the value for ^{22}Na but around ^{28}Si it must be substantially smaller. The spectra in Fig. 22 are obtained with $\kappa(m) = 0.9 - 0.05(m - 6)$, and they are now as good as those given by the universal sd model.

To determine a genuine three-body effect (i.e., the linearity of κ) a sufficiently large span of A values is necessary. In the p shell, corrections to $V_{rr'}$ become indispensable very soon and must be fitted simultaneously, as was done successfully by Abzouzi *et al.* (1991), so we do not dwell on the subject. As we have seen, in the pf shell KB3, which is nearly perfect in $A=47-50$, must be modified to KB3G for $A=50-52$, which also does well at the lower masses. To find a real problem with a two-body R

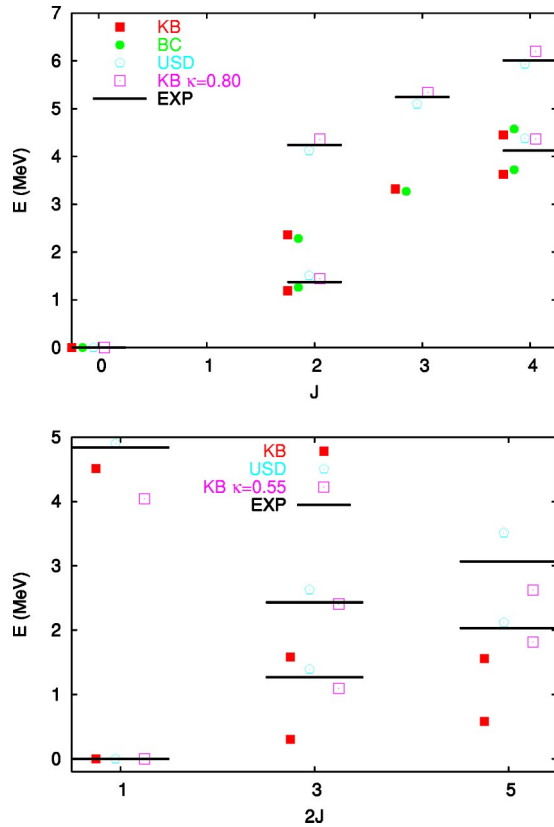


FIG. 22. (Color in online edition) The excitation spectra of ^{24}Mg (upper panel) and ^{29}Si (lower panel) for different interactions: KB, Kuo-Brown; BC, BonnC; USD, universal *sd*. Adapted from Zuker, 2003.

interaction (i.e., compatible with nucleon-nucleon data)²² we have to move to $^{56,58}\text{Ni}$. In particular the first $B(E2)(2 \rightarrow 0)$ transition in ^{58}Ni falls short of the observed value ($140 e^2 \text{fm}^4$) by a factor ≈ 0.4 with any monopole corrected KB interaction. The problem can be traced to weak quadrupole strength and it is not serious; as explained in Sec. II.D, it is due to a normalization uncertainty, and Table I shows that with equal normalizations BonnC and Kuo-Brown in the *pf* shell are as close as in the *sd* shell.

Zuker (2003) adopted BonnC. Small modifications of the V_{fr} matrix were made to improve the (already reasonable) *r* spectrum in ^{57}Ni (see Fig. 19). The particular mixture in Eq. (79) was actually chosen to make possible, in the simplest way, a good gap in ^{48}Ca and a good single-particle spectrum in ^{49}Sc . It was found that for $A=48$, $\kappa(m=8) \approx 0.43$. For $A=56$, truncated calculations yielded $\kappa(16) \leq 0.28$. The $B(E2)(2 \rightarrow 0)$ in ^{58}Ni indicated convergence to the right value.

With $\kappa(m=8)$, BonnC reproduces the yrast spectrum of ^{48}Cr almost as well as KB3, but not with a $\kappa(m=16)$, as shown in Fig. 23, indicating that the three-body drift

²²It may be possible to fit the data with a purely two-body set of matrix elements: The universal *sd* model is the prime example, but it is *R* incompatible (Dufour and Zuker, 1996).

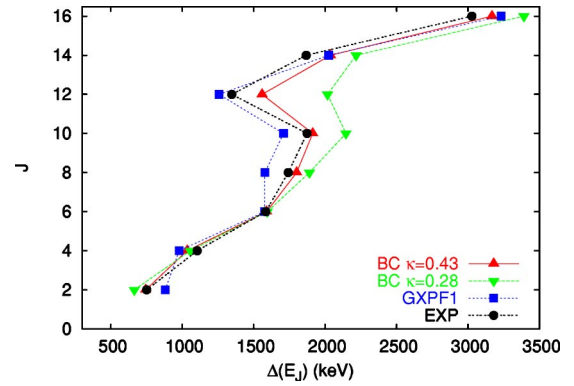


FIG. 23. (Color in online edition) Backbending plot for ^{48}Cr . The experimental data from Lenzi *et al.* (1996) (circles) are compared with the shell-model calculations using the BonnC interaction with a two-body (downward triangles) and a three-body (upward triangles) monopole correction and with the GXPF1 interaction.

is needed, though not as urgently as in the *sd* shell. Another indication comes from the $T=0$ spectrum of ^{46}V , the counterpart of ^{22}Na and ^{10}B in the *pf* shell. The realistic interactions again place the $J=1$ and $J=3$ states in the wrong order; the correct one is reestablished by the three-body monopole correction.

In Sec. II.B.2 it was shown that a good fit to $cs \pm 1$ spectra around closed shells was sufficient to define a plausible two-body monopole model \tilde{V}_{fr}^d . The trouble with this approach is that sufficient information exists around extruded-intruded (EI) closures, and very little for holes in the harmonic-oscillator ones. As a consequence, almost everything concerning $V_{rr'}$ centroids (i.e., not involving the intruder orbit) had to be invented. In addition, the very mechanism of EI shell formation was forced to be two body, which we now know must be three body. Therefore the new monopole strategy must amount to keeping the realistic two-body potentials and forcing all monopole corrections to be three body. Paradoxically, the recently released two-body-only GXPF1 (Homma *et al.*, 2004) fit to all *pf*-shell matrix elements strongly supports this strategy, as we discuss in the next section.

B. The *pf* shell

Systematic calculations of the $A=47-52$ isobars have been made by Caurier, Zuker, *et al.* (1994; $A=48$, KB3), Martínez-Pinedo *et al.* (1997; $A=47$ and 49 , KB3), and Poves *et al.* (2001; $A=50-52$, KB3G). Among the other full $0\hbar\omega$ calculations let us highlight the following:

- (i) The shell-model Monte Carlo studies using either the FPD6 interaction (Alhassid *et al.*, 1994) or the KB3 interaction (Langanke *et al.*, 1995). A comparison of the exact results with the shell-model Monte Carlo results can be found in Caurier, Martínez-Pinedo, *et al.* (1999a). For a review of

the shell-model Monte Carlo results in the pf shell, see also Koonin *et al.* (1997b).

- (ii) The recent applications of the exponential extrapolation method (Horoi *et al.*, 2002, 2003).
- (iii) The calculations of Novoselsky *et al.* (1997) for ^{51}Sc and ^{51}Ti using the DUPSM code (see also the erratum in Novoselsky *et al.*, 1998b) and for ^{52}Sc and ^{52}Ti (Novoselsky *et al.*, 1998a).
- (iv) The extensive quantum Monte Carlo diagonalizations of the spectrum of ^{56}Ni have been able to reproduce the exact result for the ground-state binding energy within 100–200 keV and to give a fairly good description of the highly deformed excited band of this doubly magic nucleus (Otsuka *et al.*, 1998; Mizusaki *et al.*, 1999, 2002).

Other applications to the pf shell can be found in Honma *et al.* (1996). The existence of excited collective bands in the $N=28$ isotones is studied by Mizusaki *et al.* (2001).

As mentioned above, a new interaction for the pf shell (GXPF1) has been produced by a Tokyo-MSU collaboration (Honma *et al.*, 2002, 2004), following the fitting procedures that lead to the universal sd interaction (plus some monopole guidance). The fit starts with the G matrix obtained from the Bonn-C nucleon-nucleon potential (Hjorth-Jensen *et al.*, 1995) and privileges the upper part of the pf shell, as seen by the very large difference in single-particle energies between the $1f_{7/2}$ and $2p_{3/2}$ orbits (3 MeV instead of the standard 2 MeV).

This approach has two noteworthy features, as can be seen in Fig. 2 of Honma *et al.* (2004) (1) The monopole matrix elements are global modulations of the realistic ones (BonnC). (2) The centroids involving the $f_{7/2}$ orbit have almost exactly the form adopted in Eq. (79) and in KB3G. Remember, though, that fine tuning is necessary since a 50-keV shift in a V_{fr} centroid amounts to an 800-keV shift in the spectrum of ^{57}Ni .

As GXPF1 is a two body-only model, its authors find it necessary to make some multipole changes, and here, something even more remarkable happens: From Table II in Honma *et al.* (2004), it appears that most of the multipole changes are made to ensure the right monopole centroids, in particular the V_{fr} ones. To give an example, the ~ 300 -keV attraction in the V_{75} centroid is achieved by making the $V_{75}^{J=5,6}$ matrix elements more attractive by ~ 600 keV. As explained in the discussion of Fig. 26 in Honma *et al.* (2004), these selective changes tend to reinforce the presence of the quadrupole force in the diagonal elements. They also transform the very nice agreement with experiment for BonnC with the proper three-body monopole corrections in Fig. 23 into a not-so-nice one. And they cause GXPF1 to differ appreciably from the realistic matrix elements, though the broad collective features are respected, as can be seen in Table II. It is not obvious that GXPF1 could do better than KB3 and KB3G below ^{56}Ni . At ^{56}Ni and above it does very well, but it is by no means clear

that three-body monopole-corrected forces could not match the GXPF1—or the universal sd —performances.

Excellent spectroscopy is obtained around ^{56}Ni . In the calcium isotopes (i.e., when only the $T=1$ neutron-neutron interaction is active) this new interaction retains the tendency of the bare G matrices (Kuo-Brown, Bonn-C, Kahana-Lee-Scott) to produce large gaps at $N=32$ and $N=34$, in contrast to FPD6 or KB3G, which only predict a large gap at $N=32$. Some early spectroscopic applications of GXPF1 to the heavy isotopes of titanium, vanadium, and chromium are those of Janssens *et al.* (2002) and Mantica *et al.* (2003), who explore the $N=32$ – 34 gaps. In particular, a recent measure (Liddick *et al.*, 2004) of the location of the 2^+ state in ^{56}Ti does not support the large $N=34$ gap predicted by the new interaction.

Each nucleus has its interest, sometimes anecdotal, sometimes fundamental. The agreement with experiment for the energies, the quadrupole and magnetic moments, and the transitions, is consistently good, often excellent. These results have been conclusive in establishing the soundness of the minimally monopole modified realistic interaction(s). There is no point in reproducing them here, and we only present a few typical examples concerning spectroscopic factors, isospin nonconserving forces, and “pure spectroscopy.” Let us, however, single out ^{60}Zn , the one with the largest m -scheme dimension (2 292 604 744), and give its ground-state energy calculated with KB3G (-84.65 MeV) for benchmarking purposes.

1. Spectroscopic factors

The basic tenet of the independent-particle model is that addition of a particle to a closed shell $a_r^\dagger|cs\rangle$ produces an eigenstate of the $|cs+1\rangle$ system. Nowadays we know better: It produces a doorway that will be fragmented. If we choose $|cs\rangle=|^{48}\text{Ca}\rangle$ and $|cs+1\rangle=|^{49}\text{Sc}\rangle$, the four pf orbits provide the doorways. The lowest, $f_{7/2}$, leads to an almost pure eigenstate. The middle ones, $p_{3/2,1/2}$, are more fragmented, but the lowest level still has most of the strength and the fragments are scattered at higher energies. Figure 24 shows what happens to the $f_{5/2}$ strength: it remains concentrated on the doorway but splits locally. The same evolution with energy of the quasiparticles (Landau’s term for single-particle doorways) was later shown to occur generally in finite systems (Altshuler *et al.*, 1997).

2. Isospin nonconserving forces

Recent experiments have identified several yrast bands in mirror pf nuclei (O’Leary *et al.*, 1997, 2002; Bentley *et al.*, 1998, 1999, 2000; Lenzi *et al.*, 2001; Brandolini, Sánchez Solano, *et al.*, 2002) for $A=47, 49, 50$, and 51. The naive view that the Coulomb energy should account for the mirror energy differences turns out to be untenable. The four pairs were analyzed by Zuker *et al.* (2002), who showed that three effects should be taken into account. A typical result is proposed in Fig. 25,

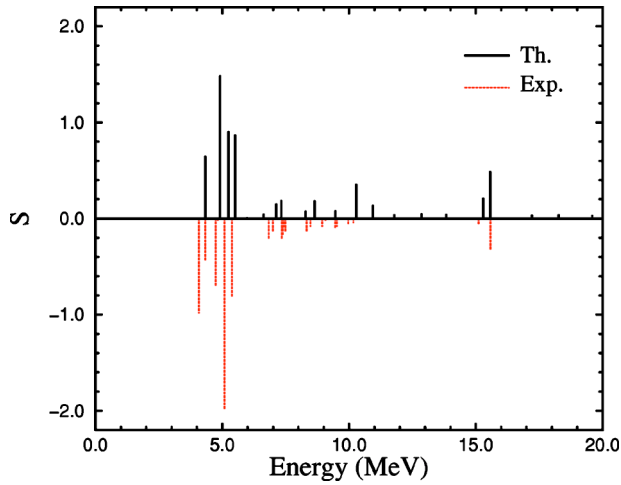


FIG. 24. (Color in online edition) Spectroscopic factors, $(2j+1)S(j, t_2)$, corresponding to stripping of a particle in the orbit $1f_{5/2}$ (Martínez-Pinedo *et al.*, 1997).

where V_{CM} and V_{BM} stand for Coulomb and nuclear isospin-breaking multipole contributions, while V_{Cm} is a monopole Coulomb term generated by small differences of radii between the members of the yrast band. The way these disparate contributions add to reproduce the observed pattern is striking.

Another calculation of the isospin-nonconserving effects, and their influence in the location of the proton drip line, is due to Ormand (1997). He has also analyzed the $A=46$ isospin triplet in Garrett *et al.* (2001).

3. Pure spectroscopy

The nucleus we have chosen to illustrate this point is also one that has been measured to complete the mirror band (Bentley *et al.*, 2000) in $A=51$, whose mirror energy differences are as well described as those of $A=49$ in Fig. 25. Such calculations require very good wave functions, and the standard test they have to pass is the “purely spectroscopic” one.

Such an analysis usually proceeds as follows:

- (i) Quadrupole effective charges for neutrons, pro-

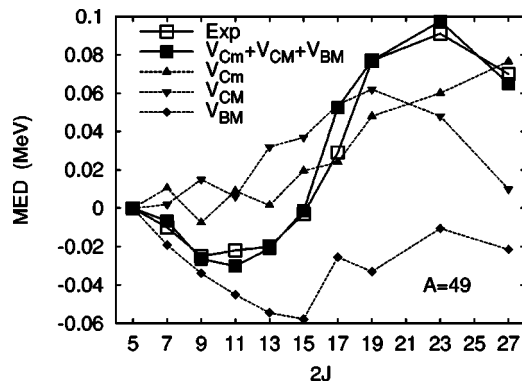


FIG. 25. Experimental (O’Leary *et al.*, 1997) and calculated (Zuker *et al.*, 2002) mirror energy differences (MED) for the pair ^{49}Cr - ^{49}Mn .

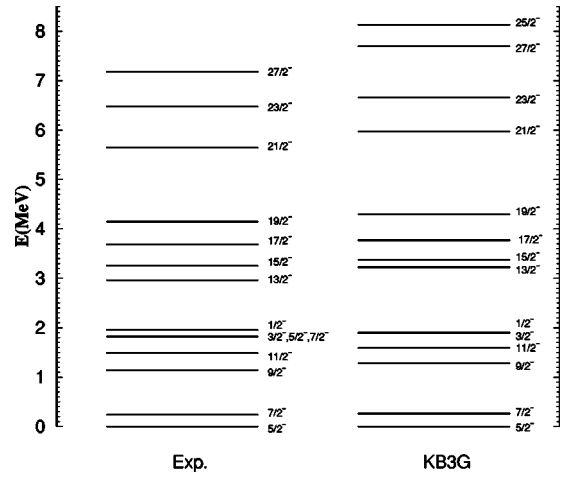


FIG. 26. Yrast band of ^{51}Mn ; experiment (Bentley *et al.*, 2000) vs shell-model calculation in the full pf -shell space. Adapted from Poves *et al.*, 2001.

tons, and bare g factors in $M1$ transitions and moments are used. First one sets the quadrupole effective charges for neutrons and protons to $q_v=0.5$ and $q_\pi=1.5$, respectively. Bare g factors of $g_\pi^s=5.5857\mu_N$, $g_\nu^s=-3.3826\mu_N$, $g_\pi^l=1.0\mu_N$, and $g_\nu^l=0.0\mu_N$ in $M1$ transitions and moments are used. Except when the $M1$ transitions are fully dominated by the spin term, the use of effective g factors does not modify the results very much due to the compensation between the spin and orbital modifications.

- (ii) Then the spectra of some relevant nuclei are computed and compared with data. For instance, we give a typical result for the nucleus ^{51}Mn , whose yrast band, calculated in the full pf -shell space, is compared in Fig. 26 with the experiment data. Here the low-lying part of the spectrum is fairly well reproduced. On the other hand, the excitation energy of the high-spin states is slightly too large.
- (iii) Then, calculated electromagnetic transitions are compared with data. An example of a satisfactory fit is given in Table IV.

Note that the abrupt change in both $B(M1)$ and $B(E2)$ for $J=(17/2)^-$ is very well reproduced by the calculation. The origin of this isomerism is the sudden alignment of two particles in the $1f_{7/2}$ orbit, which provides an intuitive physical explanation for the abrupt change in the mirror energy difference (Bentley *et al.*, 2000).

Finally, one analyzes the quality of the fit for some selected ground-state moments. Here the experimental values are known: $\mu_{\text{exp}}=3.568(2)\mu_N$ and $Q_{\text{exp}}=42(7)e\text{ fm}^2$ (Firestone, 1996) and compare quite well with the calculated $\mu_{\text{th}}=3.397\mu_N$ and $Q_{\text{th}}=35e\text{ fm}^2$.

C. Gamow-Teller and magnetic dipole strength

Out of the approximately 2500 known nuclei that are bound with respect to nucleon emission, only 253 are

TABLE IV. Transitions in ^{51}Mn .

	Expt.	Theor.
$B(M1)$	(μ_N^2)	(μ_N^2)
$\frac{7}{2}^- \rightarrow \frac{5}{2}^-$	0.207(34)	0.177
$\frac{9}{2}^- \rightarrow \frac{7}{2}^-$	0.16(5)	0.116
$\frac{11}{2}^- \rightarrow \frac{9}{2}^-$	0.662(215)	0.421
$\frac{17}{2}^- \rightarrow \frac{15}{2}^-$	0.000 12(4)	0.000 03
$\frac{19}{2}^- \rightarrow \frac{17}{2}^-$	>0.572	0.797
$B(E2)$	$(e^2 \text{ fm}^4)$	$(e^2 \text{ fm}^4)$
$\frac{7}{2}^- \rightarrow \frac{5}{2}^-$	528(146)	305
$\frac{9}{2}^- \rightarrow \frac{5}{2}^-$	169(67)	84
$\frac{9}{2}^- \rightarrow \frac{7}{2}^-$	303(112)	204
$\frac{11}{2}^- \rightarrow \frac{7}{2}^-$	236(67)	154
$\frac{11}{2}^- \rightarrow \frac{9}{2}^-$	232(75)	190
$\frac{17}{2}^- \rightarrow \frac{13}{2}^-$	1.236(337)	2.215

stable. The large majority of the rest decay by β emission or electron capture, mediated by the weak interaction. When protons and neutrons occupy the same orbits, as in our case, the dominant processes are allowed Fermi and Gamow-Teller transitions. The information obtained from the weak decays has been complemented by the (p, n) and (n, p) reactions in forward kinematics, which make it possible to obtain total Gamow-Teller strengths and strength functions that cannot be accessed by the decay data because of the limitations due to the Q_β windows. From a theoretical point of view, the comparison of calculated and observed strength functions provides invaluable insight into the meaning of the valence space and the nature of the deep correlations detected by the “quenching” effect.

The half-life for a transition between two nuclear states is given by (Behrens and Bühring, 1982; Schopper, 1966)

$$(f_A + f^e)t = \frac{6144.4 \pm 1.6}{(f_V/f_A)B(F) + B(GT)}. \quad (80)$$

The value 6144.4 ± 1.6 is obtained from the nine best-known superallowed beta decays (Tower and Hardy, 2002; see Wilkinson, 2002a, 2002b, for an alternative study). Here f_V and f_A are the Fermi and Gamow-Teller phase-space factors, respectively (Wilkinson and Macefield, 1974; Chou *et al.*, 1993). f^e is the phase space for electron capture (Bambynek *et al.*, 1977) which is only present in β^+ decays. If $t_{1/2}$ is the total lifetime, the partial lifetime of a level with branching ratio b_r is $t = t_{1/2}/b_r$.

$B(F)$ and $B(GT)$ are defined as

$$B(F) = \left[\frac{\langle f || \sum_k t_{\pm}^k || i \rangle}{\sqrt{2J_i + 1}} \right]^2, \quad (81a)$$

TABLE V. Comparison of GT_+ strengths. For ^{54}Fe , ^{55}Mn , ^{58}Ni , and ^{59}Co the calculations are truncated to $t=8$, $t=4$, $t=6$, and $t=4$, respectively. The data are from Vetterli *et al.*, 1990; Alford *et al.*, 1993; El-Kateb *et al.*, 1994; Williams *et al.*, 1995.

Nucleus	Uncorrelated	Correlated		Expt.
		Unquenched	$Q=0.74$	
^{51}V	5.15	2.42	1.33	1.2 ± 0.1
^{54}Fe	10.19	5.98	3.27	3.3 ± 0.5
^{55}Mn	7.96	3.64	1.99	1.7 ± 0.2
^{56}Fe	9.44	4.38	2.40	2.8 ± 0.3
^{58}Ni	11.9	7.24	3.97	3.8 ± 0.4
^{59}Co	8.52	3.98	2.18	1.9 ± 0.1
^{62}Ni	7.83	3.65	2.00	2.5 ± 0.1

$$B(GT) = \left[\left(\frac{g_A}{g_V} \right) \frac{\langle f || \sum_k \sigma^k t_{\pm}^k || i \rangle}{\sqrt{2J_i + 1}} \right]^2. \quad (81b)$$

Matrix elements are reduced [Eq. (A3)] with respect to spin only, \pm refers to β^\pm decay, $\sigma=2S$, and $(g_A/g_V) = -1.2720(18)$ (Hagiwara *et al.*, 2002) is the ratio of the weak interaction axial-vector and vector coupling constants.

For states of good isospin the value of $B(F)$ is fixed. It can be altered only by a small isospin-symmetry-breaking δ_C correction (Tower and Hardy, 2002). Shell-model estimates of this quantity can also be found in Ormand and Brown (1995),

$$B(F) = [T(T+1) - T_{z_i}T_{z_f}] \delta_{if} (1 - \delta_C), \quad (82)$$

where δ_{if} allows only transitions between isobaric analog states. Superallowed decays may shed light on the departures from unitarity of the Cabibbo-Kobayashi-Maskawa matrix.

The total strengths S_\pm are related by the sum rules

$$S_-(F) - S_+(F) = N - Z, \quad (83a)$$

$$S_-(GT) - S_+(GT) = 3(N - Z), \quad (83b)$$

where N and Z refer to the initial state, and $S_\pm(GT)$ does not contain the g_A/g_V factor. A comparison of the (p, n) and (n, p) data with the Gamow-Teller sum rule (Ikeda *et al.*, 1963) revealed the long-standing “quenching problem”; only approximately one-half of the sum-rule value was found in the experiments.

The Gamow-Teller strength is not protected by a conservation principle and depends critically on the wave functions used. Full $0\hbar\omega$ calculations already show a large quenching with respect to the independent-particle limit, as can be seen in Table V, where the result of a full pf calculation is compared with that obtained with an uncorrelated Slater determinant having the same occupancies:

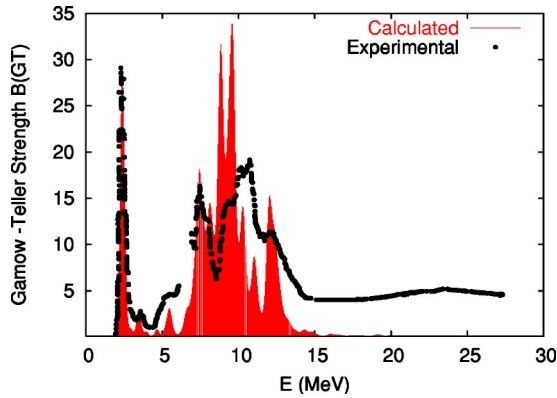


FIG. 27. (Color in online edition) Gamow-Teller strength in $^{48}\text{Ca}(p,n)^{48}\text{Sc}$ from Anderson *et al.* (1990)—after elimination of the Fermi peak at around 6 MeV—compared with the calculated peaks (KB3 interaction) after 700 Lanczos iterations (Caurier, Poves, and Zuker, 1995). The peaks have been smoothed by Gaussians having the experimental width of the first measured level.

$$S = \sum_{i,k} \frac{n_i^p n_k^h}{(2j_i + 1)(2j_k + 1)} \langle i || \sigma || k \rangle^2. \quad (84)$$

Here the sum on i runs over the proton (neutron) orbits in the valence space, and k runs over the proton (neutron) orbits for S_+ (S_-). n^p and n^h denote the number of particles and holes, respectively. The determinantal state requires a quenching factor that is almost twice as large as the standard quenching factor $Q^2 = (0.74)^2$, which brings the full calculation into line with experiment.

1. The meaning of the valence space

Before moving on to the explanation of the quenching of the Gamow-Teller strength, it is convenient to recall the meaning of the valence space, as discussed in Sec. II.A.1. The $^{48}\text{Ca}(p,n)^{48}\text{Sc}$ reaction (Anderson *et al.*, 1990) provides an excellent example. In Fig. 27, adapted from Caurier, Poves, and Zuker (1995), the experimental data are compared with the strength function produced by a calculation in the full pf shell using the interaction KB3. The peaks have all $J=1$, $T=3$. In the pf shell there are 8590 of them and the calculation has been pushed to 700 iterations in the Lanczos strength function to ensure fully converged eigenstates below 11 MeV. Of these eigenstates 30 are below 8 MeV. They are at the right energy and have the right strength profile. At higher energies the peaks are much too narrow compared with experiment. This means that they may well be eigenstates of the effective Hamiltonian in the pf shell, but not eigenstates of the full system. Therefore they should be viewed as doorway states, subject to further mixing with the background of intruders that dominates the level density after 8 MeV, as corroborated by the experimental tail that contains only intruders and can be made to start naturally at that energy.

The KB3 effective interaction is doing a very good job, but it is certainly not decoupling 8590 pf states from

the rest of the space. If the fact is not explicitly recognized we end up with the often raised (Hjorth-Jensen *et al.*, 1995) “intruder problem”: Decoupling cannot be enforced perturbatively when intruders are energetically close to model states. Figure 27 indicates that although a few eigenstates are well decoupled, it is possible to make sense of many others if one interprets them as doorways. A satisfactory description of the lowest states indicates that the model space makes sense. It ensures good decoupling at the S_2 level or simply in second-order perturbation theory, which guarantees a state-independent interaction.

Energetically we are in good shape, and we concentrate on the renormalization of the Gamow-Teller operator: the calculated strength has been quenched by a factor $\approx (0.74)^2$. Why? And why does this factor ensure the right detailed strength for about 30 states below 8 MeV?

2. Quenching

To understand the quenching problem it is best to start with a (tentative) solution. The dressed states in Eq. (4) are normalized to unity in the model space. This trick is essential in the formulation of linked cluster or exp S theories [hence Eq. (64)]. It makes possible the calculation of the energy—and some transitions, such as the $E2$ —without knowledge of the norm of the exact wave function. In general, though, we need an expectation value between exact, normalized states: $\langle \hat{f} || T || \hat{i} \rangle^2$. If we write

$$|\hat{i}\rangle = \alpha |0\hbar\omega\rangle + \sum_{n \neq 0} \beta_n |n\hbar\omega\rangle, \quad (85)$$

and a similar expression in α' , β' for $|\hat{j}\rangle$, we find

$$\langle \hat{f} || T || \hat{i} \rangle^2 = \left(\alpha\alpha' T_0 + \sum_{n \neq 0} \beta_n \beta'_n T_n \right)^2, \quad (86)$$

since the Gamow-Teller operator does not couple states with different numbers of $\hbar\omega$ excitations. Let us make two assumptions: (a) the $n \neq 0$ contributions can be neglected in the (valence) states dominated by $n=0$ ones [an estimate of Caurier, Poves, and Zuker (1995) supports this assumption]; (b) $\alpha \approx \alpha'$; it follows that if the projection of the physical wave function in the $0\hbar\omega$ space is $Q \approx \alpha^2$, its contribution to the transition will be quenched by Q^2 .

Exactly the same arguments apply to transfer reactions—for which $T = a_s$ (or a_s^\dagger)—but with these reactions the arguments are simpler because $T_{n \neq 0} = 0$. The transition strength is given by the spectroscopic factor, which can be identified with Q when one particle is removed and $1 - Q$ when it is added. The assumption that the model amplitudes in the exact wave functions are approximately constant is borne out by systematic calculations of Q in the p shell [Chou *et al.*, 1993, $Q = 0.820(15)$], the sd shell [Wildenthal *et al.*, 1983, Q

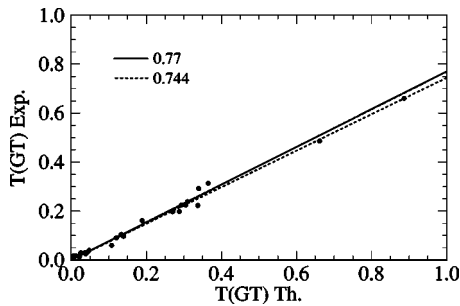


FIG. 28. Comparison of experimental and theoretical values of the quantity $T(GT)$ in the pf shell (Martínez-Pinedo, Poves, Caurier, and Zuker, 1996). The x and y coordinates correspond to theoretical and experimental values, respectively. The dashed line shows the best fit for $Q=0.744$. The solid line shows the result obtained in the sd -shell nuclei (Wildenthal *et al.*, 1983).

$=0.744(2)$], and the pf shell [illustrated in Fig. 28, Martínez-Pinedo, Poves, Caurier, and Zuker, 1996, $Q = 0.744(15)$].

These numbers square well with the existing information on spectroscopic factors from the data on d, p (Vold *et al.*, 1978, $Q \approx 0.7$) and $e, e'p$ (Cavedon *et al.*, 1982, $Q = 0.7$; see also Pandharipande *et al.*, 1997). This consistency is significant in that it backs assumption (a) above, which is trivially satisfied for spectroscopic factors. It offers the prospect of accepting the Gamow-Teller data as a measure of a very fundamental quantity that does not depend on particular processes. The proposed “solution” to the quenching problem amounts to reading data.

Experimentally, the challenge is to locate all the strength, constrained by the Ikeda sum rule, which relates the direct and inverse processes. The careful analysis of Anderson *et al.* (1985) suggests, but does not prove, that the experimental tail in Fig. 27 contains enough strength to satisfy approximately the sum rule. A similar result is obtained for $^{54}\text{Fe}(p, n)$. (Anderson *et al.*, 1990). More recent experiments by the Tokyo group establish that the strength located at accessible energies exhausts 90(5)% of the sum rule in the $^{90}\text{Zr}(n, p)$ and 84(5)% in $^{27}\text{Al}(p, n)$ (Wakasa *et al.*, 1997, 1998).

The theoretical problem is to calculate Q . It has been compounded by a sociological one: The full Gamow-Teller operator is $(g_A/g_V)\sigma\tau$, where $g_A/g_V \approx -1.27$ is the ratio of weak axial-vector and vector coupling constants. The hotly debated question is whether Q is due to non-nucleonic renormalization of g_A or nuclear renormalization of $\sigma\tau$ (Osterfeld, 1992; Arima, 2001). We have sketched above the nuclear case, along the lines proposed by Caurier, Poves, and Zuker (1995), but under a new guise that makes it easier to understand. The calculations of Bertsch and Hamamoto (1982), Drożdż *et al.* (1986), and Dang *et al.* (1997) manage to place significant amounts of strength beyond the resonance region, but they are based on $2p$ - $2h$ doorways that fall somewhat short of giving a satisfactory view of the strength func-

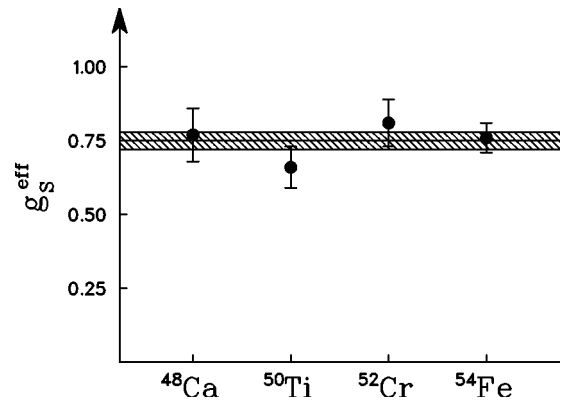


FIG. 29. Effective spin g factor of the $M1$ operator deduced from the comparison of shell-model calculations and data for the total $B(M1)$ strengths in the stable even mass $N=28$ isotones. From von Neumann-Cosel *et al.*, 1998.

tions. No-core calculations are under way that should be able to clarify the issue.

The purely nuclear origin of quenching is borne out by (p, p') , (γ, γ') , and (e, e') experiments that determine the spin and convection currents in $M1$ transitions, in which g_A/g_V play no role (see Richter, 1995, for a complete review). An analysis of the data available for the $N=28$ isotones in terms of full pf -shell calculations concluded that agreement with experiment was achieved by quenching the $\sigma\tau$ operator by a factor 0.75(2), fully consistent with the value that explains the Gamow-Teller data (von Neumann-Cosel *et al.*, 1998; see Fig. 29). These results rule out the hypothesis of a renormalization of the axial-vector constant g_A ; it is the $\sigma\tau$ operator that is quenched.

VI. SPHERICAL SHELL-MODEL DESCRIPTION OF NUCLEAR ROTATIONS

Progress in the theory of the pf shell came in stages. The first theoretical study, by McCullen, Bayman, and Zamick (1964), restricted to the $f_{7/2}$ space, was a success, but had some drawbacks: The spectra were not always symmetric by interchange of particles and holes, and the quadrupole moments had systematically the wrong sign. The first diagonalizations in the full shell (Pasquini, 1976; Pasquini and Zuker, 1978) solved these problems to a large extent, but the very severe truncations necessary at the time made it impossible to treat the pairing and quadrupole forces on the same footing. The situation improved markedly when the pure two-body $f_{7/2}$ part of the Hamiltonian H_2 , was addressed perturbing with a three-body term H_{R1} , mostly due to the quadrupole force (Poves and Zuker, 1981b). The paper of Poves and Zuker ended with these words.

“It may well happen, that in some cases, not in the pf shell but elsewhere, H_{R1} will overwhelm H_2 . Then, and we are only speculating, we shall speak, perhaps, of the rotational coupling scheme.”
Indeed, some nuclei were indicating a willingness to

become rotational but could not quite make it, simply because the perturbative treatment was inadequate. The authors' statement fell short of being prophetic for lack of one extra condition: "not in the *pf* shell" should have been "not necessarily...".

At the time it was thought impossible to describe rotational motion in a spherical shell-model context. The glorious exception, discovered by Elliott (1958a 1958b) was (apparently) associated with strict SU(3) symmetry, approximately realized only near ^{20}Ne and ^{24}Mg .

A. Rotors in the *pf* shell

A new stage in *pf*-shell theory began when the ANTOINE code (Sec. III.D) came into operation. Simulations using this code established that ^{48}Cr was definitely a well-deformed rotor (Caurier, Zuker, *et al.*, 1994). This is borne out by a comparison of the results of Caurier, Zuker, *et al.* (1994) with the experimental spectrum of Lenzi *et al.* (1996) in Fig. 30 (see also Cameron *et al.*, 1993) and the transition properties in Table VI from Brandolini *et al.* (1998), where we have used

$$Q_0(s) = \frac{(J+1)(2J+3)}{3K^2 - J(J+1)} Q_{\text{spec}}(J), \quad K \neq 1, \quad (87)$$

$$B(E2, J \rightarrow J-2) = \frac{5}{16\pi} e^2 |\langle JK20 | J-2, K \rangle|^2 Q_0(t)^2, \quad K \neq 1/2, 1 \quad (88)$$

to establish the connection with the intrinsic frame descriptions: A good rotor must have a nearly constant Q_0 , which is the case up to $J=10$; then ^{48}Cr backbends. Such a behavior had earlier been thought to occur only in much heavier nuclei.

Figure 31 compares the experimental patterns with those obtained with KB3 and with the Gogny force. The latter, when diagonalized, gives surprisingly good results. When treated in the cranked Hartree-Fock-Bogoliubov (HFB) approximation, the results are not so good. The discrepancy is more apparent than real: The predictions for the observables are very much the same in both cases (see Caurier, Egido, *et al.*, 1995, for the details). The reason is given in Fig. 32, where exact KB3 diagonalizations are done, subtracting either of the two pairing contributions, $JT=01$ or 10 (Poves and Martínez-Pinedo, 1998). It is apparent that the subtracted $JT=01$ pattern is quite close to the cranked HFB one in Fig. 31, especially in the rotational regime before the backbend. The $JT=10$ subtraction goes in the same direction. The interpretation is clear: the cranked HFB approximation does not "see" proton-neutron pairing at all, and it is not very efficient in the low-pairing regime. As it does everything else very well, the inevitable conclusion is that pairing can be treated in first-order perturbation theory, i.e., the energies are very sensitive to it, but not the wave functions. Floods of ink have gone into discussing neutron-proton pairing, which is a problem for mean-field theories but not for the Gogny force or the shell

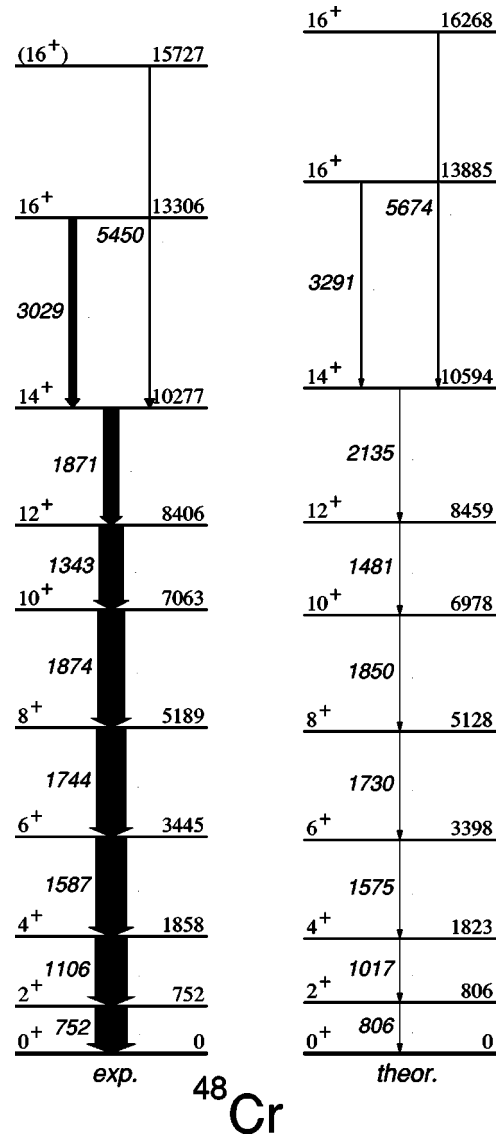


FIG. 30. ^{48}Cr level scheme: experiment (Lenzi *et al.*, 1996) vs shell-model results using the interaction KB3.

model. Furthermore, the results show that ordinary pairing is also a mean-field problem when nuclei are not superfluids.

^{48}Cr has become a benchmark for models of *pf*-shell rotors. The models proposed to date include the cranked

TABLE VI. ^{48}Cr ; quadrupole properties of the yrast band.

J	$B(E2)_{\text{expt}}$	$B(E2)_{\text{theor}}$	$Q_0(t)$	$Q_0(s)$	$Q_0(t)[f7/2, p3/2]$
2	321(41)	228	107	103	104
4	330(100)	312	105	108	104
6	300(80)	311	100	99	103
8	220(60)	285	93	93	102
10	185(40)	201	77	52	98
12	170(25)	146	65	12	80
14	100(16)	115	55	13	50
16	37(6)	60	40	15	40

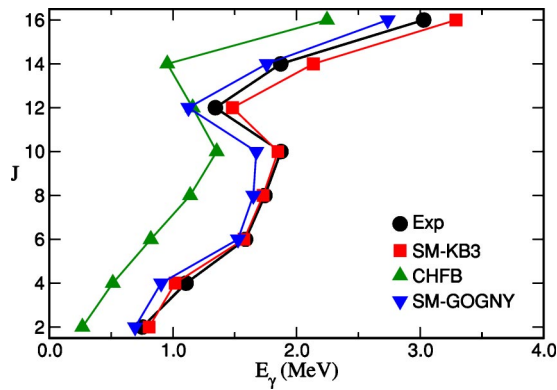


FIG. 31. (Color in online edition) The yrast band of ^{48}Cr : experiment vs the shell-model calculations with KB3 and the Gogny force, and the cranked Hartree-Fock-Bogoliubov results with the Gogny force.

HFB (Caurier, Egido, *et al.*, 1955), cranked Nilsson-Strutinsky (Juodagalvis and Åberg, 1998), projected shell model (Hara *et al.*, 1999), cluster model (Descouvemont, 2002), and others. Nuclei in the vicinity also have strong rotational features. The mirror pairs ^{47}V - ^{47}Cr and ^{49}Cr - ^{49}Mn closely follow the semiclassical picture of a particle or hole-hole strongly coupled to a rotor (Martínez-Pinedo *et al.*, 1997) in full agreement with the experiments (Cameron *et al.*, 1991, 1994; O’Leary *et al.*, 1997; Bentley *et al.*, 1998; Tonev *et al.*, 2002). ^{50}Cr was predicted to have a second backbending by Martínez-Pinedo, Poves, Robledo, *et al.* (1996). This has been confirmed experimentally (Lenzi *et al.*, 1997; see Fig. 33). When more particles or holes are added, the collective behavior fades, though even for ^{52}Fe , a rotorlike band appears at low spin with an yrast trap at $J=12^+$; both are accounted for by the shell-model calculations (Poves and Zuker, 1981b; Ur *et al.*, 1998). For spectroscopic comparisons with the odd-odd nuclei, see Brandolini *et al.* (2001) and Lenzi *et al.* (1999) for ^{46}V ; see Svensson *et al.* (1998) for ^{50}Mn . Recently, a highly deformed excited

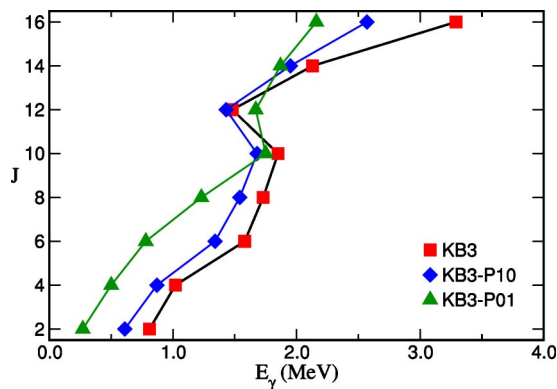


FIG. 32. (Color in online edition) Gamma-ray energies along the yrast band of ^{48}Cr (in MeV): KB3, full interaction; KB3-P10, KB3 with isoscalar pairing retired; KB3-P01, KB3 with isovector pairing retired. Adapted from Poves and Martínez-Pinedo, 1998.

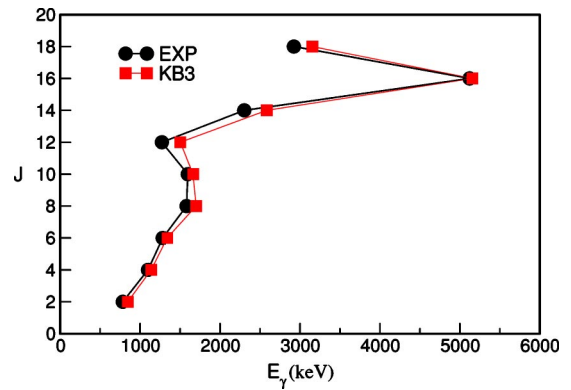


FIG. 33. (Color in online edition) The yrast band of ^{50}Cr : experiment (Lenzi *et al.*, 1997) vs the shell-model calculation with the KB3 interaction.

band has been discovered in ^{56}Ni (Rudolph *et al.*, 1999). It is dominated by the configuration $(1f_{7/2})^{12} (2p_{3/2}, 1f_{5/2}, 2p_{1/2})^4$. The calculations reproduce the band, which starts at about 5-MeV excitation energy and has a deformation close to $\beta=0.4$.

B. Quasi-SU(3)

To account for the appearance of backbending rotors, a theoretical framework was developed by Zuker *et al.* (1995) and made more precise by Martínez-Pinedo *et al.* (1997). Here we give a brief overview of the scheme, which will be shown to apply even to the classic examples of rotors in the rare-earth region.

Let us start by considering the quadrupole force alone, taken to act in a single oscillator shell, say, the p th. It will tend to maximize the quadrupole moment, which requires filling the lowest orbits obtained by diagonalizing the operator $Q_0=2q_{20}=2z^2-x^2-y^2$. Using the Cartesian representation, $2q_{20}=2n_z-n_x-n_y$, we find eigenvalues $2p, 2p-3, \dots$, etc., as shown in the left panel of Fig. 34, where spin has been included. By filling the

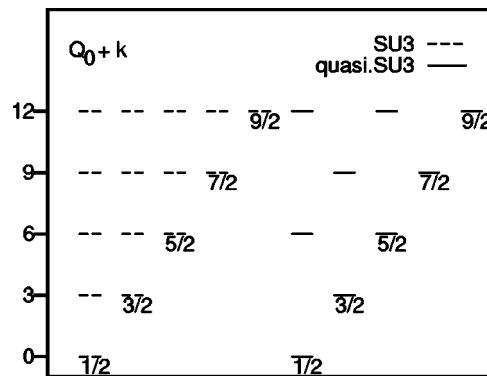


FIG. 34. Single-particle quadrupole moments of the Nilsson orbits of the SU(3) and quasi-SU(3) Hamiltonians. The quadrupole moment of the lowest orbit is $Q_0=-2p$ for SU(3) and $Q_0=-2p+1/2$ for quasi-SU(3) in units of the oscillator parameter b^2 ; p is the principal quantum number of the shell. Adapted from Zuker *et al.*, 1995.

orbits in order we obtain the intrinsic states for the lowest SU(3) representations (Elliott, 1958a, 1958b)— $(\lambda, 0)$ if all states are occupied up to a given level and (λ, μ) otherwise. For instance, putting two neutrons and two protons into the $K=1/2$ level leads to the $(4p, 0)$ representation. For four neutrons and four protons, the filling is not complete and we have the (triaxial) $(8(p-1), 4)$ representation for which we expect a low-lying γ band.

In jj coupling the angular part of the quadrupole operator $q^{20}=r^2C^{20}$ has matrix elements

$$\langle jm|C^2|j+2m\rangle \approx \frac{3[(j+3/2)^2 - m^2]}{2(2j+3)^2}, \quad (89)$$

$$\langle jm|C^2|j+1m\rangle = -\frac{3m[(j+1)^2 - m^2]^{1/2}}{2j(2j+2)(2j+4)}. \quad (90)$$

The $\Delta j=2$ numbers in Eq. (89) are—within the approximation made—identical to those in the LS scheme, obtained by replacing j by l . The $\Delta j=1$ matrix elements in Eq. (89) are small, for both large and small m , corresponding to the lowest oblate and prolate deformed orbits, respectively. If the spherical j orbits are degenerate, the $\Delta j=1$ couplings, though small, will mix strongly the two $\Delta j=2$ sequences, e.g., $(f_{7/2}p_{3/2})$ and $(f_{5/2}p_{1/2})$. The spin-orbit splittings will break the degeneracies and favor the decoupling of the two sequences. Hence the idea (Zuker *et al.*, 1995) of neglecting the $\Delta j=1$ matrix elements and exploiting the correspondence,

$$l \rightarrow j = l + 1/2, \quad m \rightarrow m + 1/2 \times \text{sgn}(m),$$

which is one-to-one except for $m=0$. The resulting “quasi-SU(3)” quadrupole operator respects SU(3) relationships, except for $m=0$, where the correspondence breaks down. The resulting spectrum for quasi- $2q_{20}$ is shown in the right panel of Fig. 34. The result is not exact for the $K=1/2$ orbits but a very good approximation.

To check the validity of the decoupling, a Hartree calculation was done for $H = \varepsilon H_{sp} + H_q$, where H_{sp} is the observed single-particle spectrum in ^{41}Ca (essentially equidistant orbits with 2-MeV spacings) and H_q is the quadrupole force in Eq. (34) with a properly renormalized coupling. The result is exactly a Nilsson (1955) calculation (Martínez-Pinedo *et al.*, 1997),

$$H_{\text{Nilsson}} = \hbar\omega \left(\varepsilon H_{sp} - \frac{\delta}{3} 2q_{20} \right), \quad (91)$$

where

$$\frac{\delta}{3} = \frac{1}{4} \frac{\langle 2q_{20} \rangle}{\langle r^2 \rangle} = \frac{\langle 2q_{20} \rangle}{(p+3/2)^4}. \quad (92)$$

In the lower panel of Fig. 35 the results are given in the usual form.

In the upper panel we have turned the representation around: since we are interested in rotors, we start from perfect ones [SU(3)] and let ε increase. At a value of ≈ 0.8 the four lowest orbits are in the same sequence as on the right side of Fig. 34. (Remember here that the

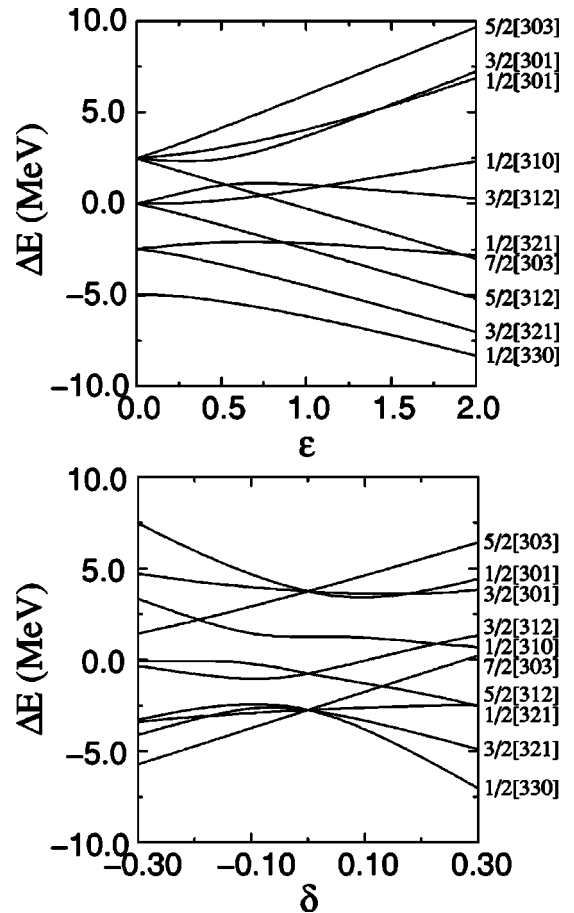


FIG. 35. Nilsson diagrams in the pf shell: upper panel, energy vs single-particle splitting ε ; lower panel, energy vs deformation δ . Adapted from Martínez-Pinedo *et al.*, 1997.

real situation corresponds to $\varepsilon \approx 1.0$.) The agreement even extends to the next group, although now there is an intruder ($1/2[310]$ orbit). The suggestion is confirmed by an analysis of the wave functions. For the lowest two orbits, the overlaps between the pure quasi-SU(3) wave functions calculated in the restricted $\Delta j=2$ space (fp from now on) and those in the full pf shell exceed 0.95 throughout the interval $0.5 < \varepsilon < 1$. More interesting still: the contributions to the quadrupole moments from these two orbits vary very little and remain close to the values obtained at $\varepsilon=0$, as shown in Fig. 34.

We have learned that—for the rotational features—calculations in the restricted $(fp)^n$ spaces account remarkably well for the results in the full major shell $(pf)^n$ (see the last column of Table VI). Let us move now to larger spaces. In Fig. 36 we have yrast transition energies for different configurations of eight particles in $\Delta j=2$ spaces. The force is that of Kahana, Lee, and Scott, $\hbar\omega = 9$ MeV, the single-particle splittings are uniform at $\varepsilon = 1$ MeV, and gds , say, is the lower sequence in the sdg , $p=4$, shell. Rotational behavior is fair to excellent at low J . As expected from the normalization property of the realistic quadrupole force [Eq. (36)] the moments of inertia in the rotational region go as $(p+3/2)^2(p'+3/2)^2$, i.e., if we multiply all the E_γ values by this factor, the

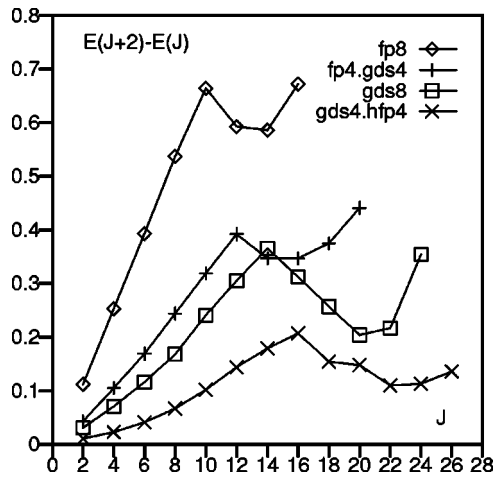


FIG. 36. Yrast transition energies $E_\gamma = E(J+2) - E(J)$ for different configurations, with the Kahana-Lee-Scott interaction. Adapted from Zuker *et al.*, 1995.

lines become parallel. The intrinsic quadrupole moment Q_0 [Eq. (87)] remains constant to within 5% up to a critical J value at which the bands backbend.

Why and how do the bands backbend? We have no simple answer, but Fig. 37 from Velázquez and Zuker (2002) shows the behavior of the $(gds)^8$ space under the influence of a symmetric random interaction, gradually made more attractive by an amount a . The similarity with Fig. 36 is clear. The appearance of backbending rotors seems to be a general result of the competition between deformation and alignment, characteristic of nuclear processes.

The group-theoretical aspects of quasi-SU3 have been recently discussed and applied to the description of the sd -shell nuclei by Vargas, Hirsch, and Draayer (2001, 2002a).

C. Heavier nuclei: Quasi+pseudo SU(3)

We have seen that quasi-SU(3) is a variant of SU(3) that obtains for moderate spin-orbit splittings. For other

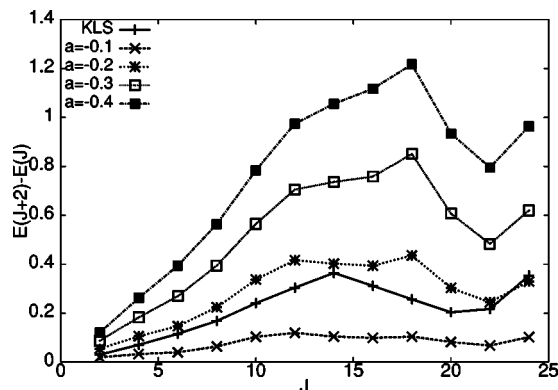


FIG. 37. Backbending patterns in the configuration $(gds)^8$ $T=0$, with the Kahana-Lee-Scott interaction and with a random interaction plus a constant $W_{rstu}^{JT} = -a$. From Velázquez and Zuker, 2002.

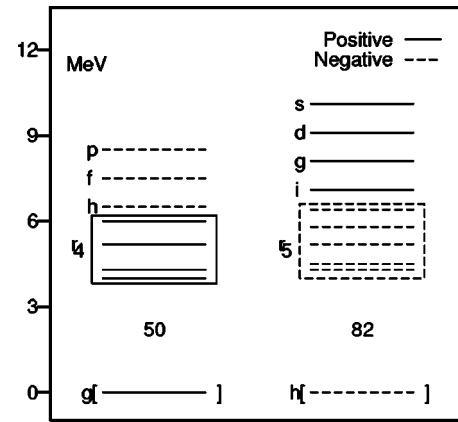


FIG. 38. Schematic single-particle spectrum above ^{132}Sn . Here r_p is the set of orbits in shell p excluding the largest. For the upper shells the label l is used for the orbits $j=l+1/2$. Adapted from Zuker *et al.*, 1995.

forms of single particle spacings, the pseudo-SU(3) scheme (Arima *et al.*, 1969; Hecht and Adler, 1969; Raju *et al.*, 1973; see also Vargas *et al.*, 2002b, for more recent applications) will be favored (in which case we have to use the left panel of Fig. 34, with pseudo- $p=p-1$). Other variants of SU(3) may be possible and are well worth exploring. In cases of truly large deformation SU(3) itself may be valid in some blocks.

To see how this works, consider Fig. 38 giving a schematic view of the single-particle energies in the space of two contiguous major shells—in protons (π) and neutrons (ν)—adequate for a shell-model description of the rare-earth region.

We want to estimate the quadrupole moments for nuclei at the onset of deformation. We shall assume quasi-SU(3) operates in the upper shells, and pseudo-SU(3) in the lower ones. The number of particles in each shell for which the energy will be lowest will depend on a balance of monopole and quadrupole effects, but Nilsson diagrams suggest that, when nuclei acquire stable deformation, two orbits $K=1/2$ and $3/2$ —originating in the upper shells of Fig. 38—become occupied, i.e., the upper blocks are precisely the eight-particle configurations we have studied at length. Their contribution to the electric quadrupole moment is then

$$Q_0 = 8[e_\pi(p_\pi - 1) + e_\nu(p_\nu - 1)], \quad (93)$$

with $p_\pi=5$, $p_\nu=6$; e_π and e_ν are the effective charges.

Consider even-even nuclei with $Z=60-66$ and $N=92-98$, corresponding to six to ten protons with pseudo- $p=3$, and six to ten neutrons with pseudo- $p=4$ in the lower shells. From the left side of Fig. 34 we obtain easily their contribution to Q_0 , which added to that of Eq. (93) yields a total

$$Q_0 = 56e_\pi + (76 + 4n)e_\nu, \quad (94)$$

for $^{152+2n}\text{Nd}$, $^{154+2n}\text{Sm}$, $^{156+2n}\text{Gd}$, and $^{158+2n}\text{Dy}$, respectively. At fixed n , the value is constant in the four cases because the orbits of the triplet $K=1/2, 3/2, 5/2$ in Fig. 34 have zero contribution for $p=3$. Q_0 (given in dimen-

TABLE VII. $B(E2) \uparrow$ in e^2b^2 compared with experiment (Raman *et al.*, 1989).

N	Nd	Sm	Gd	Dy
92	4.47	4.51	4.55	4.58
	2.6(7)	4.36(5)	4.64(5)	4.66(5)
94	4.68	4.72	4.76	4.80
			5.02(5)	5.06(4)
96	4.90	4.95	4.99	5.03
			5.25(6)	5.28(15)
98	5.13	5.18	5.22	5.26
				5.60(5)

sionless oscillator coordinates, i.e., $r \rightarrow r/b$ with $b^2 \approx 1.01A^{-1/3} \text{ fm}^2$, is related to the $E2$ transition probability from the ground state by $B(E2) \uparrow = 10^{-5} A^{2/3} Q_0^2$. The results, using effective charges of $e_\pi = 1.4$, $e_\nu = 0.6$ calculated by Dufour and Zuker (1996), are compared in Table VII with the available experimental values. The agreement is quite remarkable, and no free parameters are involved. Note in particular the quality of the prediction of constancy (or rather $A^{2/3}$ dependence) at fixed n , which does not depend on the choice of effective charges. The discrepancy in ^{152}Nd is likely to be of experimental origin, since systematics indicate, with no exception, much larger rates for a 2^+ state at such low energy (72.6 keV). It can be seen that by careful analysis of exact results one may arrive at very simple computational strategies. In the last example on $B(E2)$ rates, the simplicity is such that the computation reduces to a couple of sums.

D. The ^{36}Ar and ^{40}Ca superdeformed bands

The arguments sketched above apply to the region around ^{16}O , where a famous four-particle—four-hole ($4p-4h$) band starting at 6.05 MeV was identified by Carter *et al.* (1964), followed by an $8p-8h$ band starting at 16.75 MeV (Chevallier *et al.*, 1967). Shell-model calculations in a very small space, $p_{1/2}d_{5/2}s_{1/2}$, could account for the spectroscopy in ^{16}O , including the $4p-4h$ band (Zuker *et al.*, 1968), but the $8p-8h$ one requires at least three major shells and was tackled by an α -cluster model (Abgrall, Baron, *et al.*, 1967; Abgrall, Caurier, and Monsonogo, 1967). It is probably the first superdeformed band detected and explained.

In ^{40}Ca , the first excited 0^+ state is the $4p-4h$ bandhead. It is only recently that another low-lying highly deformed band has been found (Ideguchi *et al.*, 2001), following the discovery of a similar structure in ^{36}Ar (Svensson *et al.*, 2000).

By applying the quasi+pseudo-SU(3) recipes of Sec. VI.C we find that the maximum deformations attainable are of $8p-8h$ character in ^{40}Ca and $4p-4h$ in ^{36}Ar with $Q_0 = 180 e \text{ fm}^2$ and $Q_0 = 136 e \text{ fm}^2$, respectively.

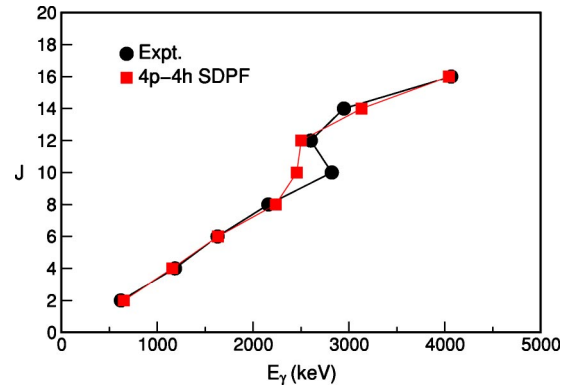


FIG. 39. (Color in online edition) The superdeformed band of ^{36}Ar ; experimental γ -ray energies as a function of J (Svensson *et al.*, 2000) vs shell-model result in the space of the $4p-4h$ configurations, with the SDPF-SM interaction.

The natural generalization of the Zuker-Buck-McGrory space consists in the $d_{3/2}s_{1/2}f_{7/2}p_{3/2}$ orbits, which keeps the space relatively free of center-of-mass spuriousness. And indeed, it describes well the rotational regime of the observed bands. However, to track them beyond the backbend, it is convenient to increase the space to $d_{3/2}s_{1/2}pf$. The adopted interaction, SDPF-SM, is the restriction to this valence space of the interaction originally constructed by Retamosa *et al.* (1997) and used by Caurier *et al.* (1998). It consists of the universal sd and KB3 interactions for the intrashell sd - and pf -shell matrix elements and the Kahana-Lee-Scott interaction for the cross-shell sd and pf matrix elements, plus the monopole adjustments dictated by new data on the single-particle structure of ^{35}Si from Nummela, Baumann, *et al.* (2001; SDPF-NR). SDPF-SM incorporates the modifications to the single-particle energies and the cross-shell monopoles needed to reproduce ^{29}Si and the evolution of the n -particle– n -hole states in the $N=Z$ nuclei.

The calculations are conducted in spaces of a fixed number of particles and holes. In Fig. 39 the calculated energy levels in ^{36}Ar are compared to the data. The agreement is excellent, except at $J=12$, where the data show a clear backbending, while the calculation produces a much smoother upbending pattern.

In Table VIII the calculated spectroscopic quadrupole moments (Q_s) and the $B(E2)$'s are used to compute the intrinsic Q as in Eqs. (87) and (88), using standard effective charges $\delta q_\pi = \delta q_\nu = 0.5$. As expected, both $Q_0(s)$ and $Q_0(t)$ are nearly equal and constant—and close to the quasi+pseudo-SU(3) estimate—up to the backbend. The calculated $B(E2)$'s agree well with the experimental ones (Svensson *et al.*, 2001). The value of Q_0 corresponds to a deformation $\beta \approx 0.5$.

Now we examine the $8p-8h$ band in ^{40}Ca (Ideguchi *et al.*, 2001). The valence space adopted for ^{36}Ar is truncated by limiting the maximum number of particles in the $1f_{5/2}$ and $2p_{1/2}$ orbits to two.

TABLE VIII. Quadrupole properties of the $4p$ - $4h$ configuration's yrast-band in ^{36}Ar (in $e^2 \text{ fm}^4$ and $e \text{ fm}^2$).

J	$B(E2)(J \rightarrow J-2)$		Q_{spec}	$Q_0(s)$	$Q_0(t)$
	Expt.	Theor.			
2		315	-36.0	126	126
4	372(59)	435	-45.9	126	124
6	454(67)	453	-50.7	127	120
8	440(70)	429	-52.8	125	114
10	316(72)	366	-52.7	121	104
12	275(72)	315	-53.0	119	96
14	232(53)	235	-54.3	120	82
16	>84	131	-56.0	122	61

The experimental (Ideguchi *et al.*, 2001) and calculated yrast gamma-ray energies are compared in Fig. 40. The patterns agree reasonably well but the change of slope at $J=10$ —where the backbend in ^{48}Cr starts (Fig. 31)—is missed by the calculation, which only backbends at $J=20$, the band termination for the configuration $f_{7/2}^8(d_{3/2}s_{1/2})^{-8}$. The extra collectivity induced by the presence of sd particles in pseudo-SU(3) orbitals is responsible for the delay in alignment, but it is apparently too strong to allow for the change in slope at $J=10$.

The experimental $Q_0(t)=180_{-29}^{+39}$ obtained from the fractional Doppler shifts corresponds to a deformation $\beta \approx 0.6$ (Ideguchi *et al.*, 2001). It is extracted from an overall fit that assumes constancy for all measured values and corresponds exactly to the quasi+pseudo-SU(3) estimate. It also squares well with the calculated $172 e \text{ fm}^2$ in Table IX, where the steady decrease in collectivity remains consistent with experiment within the quoted uncertainties. A reanalysis of the experimental lifetimes in the superdeformed band of ^{40}Ca (Chiara *et al.*, 2003) suggests that for low spins the deformation would be smaller, due to mixing with less deformed states of lower np-nh rank.

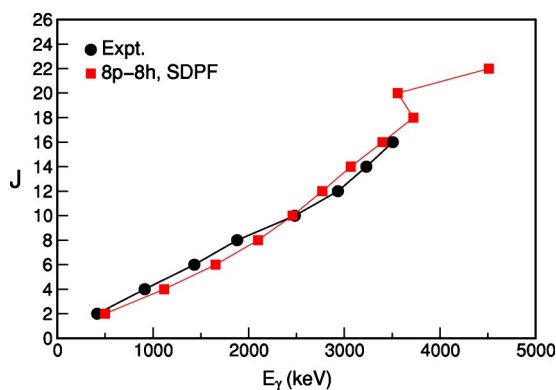


FIG. 40. (Color in online edition) The superdeformed band in ^{40}Ca ; experimental γ -ray energies as a function of J (Ideguchi *et al.*, 2001) vs shell-model result in the space of the $8p$ - $8h$ configurations, with the SDPF-SM interaction.

TABLE IX. Quadrupole properties of the $8p$ - $8h$ configuration's yrast-band in ^{40}Ca (in $e^2 \text{ fm}^4$ and $e \text{ fm}^2$), calculated in the $sdpf$ valence space.

J	$B(E2)(J \rightarrow J-2)$	Q_{spec}	$Q_0(t)$	$Q_0(s)$
2	589	-49.3	172	172
4	819	-62.4	170	172
6	869	-68.2	167	171
8	860	-70.9	162	168
10	823	-71.6	157	164
12	760	-71.3	160	160
14	677	-71.1	149	157
16	572	-72.2	128	158
18	432	-75.0	111	162
20	72	-85.1		
22	8	-79.1		
24	7	-81.5		

This calculation demonstrates that a detailed description of very deformed bands is within reach of the shell model. The next step consists in remembering that states at a fixed number of particles are doorways that will fragment in an exact calculation, which remains to be done.

The band in ^{36}Ar has also been described with the projected shell model by Long and Sun (2001). Methods beyond the mean field using the Skyrme interaction, have recently been applied to both the ^{36}Ar and the ^{40}Ca superdeformed bands by Bender, Flocard, and Heenen (2003).

E. Rotational bands of unnatural parity

The occurrence of low-lying bands of opposite parity to the ground-state band is very frequent in pf shell nuclei. Their simplest characterization is as particle-hole bands with the hole in the $1d_{3/2}$ orbit. In a nucleus whose ground state is described by the configurations $(pf)^n$ the opposite-parity intruders will be $(1d_{3/2})^{-1} (pf)^{n+1}$. The promotion of a particle from the sd to the pf shell costs an energy equivalent to the local value of the gap, which in this region is about 7 MeV. On the other side, the presence of one extra particle in the pf shell may produce an important increase of the correlation energy, which can compensate for the energy lost by the particle-hole jump. For instance, the very-low-lying positive parity band of ^{47}V can be interpreted as $(1d_{3/2})^{-1} (pf)^8$ ($T=0$). Indeed, the correlation energy of this pseudo ^{48}Cr is larger than the correlation energy of the ground state of ^{47}V and even larger than the correlation energy of the real ^{48}Cr , explaining why the band starts at only 260 keV of excitation energy (Poves and Sánchez Solano, 1998). The most extreme case is ^{45}Sc , where the intruder band based in the configuration $(1d_{3/2})^{-1}$ coupled to ^{46}Ti , barely misses (by just 12 keV) becoming the ground state. Many bands of this

type have been experimentally studied in recent years, mainly at the GASP and EUROBALL detectors (Brandolini *et al.*, 1999) and explained by shell-model calculations (Brandolini, Marginean, *et al.*, 2002).

VII. DESCRIPTION OF VERY NEUTRON-RICH NUCLEI

The study of nuclei lying far from the valley of stability is one of the most active fields in today's experimental nuclear physics. What is necessary to know specifically about these nuclei, from a shell-model point of view? As everywhere else, it is the model space and the monopole behavior of the interaction. They go together because the effective single-particle energies (see Sec. V) depend on occupancies, which in turn depend on the model space.

In broad terms, the specificity of light and medium neutron-rich nuclei is that the EI closures (corresponding to the filling of the $p+1/2$ orbit of each oscillator shell) take over as boundaries of the model spaces. As discussed in Sec. II.B.3, the harmonic-oscillator closures may be quite solid for doubly magic nuclei, but they become vulnerable in the semimagic cases.

For instance, the $d_{3/2}$ - $f_{7/2}$ neutron gap in ^{40}Ca of ≈ 7 MeV goes down to ≈ 2.5 MeV around ^{28}O . Since the $d_{5/2}$ orbit is well below its sd partners, now quite close to $f_{7/2}$, the natural model space is no longer the sd shell, but the EI space bounded by the $N=14$ and 28 closures, supplemented by the $p_{3/2}$ subshell whenever the $p_{3/2}$ - $f_{7/2}$ gap becomes small. From ≈ 6 MeV in ^{56}Ni , it drops to ≈ 4.5 MeV in ^{48}Ca , then ≈ 2 MeV in ^{40}Ca , and finally ≈ 0 MeV in ^{28}Si . As explained at the end of Sec. II.B.3, this monopole drift provides direct evidence for the need of three-body mechanisms.

For the p shell, the situation is similar; the imposing 11.5 MeV $p_{1/2}$ - $d_{5/2}$ gap in ^{16}O is down to some 3 MeV in ^{12}C . The monopole drift of the $s_{1/2}$ - $d_{5/2}$ gap brings it from about 8 MeV in ^{28}Si to nearly -1 MeV in ^{12}C . According to Ostuka, Fujimoto, *et al.* (2001) the drift may well continue. In ^8He , the $s_{1/2}$ - $p_{1/2}$ bare gap is estimated at 0.8 MeV.

All the numbers above (except the last) are experimental. The bare monopole values are smaller because correlations substantially increase the value of the gaps, but they do not qualitatively change the strong monopole drifts. Their main consequence is that “normal” states, i.e., those described by $0\hbar\omega$ p or sd calculations, often coexist with intruders that involve promotion to the next oscillator shell. Let us examine how this happens.

A. $N=8$: ^{11}Li , halos

The $1/2^+$ ground state in ^{11}Be provided one of the first examples of intrusion. The expected $0\hbar\omega$ normal state lies 300 keV higher. The explanation of this behavior has varied with time (Talmi and Unna, 1960; Sagawa *et al.*, 1993; Suzuki and Otsuka, 1994; Auman *et al.*, 2001; see

also Brown, 2001 for a recent review and Suzuki *et al.*, 2003 for a new multi- $\hbar\omega$ calculation), but the idea has remained unchanged. The normal state corresponds to a hole on the $N=8$ closure. The monopole loss of promoting a particle to the sd shell is compensated by a pairing gain for the $p_{1/2}^{-2}$ holes. A quadrupole gain due to the interaction of the sd neutron with the p^2 protons is plausible but becomes questionable when we note that the same phenomenon occurs in ^9He , which has no p^2 particles, suggesting the need for a further reduction of the monopole loss (Otsuka, Fujimoto, *et al.*, 2001).

The interest in ^{11}Be —as a “halo” nucleus—was revived by the discovery of the remarkable properties of ^{11}Li , which sits at the drip line (≈ 200 keV two-neutron separation energy) and has a very large spatial extension, due to a neutron halo (Tanihata *et al.*, 1985; Hansen and Jonson, 1987).

The shell model has no particular problem with halo nuclei, whose large size is readily attributed to the large size of the $s_{1/2}$ orbit. As shown by Kahana *et al.* (1969a) the use of Woods-Saxon wave functions affects the matrix elements involving this orbit, but the uncertainties involved are easily absorbed by the monopole field. As a

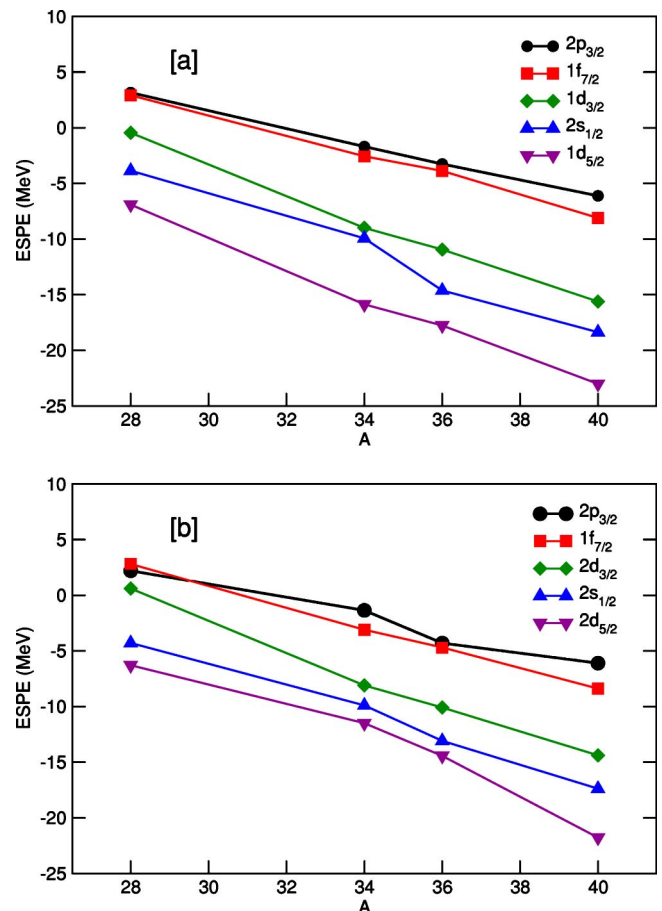


FIG. 41. (Color in online edition) Effective single-particle energies (in MeV) at $N=20$ from ^{28}O ($A=28$) to ^{40}Ca ($A=40$): (a) obtained with the SDPF-NR interaction; (b) obtained with the interaction of the Tokyo group (Utsuno *et al.*, 1999). Adapted from Caurier, Nowacki, and Poves, 2002.

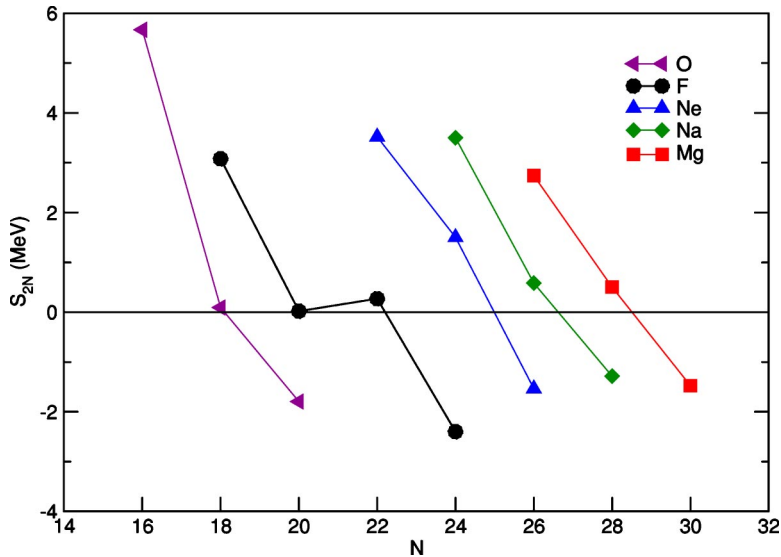


FIG. 42. (Color in online edition) Two-neutron separation energies of the neutron-rich isotopes of oxygen, fluorine, neon, sodium, and magnesium, calculated with the SDPF-NR interaction. Adapted from Caurier, Nowacki, and Poves, 2002.

consequence, the whole issue hinges on the $s_{1/2}$ contribution to the wave functions, which is sensitively detected by the β decay to the first excited $1/2^-$ state in ^{11}Be . Borge *et al.* (1997) showed that calculations producing a 50% split between the neutron closed shell and the $s_{1/2}^2 p_{1/2}^{-2}$ configuration lead to the right lifetime. This result was confirmed by Simon *et al.* (1999). Further confirmation came from Navin *et al.* (2000), with solid indications that the supposedly semimagic ^{12}Be ground state is dominated by the same $s_{1/2}^2 p_{1/2}^{-2}$ configuration.

B. $N=20$: ^{32}Mg , deformed intruders

In the mid 1970s it was the sd shell that attracted the most attention. Nobody seemed to remember ^{11}Be , and everybody (including the authors of this review active at the time) were enormously surprised when a classic experiment by Thibault *et al.* (1975) established that the mass and β -decay properties of the ^{31}Na ground state—

expected to be semimagic at $N=20$ —could not possibly be those of a normal state (Wildenthal and Chung, 1979). The next example of a frustrated semimagic was ^{32}Mg (Detraz *et al.*, 1979). Early mean-field calculations had interpreted the discrepancies as due to deformation (Campi *et al.*, 1975) but the experimental confirmation took some time (Guillemaud-Mueller *et al.*, 1984; Klotz *et al.*, 1993; Motobayashi *et al.*, 1995).

Exploratory shell-model calculations by Storm *et al.* (1983), including the $1f_{7/2}$ orbit in the valence space, were able to improve the mass predictions; however, deformation was still absent. To obtain deformed solutions demanded the inclusion of the $2p_{3/2}$ orbit, as demonstrated by Poves and Retamosa (1987). These calculations were followed by many others (Warburton *et al.*, 1990; Heyde and Woods, 1991; Fukunishi *et al.*, 1992; Poves and Retamosa, 1994; Otsuka and Fukunishi, 1996; Dean *et al.*, 1999; Siiskonen *et al.*, 1999), which mapped an *island of inversion*, i.e., a region where the intruder

TABLE X. Properties of the even magnesium isotopes. N stands for normal and I for intruder. Energies in MeV, $B(E2)$'s in $e^2 \text{fm}^4$, and Q 's in $e \text{fm}^2$.

	^{30}Mg			^{32}Mg			^{34}Mg		
	N	I	Expt.	N	I	Expt.	N	I	Expt.
$\Delta E(0_1^+)$		+3.1			-1.4			+1.1	
0^+	0.0	0.0		0.0	0.0		0.0	0.0	
2^+	1.69	0.88	1.48	1.69	0.93	0.89	1.09	0.66	0.67
4^+	4.01	2.27		2.93	2.33	(2.29)	2.41	1.86	2.13
6^+	6.82	3.75		9.98	3.81		3.52	3.50	
$B(E2)$									
$2^+ \rightarrow 0^+$	53	112	59(5)	36	98	90(16)	75	131	126(25)
$4^+ \rightarrow 2^+$	35	144		17	123		88	175	
$6^+ \rightarrow 4^+$	23	140		2	115		76	176	
$Q_{\text{spec}}(2^+)$	-12.4	-19.9		-11.4	-18.1		-15.4	-22.7	

TABLE XI. $N=28$ isotones: quasiparticle neutron gaps, difference in correlation energies between the $2p-2h$ and the $0p-0h$ configurations and their relative position.

	^{40}Mg	^{42}Si	^{44}S	^{46}Ar	^{48}Ca	^{50}Ti	^{52}Cr	^{54}Fe	^{56}Ni
Gap	3.35	3.50	3.23	3.84	4.73	5.33	5.92	6.40	7.12
ΔE_{Corr}	8.45	6.0	6.66	5.98	4.08	7.59	10.34	10.41	6.19
E_{2p-2h}^*	-1.75	1.0	-0.2	1.7	5.38	3.07	1.50	2.39	8.05

configurations are dominant in the ground states. The detailed contour of this island depends strongly on the behavior of the effective single-particle energies, in turn dictated by the monopole Hamiltonian. Let us recall that, according to what we have learned in Sec. VI.B, the configurations $(d_{5/2}s_{1/2})_p^{2-4}(f_{7/2}p_{3/2})_n^{2-4}$, corresponding to $N=20$, $Z=10-12$, have a quasi-SU(3) quadrupole coherence close to that of SU(3), i.e., maximal.

The effective single-particle energies in Fig. 41 represent H_m for the SDPF-NR (Nummela, Baumann, *et al.*, 2001) and Tokyo group interactions (Utsuno *et al.*, 1999). These models are quite similar, and both favor deformation. Both interactions lead to an “island of inversion” for $Z=10, 11$, and 12 ; and $N=19, 20$, and 21 .

Consider now some detailed information obtained with the interaction SDPF-NR, described in Sec. VI.D, by Caurier, Nowacki, and Poves (2001, 2002). The S_{2N} values of Fig. 42 locate the neutron drip line, consistent with what is known for oxygen and fluorine, where the last bound isotopes are ^{24}O and ^{31}F (Sakurai *et al.*, 1999). Note the kink due to deformed correlations in the latter. For the other chains, the behavior is smoother and the last predicted bound isotopes are ^{34}Ne , ^{37}Na , and ^{40}Mg .

Some results for the even Mg isotopes ($N=18$, $N=20$, and $N=22$) are gathered in Table X. In ^{30}Mg the normal configuration is the one that agrees with the existing experimental data (Pritychenko *et al.*, 1999). In ^{32}Mg the situation is the opposite, as the experimental data—the 2^+ excitation energy (Guillemaud-Mueller *et al.*, 1984) and the $0^+ \rightarrow 2^+$ $B(E2)$ (Motobayashi *et al.*, 1995)—clearly prefer the intruder. A preliminary measure of the 4^+ excitation energy reported by Azaiez (1999) goes in the same direction. Data and calculations suggest prolate deformation with $\beta \approx 0.5$. In ^{34}Mg the normal configuration, which contains two pf neutrons, is already quite collective. It can be seen, in the table, that it resembles the ^{32}Mg ground state. The $4p-2h$ intruder is even more deformed ($\beta \approx 0.6$) and a better rotor. Results from the RIKEN experiments of Yoneda *et al.* (2000) and Iwasaki *et al.* (2001) seem to favor the intruder option. In the quantum Monte Carlo diagonalization calculations of Utsuno *et al.* (1999), the ground-state band is dominantly $4p-2h$; the 2^+ comes at the right place, but the 4^+ is too high. Clearly, ^{34}Mg is at the edge of the island of inversion. Another manifestation of the intruder presence in the region has been found at Isolde (Nummela, Nowacki, *et al.*, 2001): The decay of ^{33}Na indicates that the ground state of ^{33}Mg has $J^\pi=3/2^+$ instead of the expected $J^\pi=3/2^-$ or $J^\pi=7/2^-$. This inver-

sion is nicely reproduced by the SDPF-NR calculation.

C. $N=28$: Vulnerability

Let us return briefly to Fig. 41. The scale does not do justice to a fundamental feature—the drift of the $p_{3/2}-f_{7/2}$ gap, which decreases as protons are removed. As explained at the end of Sec. II.B.3, this behavior is contrary to a very general trend in heavier nuclei, and demands a three-body mechanism to resolve the contradiction. We recall that the oscillator closures are quite vulnerable, even at the strict monopole level. As we have seen, quadrupole coherence takes full advantage of this vulnerability. By contrast, the EI closures are very robust. However, because of the drift of the $p_{3/2}-f_{7/2}$ gap, even the $N=28$ closure becomes vulnerable. The

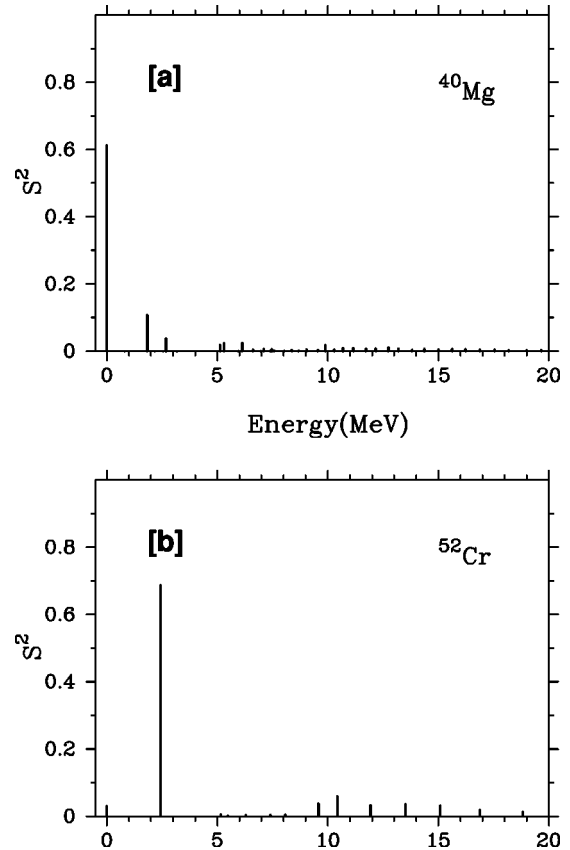


FIG. 43. Lanczos structure function of the $2p-2h$ 0^+ bandheads of (a) ^{40}Mg and (b) ^{52}Cr in the full $0\hbar\omega$ space. The bars give the square of the amplitude S of the bandhead in the physical state located at this energy.

TABLE XII. $N=28$ isotones: spectra, quadrupole properties, and occupancies.

	^{40}Mg	^{42}Si	^{44}S	^{46}Ar
$E^*(2^+)$ (MeV)	0.81	1.49	1.22	1.51
$E^*(4^+)$	2.17	2.68	2.25	3.46
$E^*(0_2^+)$	1.83	1.57	1.26	2.93
$Q(2^+)$ ($e\text{ fm}^2$)	-21	16	-17	20
$B(E2)$ ($e^2\text{ fm}^2$)	108	71	93	93
$\langle n_{7/2} \rangle$	5.54	6.16	6.16	6.91
$(f_{7/2})^{8\%}$	3	28	24	45

SPDF-NR interaction leads to a remarkable result summarized in Table XI: The decrease of the gap combined with the gain of correlation energy of the $2p$ - $2h$ leads to a breakdown of the $N=28$ closure for ^{44}S , ^{42}Si , and ^{40}Mg . Towards $N=Z$, ^{52}Cr and ^{54}Fe exhibit large correlation energies associated with the prolate deformed character of their $2p$ - $2h$ neutron configurations ($\beta \sim 0.3$).

When the $2p$ - $2h$ bandheads of ^{40}Mg and ^{52}Cr are allowed to mix in the full $0\hbar\omega$ space, using them as pivots in the Lanczos strength function procedure, they keep their identity to a large extent. This can be seen in Fig. 43, where we have plotted the strength functions of the $2p$ - $2h$ 0^+ states in the full space. In ^{40}Mg the $2p$ - $2h$ state represents 60% of the ground state, while in ^{52}Cr it is the dominant component (70%) of the first excited 0^+ . This is a very interesting illustration of the mechanism of intrusion; the intruder state is present in both nuclei, but it is only in the very neutron-rich one that it becomes the ground state.

Table XII gives an idea of the properties of the isotones in which configuration mixing is appreciable. In Fig. 44 we have plotted the low-energy spectra of the heaviest known sulfur isotopes. The agreement with the accumulated experimental results (see Glasmacher, 1988, for a recent review) is excellent and extends to the new data of Sohler *et al.* (2002). Analyzing their proton

occupancies we conclude that the rise in collectivity along the chain is correlated with the equal filling of the $d_{3/2}$ and $s_{1/2}$ orbitals (the $d_{5/2}$ orbital remains always nearly closed). The maximum proton collectivity is achieved when both orbitals are degenerate, which corresponds to the pseudo-SU(3) limit. For the neutrons, maximum collectivity occurs at $N=24$, the $f_{7/2}$ midshell. According to the calculation, ^{42}S is a prolate rotor with an incipient γ band. In ^{44}S the spherical and deformed configurations mix equally.

The $N=27$ isotones also reflect the regular transition from sphericity to deformation in their low-lying spectrum. The excitation energy of the $3/2^-$ state should be sensitive to the correlations and to the neutron gap. While in ^{47}Ca , it lies quite high (at around 2 MeV) due to the strong $f_{7/2}$ closure, in ^{45}Ar it appears at about 0.4 MeV. Concerning ^{43}S , the information comes from two recent experiments: the mass measurements at Ganil by Sarazin *et al.* (2000), which observed a low-lying isomer around 400-keV excitation energy, and the Michigan State University Coulex experiment of Ibbotson *et al.* (1999), which detected a strong $E2$ transition from the ground state to an excited state around 940 keV. According to our calculations, the ground state corresponds to the deformed configuration and has spin

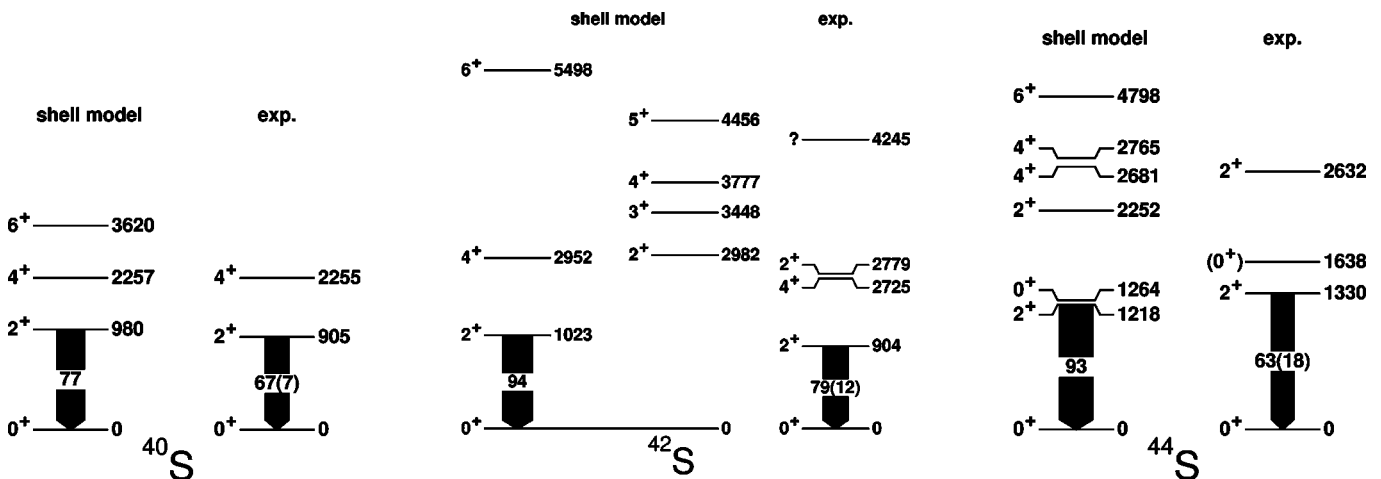


FIG. 44. Predicted level schemes of the heavy sulphur isotopes, compared with experiment (Sohler *et al.*, 2002). Energies in keV, $B(E2)$'s in $e^2\text{ fm}^4$.

TABLE XIII. 2_1^+ energies and $g_{9/2}$ intruder occupation in the nickel isotopic chain, from Sorlin *et al.*, 2002.

	^{62}Ni	^{64}Ni	^{66}Ni	^{68}Ni	^{70}Ni	^{72}Ni	^{74}Ni
$E(2^+)_{calc}$	1.11	1.24	1.49	1.73	1.50	1.42	1.33
$E(2^+)_{expt}$	1.173	1.346	1.425	2.033	1.259		
$B(E2\uparrow)_{calc}$	775	755	520	265	410	505	690
$\langle n_{9/2} \rangle$	0.24	0.43	0.67	1.07	0.84	0.55	0.45

$3/2^-$. The spherical single-hole state $7/2^-$ would be the first excited state and its lifetime is consistent with that of the experimental isomer. The third known state is short lived and should correspond to the $7/2^-$ member of the ground-state band.

D. $N=40$: From “magic” ^{68}Ni to deformed ^{64}Cr

Systematics is a most useful guide, but it has to be used with care. The p and sd shells can be said to be “full” $0\hbar\omega$ spaces, in the sense that the region boundaries are well defined by the $N=4, 8,$ and 20 closures, with the exception of the very neutron-rich halo nuclei and the island of inversion discussed previously. In the pf shell the $0\hbar\omega$ model space collapses at $N=Z \approx 32-34$ under the invasion of $g_{9/2}$ intruder orbital. Naturally, we expect something similar in the neighborhood of $N=40$ isotones. Recent experiments involving the Coulomb excitation of $^{66-68}\text{Ni}$ (Sorlin *et al.*, 2002), the β decay of $^{60-63}\text{V}$ (Sorlin *et al.*, 2003), and the decay and spectroscopy of the ^{67m}Fe (Sawicka *et al.*, 2003), support this hypothesis. In addition, the β decays of the neutron-rich isotopes ^{64}Mn and ^{66}Mn , investigated at Isolde (Hannawald *et al.*, 1999), which show a sudden drop of the 2^+ energies in the daughter nuclei ^{64}Fe and ^{66}Fe , also point in the same direction.

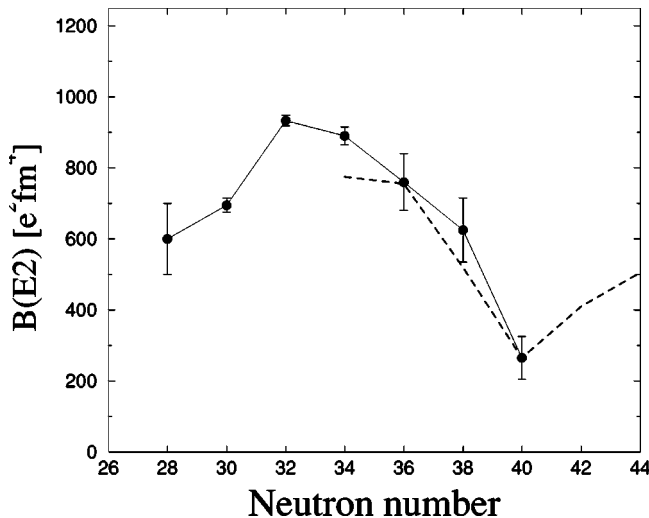


FIG. 45. Experimental $B(E2)$'s ($0^+ \rightarrow 2^+$) in $e^2 \text{fm}^4$ for the isotopes ^{56}Ni – ^{68}Ni (filled circles) (Sorlin *et al.*, 2002). The dashed line links the shell-model results.

The direct inclusion of the $g_{9/2}$ orbital in the fp valence space would have the drawback of increasing dramatically the size of the problems to be treated and allowing spurious center-of-mass contaminations. Moreover, its validity would be restricted to nearly spherical or moderately deformed states. Deformation requires the addition of the $d_{5/2}$ subshell. A compromise is obtained with a ^{48}Ca core with fp orbitals for protons, to take explicitly into account core excitations from $f_{7/2}$ to r_3 orbitals and with $r_3 g_{9/2}$ neutron orbitals. For the most deformed cases, this valence space can be enlarged to the $d_{5/2}$ orbital.

The effective interaction is based on three blocks: (i) the two-body matrix element from the KB3G effective interaction (Poves *et al.*, 2001); (ii) the G matrix of Hjorth-Jensen *et al.* (1995) with the modifications of Nowacki (1996); and (iii) the Kahana, Lee, and Scott G matrix (Kahana *et al.*, 1969b) for the remaining matrix elements. We have computed all the nickel isotopes and followed their behavior at and beyond $N=40$. In Table XIII we compare the excitation energy of the 2^+ states in the nickel chain with the available experimental data, including the very recent ^{70}Ni value (Sorlin *et al.*, 2002). The agreement is quite good, although the experiment gives a larger peak at $N=40$. Similarly the $B(E2)$'s in Fig. 45 follow the experimental trends, including the drop at ^{68}Ni recently measured by Sorlin *et al.* (2002). Note that for a strict closure the transition probability vanishes. The ground-state wave function of ^{68}Ni is 50% closed shell and the extra occupancy of the $g_{9/2}$ orbital, maximum at $N=40$, reflects the erosion of the $N=40$ shell gap. These numbers are very sensitive to modifications of the pf - g gap, and smaller values of the closed-shell probability can be obtained without altering drastically the rest of the properties. The shell-model results have been compared with those of other methods by Langanke, Terasaki, *et al.* (2003).

The β decays of ^{60}V and ^{62}V indicate very low energies for the 2_1^+ states in ^{60}Cr and ^{62}Cr (Sorlin *et al.*, 2000, 2003). If $N=40$ were a magic number, one would expect higher 2^+ energies as the shell closure approaches, particularly in ^{64}Cr . As can be seen in Fig. 46, exactly the opposite seems to happen experimentally. The three possible model spaces tell an interesting story: $pf \equiv r_3$ is acceptable at $N=32, 34$. The addition of $g_{9/2}$ does more harm than good because the gaps have been arbitrarily reduced to reproduce the $N=36$ experimental point by

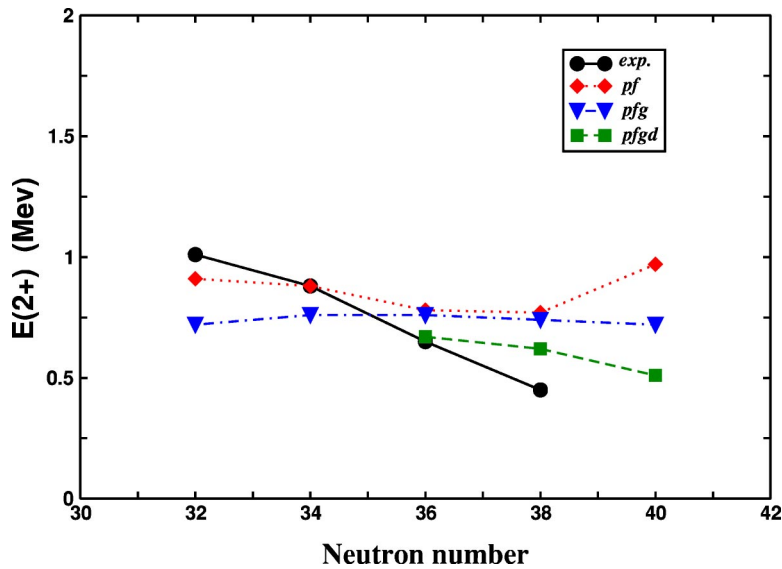


FIG. 46. (Color in online edition) Experimental (Sorlin *et al.*, 2000, 2003) and calculated 2^+ energies of the very-neutron-rich chromium isotopes in the pf , pfg , and $pfgd$ spaces.

allowing $2p$ - $2h$ jumps including $d_{5/2}$. But then, in $N=38$ the 2^+ is too high, and the experimental trend promises no improvement at $N=40$.

Properties of the 2^+ energies given by the $pfgd$ calculation are collected in Table XIV. They point to prolate structures with deformation $\beta \approx 0.3$.

VIII. OTHER REGIONS AND THEMES

A. Astrophysical applications

Astrophysical environments involve temperatures and densities that are normally not accessible in laboratory experiments. The description of the different nuclear processes thus requires theoretical estimates. As discussed in previous sections, shell-model calculations are able to satisfactorily reproduce many experimental results so that it should be possible to obtain reliable predictions for nuclei and/or conditions not yet accessible experimentally.

As a first example, consider the decay properties of nuclei totally stripped of the atomic electrons at typical cosmic-ray energies of 300 MeV/A. A nucleus such as

^{53}Mn , unstable in normal conditions, becomes stable. Another isotope, ^{54}Mn , could be used as a chronometer to study the propagation of iron-group nuclei on cosmic rays (Duvernois, 1997), provided its half-life under cosmic-ray conditions is known. The necessary calculation involves decay by second-forbidden unique transitions to the ground states of ^{54}Cr and ^{54}Fe . Due to phase-space arguments the β^- decay to ^{54}Fe is expected to dominate. In two difficult and elegant experiments the very small branching ratio for the β^+ decay to the ground state of ^{54}Cr has been measured: $(1.8 \pm 0.8) \times 10^{-9}$ by Zaerpoor *et al.* (1997) and $(1.20 \pm 0.26) \times 10^{-9}$ by Wuosmaa *et al.* (1998). Taking the weighted mean of these values, $(1.26 \pm 0.25) \times 10^{-9}$, and knowing that of ^{54}Mn , 312.3(4) d, we obtain a partial β^+ half-life of $(6.8 \pm 1.3) \times 10^8$ yr, as compared with 5.6×10^8 yr from the shell-model calculation of Martínez-Pinedo and Vogel (1998), which yields 5.0×10^5 yr for the dominant β^- branch. Both theoretical results are sensitive to uncertainties in the renormalization of the unique second-forbidden operators, which should be removed when taking the ratio of the β^- and β^+ half-lives. Multiplying

TABLE XIV. Spectroscopic properties of $^{60-64}\text{Cr}$ in the $pfgd$ valence space.

	^{60}Cr	^{62}Cr	^{64}Cr
$E^*(2^+)$ (MeV)	0.67	0.65	0.51
Q_s ($e \text{ fm}^2$)	-23	-27	-31
$B(E2)_{\downarrow}$ ($e^2 \text{ fm}^4$)	288	302	318
Q_i ($e \text{ fm}^2$) from Q_s	82	76	109
Q_i ($e \text{ fm}^2$) from $B(E2)$	101	103	106
$E^*(4^+)$ (MeV)	1.43	1.35	1.15
Q_s ($e \text{ fm}^2$)	-37	-30	-43
$B(E2)_{\downarrow}$ ($e^2 \text{ fm}^4$)	426	428	471
Q_i ($e \text{ fm}^2$) from Q_s	102	84	119
Q_i ($e \text{ fm}^2$) from $B(E2)$	117	117	123

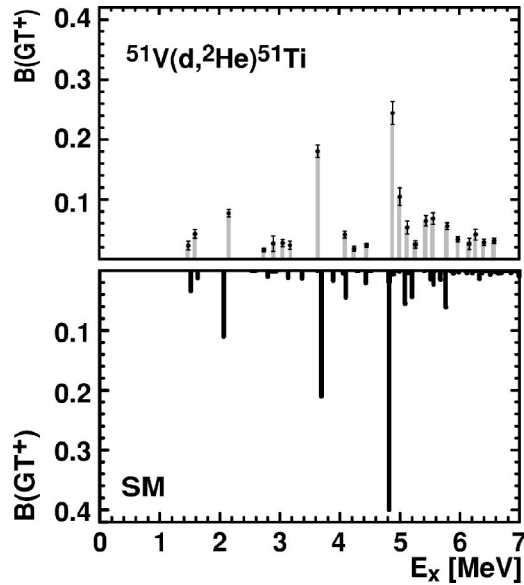


FIG. 47. Comparison of the shell-model GT_+ distribution (lower panel) for ^{51}V with the high-resolution $(d,^2\text{He})$ data (from Bäumer *et al.*, 2003). The shell-model distribution includes a quenching factor of $(0.74)^2$.

the theoretical ratio by the experimental value of the β^+ half-life yields a value of $(6.0 \pm 1.2) \times 10^5$ yr for the β^- branch. Using a similar argument, Wuosmaa *et al.* (1998) estimate the partial β^- half-life to be $(6.0 \pm 1.3[\text{stat}] \pm 1.1[\text{theor}]) \times 10^5$. The influence of this half-life on the age of galactic cosmic rays has been discussed recently by Yanasak *et al.* (2001). Another possible cosmic-ray chronometer, ^{56}Ni , could measure the time between production of iron-group nuclei in supernovae and the acceleration of part of this material to form cosmic rays (Fisker *et al.*, 1999). Before acceleration, the decay of ^{56}Ni proceeds by electron capture to the 1^+ state in ^{56}Co with a half-life of 6.075(20) d. After acceleration ^{56}Ni is stripped of its electrons, the transition to the 1^+ state is no longer energetically allowed, and the decay proceeds to the 3^+ state at 158 keV via a second-forbidden unique transition. Currently only a lower limit for the half-life of totally ionized ^{56}Ni has been established (2.9×10^4 yr) (Sur *et al.*, 1990). A recent shell-model calculation by Fisker *et al.* (1999) predicts a half-life of 4×10^4 yr that is too short for ^{56}Ni to serve as a cosmic-ray chronometer.

Nuclear beta decay and electron capture are important during the late stages of stellar evolution (see Langanke and Martínez-Pinedo, 2003, for a recent review). At the relevant conditions in the star, electron capture and β decay are dominated by Gamow-Teller (and Fermi) transitions. Earlier determinations of the appropriate weak-interaction rates were based in the phenomenological work of Fuller, Fowler, and Newman (1980, 1982a, 1982b, 1985). The shell model makes it possible to refine these estimates. For the *sd*-shell nuclei, important in stellar oxygen and silicon burning, we refer the reader to Oda *et al.* (1994). More recently, it has been

possible to extend these studies to *pf*-shell nuclei relevant for presupernova evolution and collapse (Caurier, Langanke, *et al.*, 1999; Langanke and Martínez-Pinedo, 2000, 2001). The astrophysical impact of the shell-model-based weak-interaction rates have recently been studied by Heger, Langanke, *et al.* (2001), and Heger, Woosley, *et al.* (2001).

The basic ingredient in the calculation of the different weak-interaction rates is the Gamow-Teller (GT) strength distribution. The GT_+ sector directly determines the electron-capture rate and also contributes to the beta-decay rate through the thermal population of excited states (Fuller *et al.*, 1982a). The GT_- strength contributes to the determination of the β -decay rate. To be applicable to stellar weak-interaction rates, the shell-model calculations should reproduce the available GT_+ [measured by (n,p) -type reactions] and GT_- [measured in (p,n) -type reactions]. Many such comparisons with the pioneering (n,p) measurements performed at TRIUMF (Alford *et al.*, 1993; Rönnqvist *et al.*, 1993; El-Katab *et al.*, 1994), with a typical energy resolution of ≈ 1 MeV, can be found in Caurier, Langanke, *et al.* (1999). Recently developed techniques, involving $(d,^2\text{He})$ charge-exchange reactions at intermediate energies (Rakers *et al.*, 2002), have improved the energy resolution by an order of magnitude or more. Figure 47 compares the shell-model GT_+ distribution computed using the KB3G interaction (Poves *et al.*, 2001) with a recent experimental measurement of the $^{51}\text{V}(d,^2\text{He})$ performed at KVI (Bäumer *et al.*, 2003).

Detailed comparisons of the shell-model GT_- distributions with the data obtained in (p,n) charge-exchange reaction measurements for $^{54,56}\text{Fe}$ and $^{58,60}\text{Ni}$ (Rapaport *et al.*, 1983; Anderson *et al.*, 1990) can also be found in Caurier, Langanke, *et al.* (1999). The GT_- operator acting on a nucleus with neutron excess and ground-state isospin T can lead to states in the daughter nucleus with three different isospin values ($T-1, T, T+1$). As a consequence, the GT_- strength distributions have significantly more structure and extend over a larger excitation-energy interval than the GT_+ distributions, making their theoretical reproduction more challenging. Nevertheless, the agreement with the experimental data is quite satisfactory. The shell-model results for ^{58}Ni have recently been compared with high-resolution data (50 keV) obtained using the $(^3\text{He},t)$ reaction (Fujita *et al.*, 2002).

Shell-model diagonalization techniques have been used to determine astrophysically relevant weak-interaction rates for nuclei with $A \leq 65$. Nuclei with higher masses are relevant to the study of the collapse phase of core-collapse supernovae (Langanke and Martínez-Pinedo, 2003). The calculation of the relevant electron-capture rates is currently beyond the capabilities of shell-model diagonalization due to the enormous dimensions of the valence space. However, this dimensionality problem does not apply to shell-model Monte Carlo methods (see Sec. IV.B.3). Moreover, the high temperatures present in the astrophysical environment

make necessary a finite-temperature treatment of the nucleus; this makes shell-model Monte Carlo methods the natural choice for this type of calculation. Initial studies by Langanke *et al.* (2001) showed that the combined effect of nuclear correlations and finite temperature was rather efficient in unblocking Gamow-Teller transitions on neutron-rich germanium isotopes. More recently these calculations have been extended to cover all the relevant nuclei in the range $A=65-112$ by Langanke, Martínez-Pinedo, *et al.* (2003). The resulting electron-capture rates have a very strong influence in the collapse (Langanke, Martínez-Pinedo, *et al.*, 2003) and postbounce (Hix *et al.*, 2003).

The astrophysical r process²³ is responsible for the synthesis of at least half of the elements heavier than $A \approx 60$ (Wallerstein *et al.*, 1997). Simulations of the r process require a knowledge of nuclear properties far from the valley of stability (Kratz *et al.*, 1998; Pfeiffer *et al.*, 2001). As the relevant nuclei are not experimentally accessible, theoretical predictions for the relevant quantities (i.e., neutron separation energies and half-lives) are needed. The calculation of β -decay half-lives usually requires two ingredients: the Gamow-Teller strength distribution in the daughter nucleus and the relative energy scale between parent and daughter (i.e., the Q_β value). Due to the huge number of nuclei relevant for the r process, the estimates of the half-lives are so far based on a combination of global mass models and the quasi-particle random-phase approximation (see Langanke and Martínez-Pinedo, 2003, for a description of the different models). However, recently shell-model calculations have become available for some key nuclei with a magic neutron number $N=50$ (Langanke and Martínez-Pinedo, 2003), $N=82$ (Martínez-Pinedo and Langanke, 1999; Brown *et al.*, 2003), and $N=126$ (Martínez-Pinedo, 2001). All these calculations suffer from a lack of spectroscopic information on the regions of interest, which is necessary to fine-tune the effective interactions. This situation is improving at least for $N=82$, thanks to the recent spectroscopic data on ^{130}Cd (Dillmann *et al.*, 2003).

Nuclear reaction rates are the key input data for simulations of stellar burning processes. Experiment-based reaction rates for the simulation of explosive processes such as novae, supernovae, x-ray bursts, x-ray pulsars, and merging neutron stars are scarce because of the experimental difficulties associated with radioactive-beam measurements (Käppeler *et al.*, 1998.) Most of the reaction-rate tables are therefore based on global model predictions.

²³The r process was originally described as the rapid capture of free neutrons by iron-peak and heavier nuclei during a supernova. While the actual process of building heavy nuclei in a supernova is more complicated, the term is still applied to heavy-element production during type-II supernovae which occur at the end of the lifetime of stars greater than about ten solar masses.

The most frequently used model is the statistical Hauser-Feshbach approach (Rauscher and Thielemann, 2000). For nuclei near the driplines or near closed-shell configurations, the density of levels is not high enough for the Hauser-Feshbach approach to be applicable. For these cases alternative theoretical approaches such as the nuclear shell model need to be applied. Shell-model calculations were used for the determination of the relevant proton-capture reaction rates for sd -shell nuclei necessary for rp process studies (Herndl *et al.*, 1995). These calculations have recently been extended to include pf -shell nuclei (Fisker *et al.*, 2001).

Knowledge of neutrino-nucleus reactions is necessary for many applications, e.g., neutrino oscillation studies, detection of supernova neutrinos, description of neutrino transport in supernovae, and nucleosynthesis studies. Most of the relevant neutrino reactions have not been studied experimentally so far, and their cross sections are typically based on nuclear theory (see Kolbe *et al.*, 2003, for a recent review). The model of choice for the theoretical description of neutrino reactions depends of the energy on the neutrinos that participate in the reaction.

For low neutrino energies, comparable to the nuclear excitation energy, neutrino-nucleus reactions are very sensitive to the appropriate description of the nuclear response, which is very sensitive to correlations among nucleons. The model of choice is then the nuclear shell model. $0\hbar\omega$ calculations have been used for the calculation of neutrino absorption cross sections (Sampaio *et al.*, 2001) and scattering cross sections (Sampaio *et al.*, 2002) for selected pf -shell nuclei relevant for supernovae evolution. For lighter nuclei complete diagonalizations can be performed in larger model spaces, e.g., $4\hbar\omega$ calculations for ^{16}O (Haxton, 1987; Haxton and Johnson, 1990) and $6\hbar\omega$ calculations for ^{12}C (Hayes and Towner, 2000; Volpe *et al.*, 2000). Another example of shell-model calculations of neutrino cross sections is the series of neutrino absorption cross sections on ^{40}Ar of Ormand *et al.* (1995) for solar neutrinos (see Bhattacharya *et al.*, 1998, for an experimental evaluation of the same cross section). This cross section has recently been evaluated by Kolbe *et al.* (2003) for supernova neutrinos. And the evaluation by Haxton (1998) of the solar neutrino absorption cross section on ^{71}Ga is relevant for the GALLEX and SAGE solar neutrino experiments.

For higher neutrino energies the standard method of choice is the random-phase approximation, as neutrino reactions are sensitive mainly to the total strength and energy centroids of the different multipoles contributing to the cross section. In some selected cases, the Fermi and Gamow-Teller contribution to the cross section could be determined from a shell-model calculation supplemented by RPA calculations for higher multipoles. This type of mixed calculation has been carried out for several iron isotopes (Kolbe *et al.*, 1999; Toivanen *et al.*, 2001) and for ^{20}Ne (Heger *et al.*, 2005).

B. $\beta\beta$ decays

The double-beta decay is the rarest nuclear weak process. It takes place between two even-even isobars, when decay to the intermediate nucleus is energetically forbidden or hindered by the large spin difference between the parent ground state and the available states in the intermediate nuclei. It comes in three forms: The two-neutrino decay $\beta\beta_{2\nu}$,

$${}^A_Z X_N \rightarrow {}^A_{Z+2} X_{N-2} + e_1^- + e_2^- + \bar{\nu}_1 + \bar{\nu}_2,$$

is just a second-order process mediated by the Standard Model weak interaction. It conserves lepton number and has already been observed in a few nuclei.

The second mode, the neutrinoless decay $\beta\beta_{0\nu}$,

$${}^A_Z X_N \rightarrow {}^A_{Z+2} X_{N-2} + e_1^- + e_2^-,$$

needs an extension of the Standard Model of electroweak interactions as it violates lepton number. A third mode, $\beta\beta_{0\nu,\chi}$ is also possible,

$${}^A_Z X_N \rightarrow {}^A_{Z+2} X_{N-2} + e_1^- + e_2^- + \chi,$$

in some extensions of the Standard Model and proceeds via emission of a light neutral boson, a majoron χ . The last two modes, not yet experimentally observed, require massive neutrinos—an issue already settled by the recent measurements at Super-Kamiokande (Fukuda *et al.*, 1998), SNO (Ahmad *et al.*, 2002), and KamLAND (Eguchi *et al.*, 2003). Interestingly, double-beta decay without emission of neutrinos would be the only way to signal the Majorana character of the neutrino and to distinguish between the different scenarios for the neutrino mass differences. Experimentally, the three modes show different electron energy spectra (see Fig. 2 in Zdesenko, 2002). The $\beta\beta_{2\nu}$ and $\beta\beta_{0\nu,\chi}$ are characterized by a continuous spectrum ending at the maximum available energy $Q_{\beta\beta}$, while the $\beta\beta_{0\nu}$ spectrum consists in a sharp peak at the end of the $Q_{\beta\beta}$ spectrum. This should, in principle, make it easier to observe the signature of this mode. In what follows we shall concentrate on the $\beta\beta_{2\nu}$ and $\beta\beta_{0\nu}$ modes.

The theoretical expression of the half-life of the 2ν mode can be written as

$$[T_{1/2}^{2\nu}]^{-1} = G_{2\nu} |M_{GT}^{2\nu}|^2, \quad (95)$$

with

$$M_{GT}^{2\nu}(J) = \sum_m \frac{\langle J^+ || \vec{\sigma}t_- || 1_m^+ \rangle \langle 1_m^+ || \vec{\sigma}t_- || 0^+ \rangle}{E_m + E_0(J)} \quad (96)$$

(there is an implicit sum over all the nucleons). $G_{2\nu}$ contains the phase-space factors and the axial coupling constant g_A . The calculation of $M_{GT}^{2\nu}$ requires a precise knowledge of the ground state of the parent nuclei plus the ground state and occasionally a few excited states of the granddaughter, both even-even. In addition, it is necessary to have a good description of the Gamow-Teller strength functions of both of them, which implies a detailed description of the odd-odd intermediate nucleus. This is why this calculation is a challenge for the nuclear

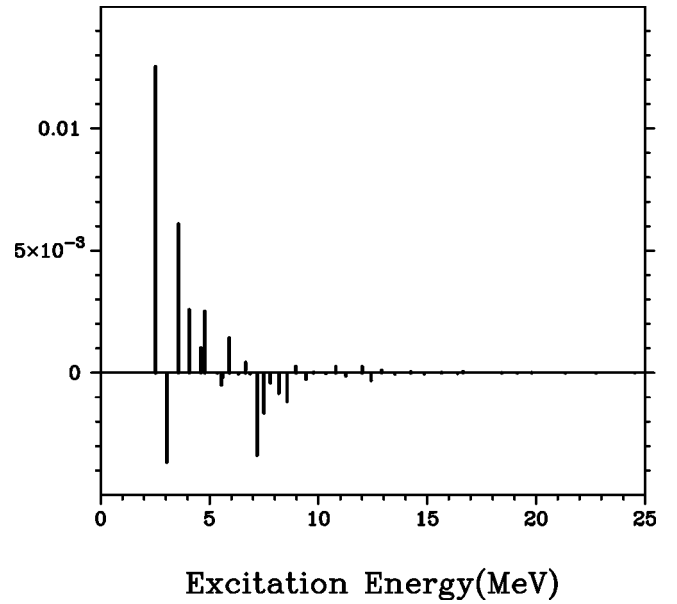


FIG. 48. Lanczos strength function for the ${}^{48}\text{Ca} \rightarrow {}^{48}\text{Ti}$ 2ν decay. Each bar corresponds to the contribution of one intermediate state to the matrix element. Notice the interfering positive and negative contributions. From Caurier *et al.*, 1990.

models, and why agreement with experiment in this channel is taken as a quality factor to be applied to the predictions of the models for the neutrinoless mode.

It is also a showcase for the use of the Lanczos strength function method. This works as follows: Once the relevant wave functions of parent and granddaughter are obtained, it is straightforward to build the doorway states $\vec{\sigma}t_- |0_{initial}^+\rangle$ and $\vec{\sigma}t_+ |J_{final}^+\rangle$. In a second step, one of these is fragmented using the Lanczos strength function, producing, at iteration N , $N+1$ states in the intermediate nucleus, with excitation energies E_m . Overlapping these vectors with the other doorway, entering the appropriate energy denominators, and adding up the N contributions gives an approximation to the exact value of $M_{GT}^{2\nu}$ ($N=1$ gives just the closure approximation). Finally, the number of iterations is increased until full convergence is reached. The method is very efficient. For instance, in the $A=48$ case, 20 iterations usually suffice. The contributions of the different intermediate states to the final matrix element are plotted in Fig. 48.

In the pf shell there is only one double-beta emitter, namely, ${}^{48}\text{Ca}$. For many years, the experimental information was limited to a lower limit on the 2ν - $\beta\beta$ half-life $T_{1/2}^{2\nu} > 3.6 \times 10^{19}$ yr (Bardin *et al.*, 1970). The calculation of the ${}^{48}\text{Ca}$ half-life was one of the first published results stemming from the full pf shell calculations using the code ANTOINE. The resulting matrix elements are $M_{GT}^{2\nu}(0^+) = 0.083$ and $M_{GT}^{2\nu}(2^+) = 0.051$. For the ground-state to ground-state decay ${}^{48}\text{Ca} \rightarrow {}^{48}\text{Ti}$, $G_{2\nu} = 1.1 \times 10^{-17} \text{ yr}^{-1}$ (Tsuboi *et al.*, 1984). The phase-space factor hinders the transition to the 2^+ , which represents only about 3% of the total probability. Putting everything together, and using the Gamow-Teller quenching factor al-

TABLE XV. Calculated $T_{1/2}^{2\nu}$ half-lives for several nuclei and $0^+ \rightarrow 0^+$ transitions.

Parent	^{48}Ca	^{76}Ge	^{82}Se
$T_{1/2}^{2\nu}$ theor. (y)	3.7×10^{19}	2.6×10^{21}	3.7×10^{19}
$T_{1/2}^{2\nu}$ expt. (y)	4.3×10^{19}	1.8×10^{21}	8.0×10^{19}

ready discussed, the resulting half-life is $T_{1/2}^{2\nu} = 3.7 \times 10^{19}$ yr (Caurier *et al.*, 1990; see also the erratum, Caurier *et al.*, 1994). The prediction was a success, because a later measure gave $T_{1/2}^{2\nu} = 4.3_{-1.1}^{+2.4}[\text{stat}] \pm 1.4[\text{syst}] \times 10^{19}$ yr (Balys *et al.*, 1996).

Among the other $\beta\beta$ emitters in nature (around 30), only a few are potentially interesting for experiment because they have a $Q_{\beta\beta}$ value sufficiently large (≥ 2.5 MeV) for the 0ν signal not to be drowned in the surrounding natural radioactivity. With the exception of ^{150}Nd , all of them can be described within a shell-model approach. The results for the 2ν mode of the lightest emitters, ^{48}Ca , ^{76}Ge , and ^{82}Se , for which full space calculations are doable, are gathered in Table XV (Caurier *et al.*, 1996). The shell-model Monte Carlo method has also been applied to the calculation of 2ν double-beta decays by Radha *et al.* (1996).

The expression for the neutrinoless beta-decay half-life, in the $0^+ \rightarrow 0^+$ case, can be brought to the following form (Takasugi, 1981; Doi *et al.*, 1985):

$$[T_{1/2}^{(0\nu)}(0^+ \rightarrow 0^+)]^{-1} = G_{0\nu} \left[M_{GT}^{(0\nu)} - \left(\frac{g_V}{g_A} \right)^2 M_F^{(0\nu)} \right]^2 \times \left(\frac{\langle m_\nu \rangle}{m_e} \right)^2,$$

where $\langle m_\nu \rangle$ is the effective neutrino mass, $G_{0\nu}$ the kinematic space factor, and $M_{GT}^{(0\nu)}$ and $M_F^{(0\nu)}$ the following matrix elements (m and n sum over nucleons):

$$M_{GT}^{(0\nu)} = \langle 0_f^+ | \sum_{n,m} h(r) (\vec{\sigma}_n \cdot \vec{\sigma}_m) t_{n-} t_{m-} | 0_i^+ \rangle, \quad (97)$$

$$M_F^{(0\nu)} = \langle 0_f^+ | \sum_{n,m} h(r) t_{n-} t_{m-} | 0_i^+ \rangle. \quad (98)$$

Here, due to the presence of the neutrino propagator, the “neutrino potential” $h(r)$ is introduced. In this case, the matrix elements are just expectation values of two-body operators, without a sum over intermediate states. This was believed to make the results less dependent on the nuclear model employed to obtain the wave function, an assumption that has not survived to the actual calculations. Full details of the calculations, as well as predictions for other 0ν and 2ν decays in heavier double-beta emitters, can be found in Retamosa *et al.* (1995) and Caurier *et al.* (1996); see also Suhonen and Civitarese (1998) for a recent and very comprehensive review of the nuclear aspects of double-beta decay. The upper bounds on the neutrino mass resulting from our

TABLE XVI. 0ν matrix elements and upper bounds on the neutrino mass for $T_{1/2}^{0\nu} \geq 10^{25}$ yr $\langle m_\nu \rangle$ in eV.

Parent	^{48}Ca	^{76}Ge	^{82}Se
$M_{GT}^{0\nu}$	0.63	1.58	1.97
$M_F^{0\nu}$	-0.09	0.19	-0.22
$\langle m_\nu \rangle$	0.94	1.33	0.49

shell-model calculations, assuming a reference half-life $T_{1/2}^{0\nu} \geq 10^{25}$ yr are collected in Table XVI.

For the heavier emitters, some truncation scheme has to be employed, and seniority truncation seems to be the best, because the dimensions are strongly reduced, in particular for 0^+ states. An interesting feature in the calculation of the double-beta decay matrix elements is shown in Fig. 49 for the ^{76}Ge case. The convergence of the $M_{GT}^{0\nu}$ matrix element is displayed as a function of the truncation of the valence space, either by seniority ν or by configurations t (t is the maximum number of particles in the $g_{9/2}$ orbital). The $t=16$ and $\nu=16$ values correspond to the full space calculation and are consequently equal. The two truncation schemes show very distinct patterns, with the seniority truncation being the more efficient. Such patterns have also been observed in the tellurium and xenon isotopes. This seems to indicate that the most favorable nuclei for the theoretical calculation of the 0ν mode would be the spherical emitters, in which seniority is an efficient truncation scheme.

C. Charge radius shifts in the calcium isotopes

We have already seen in Sec. VI.E that deformed n -particle– n -hole configurations can appear at very low excitation energy around shell closures and even become yrast in the case of neutron-rich nuclei. This situation simply reflects the limitation of the spherical mean-field description of the nucleus, and it shows that, even in magic cases, the correlations produce a sizable erosion of the Fermi surface. This is the case in the cal-

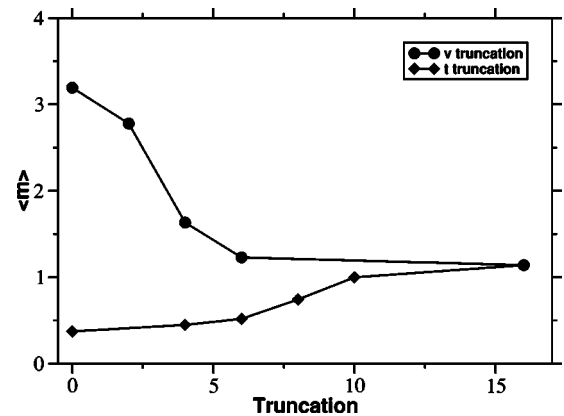


FIG. 49. Variation of the upper bound on the neutrino mass $\langle m_\nu \rangle$ when the seniority truncations (circles) and the configuration truncations (diamonds) are made less restrictive.

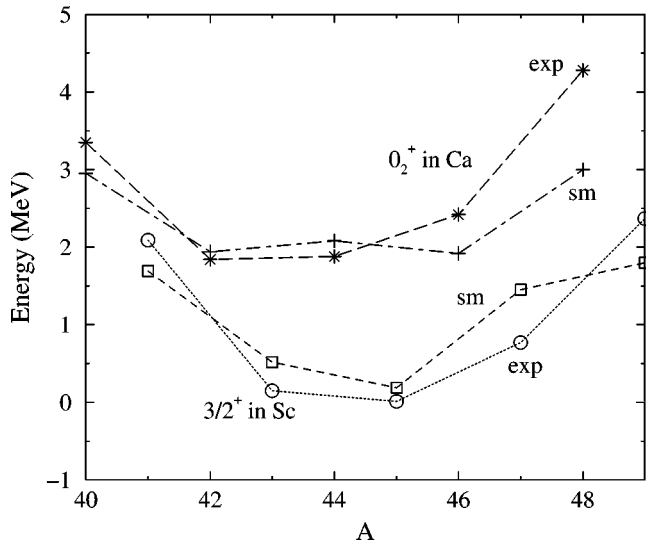


FIG. 50. Comparison between calculated (sm) and experimental (Firestone, 1996) intruder excitation energies in the calcium and scandium isotopic chains. From Caurier, Langanke, *et al.*, 2001.

cium isotopic chain. Experiments based on optical isotope shifts or muonic atom data reveal that the nuclear charge radii $\langle r_c^2 \rangle$ follow a characteristic parabolic shape with a pronounced odd-even staggering (Palmer, 1984; Fricke *et al.*, 1995).

For a description of the nuclei around $N=Z=20$, a model space comprising the orbits $d_{3/2}$, $2s_{1/2}$, $1f_{7/2}$, and $2p_{3/2}$, is a judicious choice (see Caurier, Langanke, *et al.*, 2001). The interaction is the same as that used to describe the neutron-rich nuclei in the sd - pf valence space, called SPDF-NR in Sec. VII, with modified single-particle energies to reproduce the spectrum of ^{29}Si (SDPF-SM).

Several important features of the nuclei at the sd/pf interface are reproduced by the calculation, among others, the excitation energies of the intruder 0_2^+ states in the calcium isotopes, the location of the $3/2^+$ states in the scandium isotopes (see Fig. 50), and the excitation energies of the 2^+ and 3^- and the $B(E2)$'s between the 2_1^+ and the 0_1^+ states in the calcium isotopes.

Due to the cross-shell pairing interaction, protons and neutrons are lifted from the sd to the fp orbitals. The former produce an increase of $\langle r_c^2 \rangle$ that, using harmonic-oscillator wave functions, can be expressed as

$$\delta r_c^2(A) = \frac{1}{Z} n_{pf}^\pi(A) b^2, \quad (99)$$

where $Z=20$ for the calcium chain, b is the oscillator parameter, and n_{pf}^π is extracted from the calculated wave functions. The charge radius shifts of the calcium isotopes relative to ^{40}Ca are shown in Fig. 51, together with the experimental values. The global trends are very well reproduced, although the calculated shifts are a bit smaller than the experimental ones. This is probably due

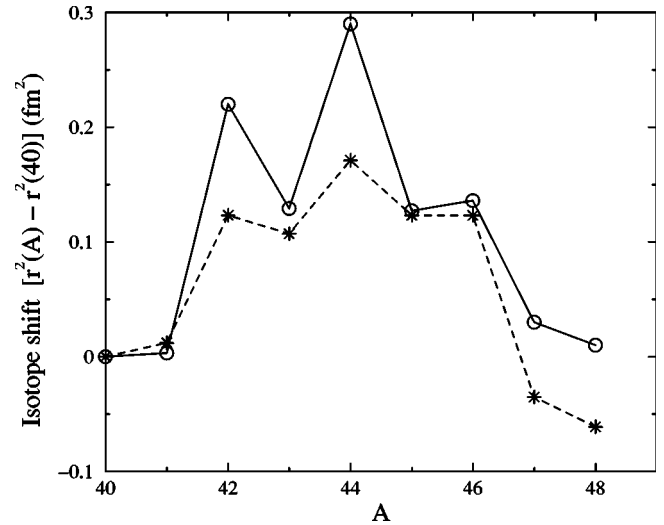


FIG. 51. Isotope shifts in the calcium chain: \circ , experiment (Palmer, 1984; Fricke *et al.*, 1995); stars, shell-model calculations. From Caurier, Langanke, *et al.*, 2001.

to the limitations in the valence space, which excludes the $1d_{5/2}$, the $1f_{5/2}$, and the $2p_{1/2}$ orbits.

D. Shell-model calculations in heavier nuclei

There are some regions of heavy nuclei in which physically sound valence spaces can be designed that are at the same time tractable. A good example is the space comprising the neutron orbits between $N=50$ and $N=82$ for the tin isotopes (Hjorth-Jensen *et al.*, 1995; Nowacki, 1996). When protons are allowed, the dimensions grow rapidly and the calculations have been limited until now to nuclei with few particle or holes on the top of the closed shells (see Covello *et al.*, 1997, for a review of the work of the Napoli group).

The shell-model Monte Carlo approach, which can overcome these limitations, has been applied in this region to ^{128}Te and ^{128}Xe , which are candidates for γ soft nuclei, by Alhassid *et al.* (1996). It has also been applied to several dysprosium isotopes, $A=152$ – 162 , in the Kumar-Baranger space by White *et al.* (2000). Quantum Monte Carlo diagonalization has also been applied to the study of the spherical-to-deformed transition in the even barium isotopes with $A=138$ – 150 by Shimizu *et al.* (2001).

Hints on the location of the hypothetical islands of superheavy elements can often be found in mean-field calculations of the single-particle structure. The predictions for nuclei far from stability can also be tested in nuclei much closer to stability, where shell-model calculations are now feasible. In particular, recent systematic mean-field calculations suggest a substantial gap for $Z=92$ and $N=126$ (^{218}U) corresponding to the $1h_{9/2}$ shell closure. On the other hand, the single-quasiparticle energies extrapolated from lighter $N=126$ isotones, up to ^{215}Ac , do not support this conclusion. To shed light on these controversial predictions, shell-model calculations

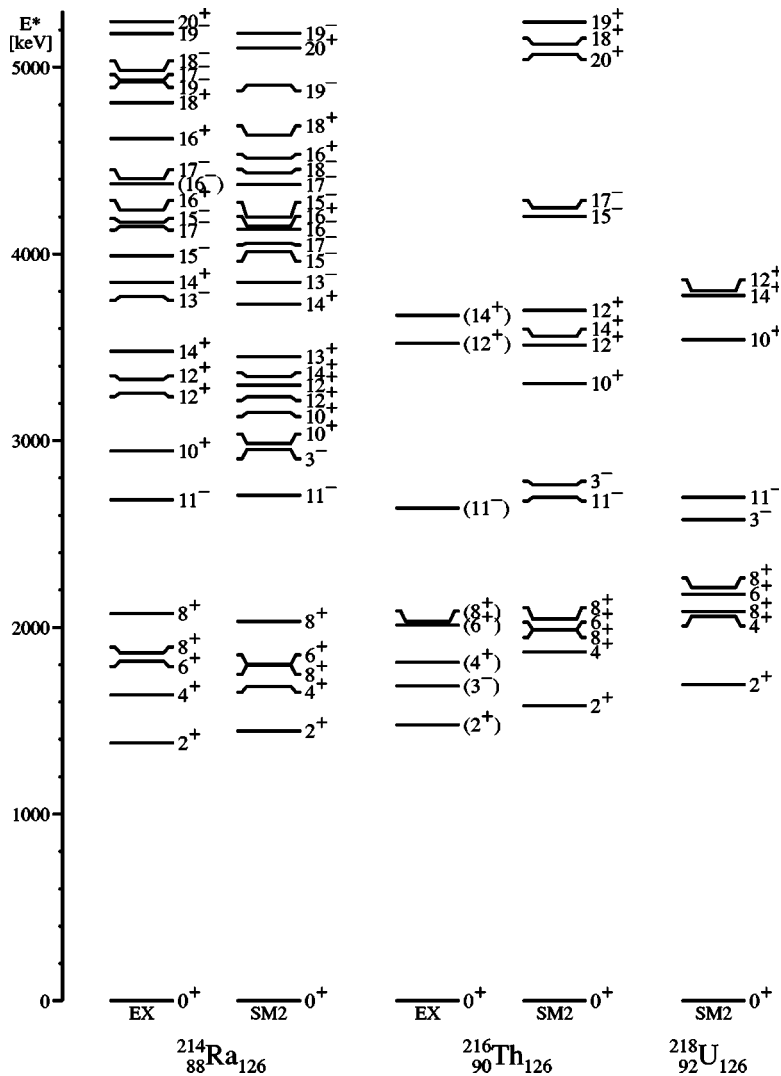


FIG. 52. Experimental (Hauschild *et al.*, 2001) vs theoretical spectra of ^{214}Ra , ^{216}Th , and ^{218}U .

[as well as experimental spectroscopic studies of ^{216}Th by Hauschild *et al.* (2001)] were undertaken by the present authors. The shell-model calculations were for the $N=126$ isotones up to ^{218}U . These calculations were performed in the $1h_{9/2}$, $2f_{7/2}$, $1i_{13/2}$, $3p_{3/2}$, $2f_{5/2}$, $3p_{1/2}$ proton valence space, using the realistic Kuo-Herling interaction (Kuo and Herling, 1971) as modified by Brown and Warburton (Warburton and Brown, 1991). The calculation reproduces nicely the ground-state energies, the 2^+ energy systematics, and the high-spin trends. The cases of ^{214}Ra , ^{216}Th , and ^{218}U are shown in Fig. 52. The only deviations between theory and experiment are in the 3^- energy. These reflect the particular nature of these states, which are known to be very collective, and correspond to particle-hole excitations of the ^{208}Pb core.

No shell gap for $Z=92$, corresponding to the $1h_{9/2}$ closure, is predicted. On the contrary, the ground state of the $N=126$ isotones is characteristic of a superfluid regime with zero-seniority components representing more than 95% of the wave functions for all nuclei.

E. Random Hamiltonians

The study of random Hamiltonians is a vast interdisciplinary subject that is beyond the scope of this review

(see Porter, 1965, for a collection of the pioneering papers). Therefore we shall only give here a bibliographical guide to work that has recently attracted wide attention and that may have consequences for future shell-model studies.

Johnson *et al.* (1998, 1999) noticed that random interactions had a strong tendency to produce $J=0$ ground states. This is an empirical fact that was hitherto attributed to the pairing force. Bijker and Frank (2000a, 2000b) and Bijker *et al.* (1999) showed that this also occurred in an interacting boson context and was associated with the typical forms of collectivity found in the interacting boson model. For the fermion problem no collectivity occurs for purely random interactions (Horoi *et al.*, 2001). The origin of $J=0$ ground-state dominance was attributed to “geometric chaoticity” by Mulhall *et al.* (2000). The geometric aspects of the phenomenon were investigated in some simple cases by Zhao and Arima (2001), Zhao *et al.* (2001), and Chau Huu-Tai *et al.* (2002). Velázquez and Zuker (2002) argued that the general cause of $J=0$ ground-state dominance was to be found in time-reversal invariance. They showed that when the random matrix elements were displaced to have a negative centroid, well-developed rotational mo-

tion appeared in the valence spaces where the realistic interactions would also produce it (as in Fig. 37). This is very much in line with what was found by Cortes *et al.* (1982), and the interesting point is that the collective ingredient induced by the displacement of the matrix elements is the quadrupole force.

It is unlikely that we shall learn much more from purely random Hamiltonians. However, the interplay of random and collective interactions may deserve further study. In particular, we know that a monopole plus pairing Hamiltonian is a good approximation. Would it be a good idea to replace the rest of the interaction by a random one, instead of neglecting it?

IX. CONCLUSION

Nuclei are idiosyncratic, especially the lighter ones accessible to shell-model treatment. Energy scales that are well separated in other systems (such as vibrational and rotational states in molecules) do overlap here, leading to a strong interplay of collective and single-particle modes. Nonetheless, secular behavior—both in the masses and the spectra—eventually emerges, and the *pf* shell is the boundary region where rapid variation from nucleus to nucleus is replaced by smoother trends. As a consequence, larger calculations become associated with more transparent physics and give hints on how to extend the shell-model philosophy into heavier regions where exact diagonalizations become prohibitive. In this review we have not hesitated to advance some ideas on how this could be achieved, by suggesting some final solution to the monopole problem and exploiting the formal properties of the Lanczos construction.

The shell model has been both a craft and a science: one invented model spaces and interactions and tried to impose them on the spectra. Sometimes it worked very well. Then one wondered why such a phenomenology succeeded, only to discover that there was not so much phenomenology after all. It is to be hoped that this state of affairs will persist.

ACKNOWLEDGMENTS

This review owes much to many colleagues: in the first place to Joaquín Retamosa, who has been a member of the Strasbourg-Madrid Shell-Model Collaboration for many years, then to Mike Bentley, Franco Brandolini, David Dean, Jean Duflo, Marianne Dufour, Luis Egido, José María Gómez, Hubert Grawe, María José García Borge, Morten Hjorth-Jensen, Karlheinz Langanke, Silvia Lenzi, Peter Navrátil, Peter von Neumann-Cosel, Achim Richter, Luis Miguel Robledo, Dirk Rudolph, Jorge Sánchez Solano, Olivier Sorlin, Carl Svensson, Petr Vogel, and Guy Walter to name only a few. This work has been partly supported by the IN2P3-France, CICYT-Spain agreements and by a grant of the MCyT-Spain, Grant No. BFM2000-030. Many thanks are given to Benoit Speckel for his continuous computational support.

APPENDIX A: BASIC DEFINITIONS AND RESULTS

- (i) p is the principal oscillator quantum number;
- (ii) $D_p = (p+1)(p+2)$ is the (single fluid) degeneracy of shell p ;
- (iii) orbits are called r, s , etc. $D_r = 2j_r + 1$;
- (iv) $\hat{\delta}_{rs} = \delta_{j_r j_s}$ but $r \neq s$, and both have the same parity;
- (v) m_r is the number of particles in orbit r , T_r is used for both the isospin and the isospin operator. In neutron-proton (np) schemes, m_{rx} specifies the fluid x . Alternatively we use n_r and z_r ;
- (vi) V_{rstu}^Γ or $\mathcal{V}_{rstu}^\Gamma$ are two-body matrix elements. W_{rstu}^Γ is used after the monopole part has been subtracted.

A few equations have to exhibit explicitly angular momentum (J), and isospin (T) conservation. We use Bruce French's notations (French, 1966): Γ stands for JT . Then $(-1)^\Gamma = (-1)^{J+T}$, $[\Gamma] = (2J+1)(2T+1)$, and in general $F(\Gamma) = F(J)F(T)$. Also $(-1)^r = (-1)^{j_r+1/2}$, $[r] = 2(2j_r+1)$. Expressions are carried over to a neutron-proton formalism simply by dropping the isospin factor.

The one-particle creation and annihilation operators

$$A_{rr_z} = a_{rr_z}^\dagger, \quad B_{rr_z} = \tilde{a}_{rr_z} = (-1)^{r+r_z} a_{r-r_z} \quad (\text{A1})$$

can be coupled to quadratics in A and B ,

$$X_{\Gamma_z}^\dagger(rs) = (A_r A_s)_{\Gamma_z}^\dagger, \quad X_{\Gamma_z}(rs) = (B_r B_s)_{\Gamma_z},$$

$$S_{\gamma_z}^\gamma(rt) = (A_r B_t)_{\gamma_z}^\gamma. \quad (\text{A2})$$

$Z_{\Gamma_z}^\dagger(rs) = (1 + \delta_{rs})^{-1/2} X_{\Gamma_z}^\dagger(rs)$ is the normalized pair operator and $Z_{\Gamma_z}(rs)$ its Hermitian conjugate.

For reduced matrix elements we use Racah's definition

$$\langle \alpha \alpha_z | P_{\gamma_z}^\gamma | \beta \beta_z \rangle = (-1)^{\alpha - \alpha_z} \begin{pmatrix} \alpha & \gamma & \beta \\ -\alpha_z & \gamma_z & \beta_z \end{pmatrix} \langle \alpha || P^\gamma || \beta \rangle. \quad (\text{A3})$$

The normal and multipole representations of H are obtained through the basic recoupling

$$- [X_\Gamma^\dagger(rs) X_\Gamma(tu)]^0 = - (-1)^{u+t-\Gamma} \left[\frac{\Gamma}{r} \right]^{1/2} \delta_{sr} S_{ru}^0$$

$$+ \sum_{\gamma} [\Gamma \gamma]^{1/2} (-1)^{s+t-\gamma-\Gamma}$$

$$\times \left\{ \begin{matrix} r & s & \Gamma \\ u & t & \gamma \end{matrix} \right\} (S_{rt}^\gamma S_{su}^\gamma)^0, \quad (\text{A4})$$

whose inverse is

$$(S_{rt}^\gamma S_{su}^\gamma)^0 = (-1)^{u-t+\gamma} \left[\frac{\gamma}{r} \right]^{1/2} \delta_{st} S_{ru}^0 - \sum_{\Gamma} [\Gamma \gamma]^{1/2} (-1)^{s+t-\gamma-\Gamma} \times \begin{Bmatrix} r & s & \Gamma \\ u & t & \gamma \end{Bmatrix} [X_{\Gamma}^\dagger(rs) X_{\Gamma}(tu)]^0. \quad (\text{A5})$$

The “normal” representation of \mathcal{V} is then

$$\mathcal{V} = \sum_{r \leq s \leq u, \Gamma} \mathcal{V}_{rstu}^\Gamma Z_{rs\Gamma}^\dagger \cdot Z_{tu\Gamma} - \sum_{(rstu)\Gamma} \xi_{rs} \xi_{tu} [\Gamma]^{1/2} \mathcal{V}_{rstu}^\Gamma (X_{rs\Gamma}^\dagger X_{tu\Gamma})^0, \quad (\text{A6})$$

where we have used

$$\xi_{rs} = \begin{cases} (1 + \delta_{rs})^{-1/2} & \text{if } r \leq s, \\ (1 + \delta_{rs})^{1/2}/2 & \text{if no restriction,} \end{cases} \quad (\text{A7})$$

so as to have complete flexibility in the sums. According to Eq. (A4), \mathcal{V} can be transformed into the “multipole” representation

$$\mathcal{V} = \sum_{(rstu)\gamma} \xi_{rs} \xi_{tu} \{ [\gamma]^{1/2} \omega_{rtsu}^\gamma (S_{rt}^\gamma S_{su}^\gamma)^0 + \delta_{st} \hat{\delta}_{ru} [s]^{1/2} \omega_{russ}^0 S_{ru}^0 \}, \quad (\text{A8})$$

where (sum only over Pauli-allowed Γ)

$$\omega_{rtsu}^\gamma = \sum_{\Gamma} (-1)^{s+t-\gamma-\Gamma} \begin{Bmatrix} r & s & \Gamma \\ u & t & \gamma \end{Bmatrix} W_{rstu}^\Gamma[\Gamma], \quad (\text{A9})$$

$$W_{rstu}^\Gamma = \sum_{\gamma} (-1)^{s+t-\gamma-\Gamma} \begin{Bmatrix} r & s & \Gamma \\ u & t & \gamma \end{Bmatrix} \omega_{rtsu}^\gamma[\gamma]. \quad (\text{A10})$$

Equation (A5) suggests an alternative to Eq. (A8):

$$\mathcal{V} = \sum_{(rstu)\gamma} \xi_{rs} \xi_{tu} [\gamma]^{1/2} \omega_{rstu}^\gamma \times \left[(S_{rt}^\gamma S_{su}^\gamma)^0 - (-1)^{\gamma+r-s} \left(\frac{\gamma}{r} \right)^{1/2} \delta_{st} \hat{\delta}_{ru} S_{ru}^0 \right], \quad (\text{A11})$$

where each term is associated with a pure two-body operator.

APPENDIX B: FULL FORM OF \mathcal{H}_m

If we were interested only in extracting the diagonal parts of the monopole Hamiltonian at fixed mT , \mathcal{H}_{mT} , the solution would consist in calculating traces of \mathcal{H} and showing that they can be written solely in terms of number and isospin operators. Before we describe the technique for dealing with the nondiagonal parts of \mathcal{H}_{mT} , i.e., for generalizing to them the notion of the centroid, some remarks on the appeal of such an operation may be in order.

The full \mathcal{H}_m contains all that is required for Hartree-Fock (HF) variation, but it goes beyond. Minimizing the energy with respect to a determinantal state will invariably lead to an isospin violation because neutron and proton radii tend to equalize (Duflo and Zuker, 2002),

which demands different orbits of neutrons and protons. Therefore, to assess accurately the amount of isospin violation in the presence of isospin-breaking forces, we must ensure conservation of isospin in their absence. More generally, a full diagonalization of \mathcal{H}_m would be of great intrinsic interest, though it has never been carried out. Now, the technical details.

Define the generalized number and isospin operators

$$S_{rs} = \hat{\delta}_{rs} [r]^{1/2} S_{rs}^{00}, \quad T_{rs} = \frac{1}{2} \hat{\delta}_{rs} [r]^{1/2} S_{rs}^{01}, \quad (\text{B1})$$

which, for $\delta_{rs}=1$, reduce to $S_{rr}=n_r$, $T_{rr}=T_r$. By definition \mathcal{H}_m contains the two-body quadratic forms in S_{rs} and T_{rs} ,

$$S_{rtsu} = \zeta_{rs} \zeta_{tu} (S_{rt} S_{su} - \delta_{st} S_{ru}), \quad (\text{B2a})$$

$$T_{rtsu} = \zeta_{rs} \zeta_{tu} \left(T_{rt} \cdot T_{su} - \frac{3}{4} \delta_{st} S_{ru} \right), \quad (\text{B2b})$$

which in turn become for $\delta_{rt}=\delta_{su}=1$, m_{rs} and T_{rs} in Eqs. (10a) and (10b).

It follows that the form of \mathcal{H}_{mT} must be

$$\mathcal{H}_{mT} = \mathcal{K} + \sum_{all} (a_{rtsu} S_{rtsu} - b_{rtsu} T_{rtsu}) \hat{\delta}_{rt} \hat{\delta}_{su}, \quad (\text{B3})$$

where the sum is over all possible contributions. This is a special Hamiltonian containing only $\lambda=0$ terms. Transforming to the normal representation through Eq. (A10), we have

$$\omega^{00} = \delta_{\lambda 0} \delta_{\tau 0} \Rightarrow \mathcal{V}_{rtsu}^{J0} = \mathcal{V}_{rstu}^{J1} = [rs]^{-1/2},$$

$$\omega^{01} = \delta_{\lambda 0} \delta_{\tau 1} \Rightarrow \mathcal{V}_{rtsu}^{J0} = 3[rs]^{-1/2}, \quad \mathcal{V}_{rtsu}^{J1} = -[rs]^{-1/2}$$

and therefore

$$S_{rtsu} = \sum_{\Gamma} Z_{rs\Gamma}^\dagger \cdot Z_{tu\Gamma} = \sum_J Z_{rsJ0}^\dagger \cdot Z_{tuJ0} + \sum_J Z_{rsJ1}^\dagger \cdot Z_{tuJ1}, \quad (\text{B4a})$$

$$-T_{rtsu} = \frac{3}{4} \sum_J Z_{rsJ0}^\dagger \cdot Z_{tuJ0} - \frac{1}{4} \sum_J Z_{rsJ1}^\dagger \cdot Z_{tuJ1}. \quad (\text{B4b})$$

Inverting, we obtain

$$\sum_J Z_{rsJ0}^\dagger \cdot Z_{tuJ0} = \frac{1}{4} (S_{rtsu} - 4T_{rtsu}), \quad (\text{B5a})$$

$$\sum_J Z_{rsJ1}^\dagger \cdot Z_{tuJ1} = \frac{1}{4} (3S_{rtsu} + 4T_{rtsu}). \quad (\text{B5b})$$

When $j_r=j_s=j_t=j_u$ and $r \neq s$ and $t \neq u$, both S_{rust} , T_{rust} and S_{rtsu} , T_{rtsu} are present. They can be calculated from Eqs. (B5a) and (B5b) by exchanging t and u ,

$$\sum_J Z_{rsJ0}^\dagger \cdot Z_{tuJ0} = - \sum_J (-1)^J Z_{rsJ0}^\dagger \cdot Z_{tuJ0} = \frac{1}{4} (S_{rust} - 4T_{rust}), \quad (\text{B6a})$$

$$\begin{aligned} \sum Z_{rsJ1}^\dagger \cdot Z_{tuJ1} &= \sum (-1)^J Z_{rsJ1}^\dagger \cdot Z_{tuJ1} \\ &= \frac{1}{4}(3S_{rust} + 4T_{rust}) \end{aligned} \quad (\text{B6b})$$

and by combining Eqs. (B5a), (B5b), (B6a), and (B6b),

$$\begin{aligned} \sum_J Z_{rsJ0}^\dagger \cdot Z_{tuJ0} \frac{[1 \pm (-1)^J]}{2} \\ = \frac{1}{8}[(S_{rtsu} - 4T_{rtsu}) \mp (S_{rust} - 4T_{rust})], \end{aligned} \quad (\text{B7a})$$

$$\begin{aligned} \sum_J Z_{rsJ1}^\dagger \cdot Z_{tuJ1} \frac{[1 \pm (-1)^J]}{2} \\ = \frac{1}{8}[(3S_{rtsu} + 4T_{rtsu}) \pm (3S_{rust} + 4T_{rust})]. \end{aligned} \quad (\text{B7b})$$

To write \mathcal{H}_{mT} we introduce the notations

$$\Phi(P) = 1 - (1 - \delta_{rs})(1 - \delta_{tu}), \quad (\text{B8})$$

$$\Phi(e) \equiv (\hat{\delta}_{rs} - \delta_{rs})(\hat{\delta}_{tu} - \delta_{tu}). \quad (\text{B9})$$

So for $r=s$ or $t=u$, $\Phi(P)=1$ and for $j_r=j_s=j_t=j_u$ and $\Phi(P)=0$, $\Phi(e)=1$. Then

$$\begin{aligned} \mathcal{H}_{mT} &= \mathcal{K} + \sum_{\substack{r \leq s \\ t \leq u \\ T, \rho = \pm}} \hat{\delta}_{rt} \hat{\delta}_{su} \{ [1 - \Phi(e)] \bar{\mathcal{V}}_{rstu}^T \Omega_{rstu}^T \\ &\quad + \Phi(e) \bar{\mathcal{V}}_{rstu}^{\rho T} \Omega_{rstu}^{\rho T} \}, \\ \rho &= \text{sgn}(-1)^J, \quad \Omega_{rstu}^T = \sum_J Z_{rsJT}^\dagger \cdot Z_{tuJT}, \\ \Omega_{rstu}^{\pm T} &= \sum_J Z_{rsJT}^\dagger \cdot Z_{tuJT} \frac{[1 \pm (-1)^J]}{2}. \end{aligned} \quad (\text{B10})$$

The values of the generalized centroids $\bar{\mathcal{V}}_{rstu}^T$ and $\bar{\mathcal{V}}_{\rho T}$ are determined by demanding that $\mathcal{H} - \mathcal{H}_{mT} = \mathcal{H}_M$ contain no contributions with $\lambda=0$. In other words,

$$\mathcal{W}_{rstu}^{JT} = \mathcal{V}_{rstu}^{JT} - \hat{\delta}_{rt} \hat{\delta}_{su} \{ [1 - \Phi(e)] \bar{\mathcal{V}}_{rstu}^T + \Phi(e) \bar{\mathcal{V}}_{rstu}^{\rho T} \} \quad (\text{B11})$$

must be such that $\omega_{rstu}^{0T} = 0$, and from Eq. (A10)

$$\sum_{(J)} [J] \mathcal{W}_{rstu}^{JT} = 0 \therefore \bar{\mathcal{V}}_{rstu}^T = \sum_{(J)} [J] \mathcal{V}_{rstu}^{JT} / \sum_{(J)} [J]. \quad (\text{B12})$$

Applying this prescription to all the terms leads to (obviously $\hat{\delta}_{rt} \hat{\delta}_{su} = 1$ in all cases)

$$\begin{aligned} \bar{\mathcal{V}}_{rstu}^T &= \sum_{(J)} \mathcal{V}_{rstu}^{JT} [J] / \sum_{(J)} [J], \\ \sum_{(J)} [J] &= \frac{1}{4} \frac{D_r [D_s + 2\Phi(P)(-1)^T]}{1 + \Phi(P)}, \\ \bar{\mathcal{V}}_{rstu}^{\pm T} &= \sum_J \mathcal{V}_{rstu}^{JT} [J] [1 \pm (-1)^J] / \sum_J [J] [1 \pm (-1)^J], \end{aligned}$$

$$\sum_J [J] [1 \pm (-1)^J] = \frac{1}{4} D_r (D_r \mp 2),$$

$$D_r = [r], \quad \Phi(e) = 1, \quad \text{for } \bar{\mathcal{V}}_{rstu}^{\pm T}. \quad (\text{B13})$$

Through Eqs. (B5a), (B5b), (B7a), and (B7b) we can obtain the form of \mathcal{H}_{mT} in terms of the monopole operators by regrouping the coefficients affecting each of them. To simplify the presentation we adopt the following convention:

$$\begin{cases} \alpha \equiv rstu & r \leq s, t \leq u, \quad \hat{\delta}_{rt} \hat{\delta}_{su} = 1, \quad \text{BUT} \\ S_\alpha = S_{rstu}, \quad S_{\bar{\alpha}} = S_{rust}, \quad T_\alpha = T_{rstu}, \quad T_{\bar{\alpha}} = T_{rust}. \end{cases}$$

Then

$$\begin{aligned} \mathcal{H}_{mT} &= \mathcal{K} + \sum_\alpha [1 - \Phi(e)] (a_\alpha S_\alpha + b_\alpha T_\alpha) + \Phi(e) (a_\alpha^d S_\alpha \\ &\quad + b_\alpha^d T_\alpha + a_\alpha^e S_{\bar{\alpha}} + b_\alpha^e T_{\bar{\alpha}}), \end{aligned} \quad (\text{B14a})$$

with

$$\begin{aligned} a_\alpha &= \frac{1}{4} (3\bar{\mathcal{V}}_\alpha^1 + \bar{\mathcal{V}}_\alpha^0), \\ b_\alpha &= \frac{1}{4} (\bar{\mathcal{V}}_\alpha^1 - \bar{\mathcal{V}}_\alpha^0), \end{aligned} \quad (\text{B14b})$$

$$a_\alpha^d = \frac{1}{8} (3\bar{\mathcal{V}}_\alpha^{+1} + 3\bar{\mathcal{V}}_\alpha^{-1} + \bar{\mathcal{V}}_\alpha^{+0} + \bar{\mathcal{V}}_\alpha^{-0}),$$

$$a_\alpha^e = \frac{1}{8} (3\bar{\mathcal{V}}_\alpha^{+1} - 3\bar{\mathcal{V}}_\alpha^{-1} - \bar{\mathcal{V}}_\alpha^{+0} + \bar{\mathcal{V}}_\alpha^{-0}),$$

$$b_\alpha^d = \frac{1}{2} (3\bar{\mathcal{V}}_\alpha^{+1} + 3\bar{\mathcal{V}}_\alpha^{-1} - \bar{\mathcal{V}}_\alpha^{+0} - \bar{\mathcal{V}}_\alpha^{-0}),$$

$$b_\alpha^e = \frac{1}{2} (3\bar{\mathcal{V}}_\alpha^{+1} - \bar{\mathcal{V}}_\alpha^{-1} + \bar{\mathcal{V}}_\alpha^{+0} - \bar{\mathcal{V}}_\alpha^{-0}). \quad (\text{B14c})$$

1. Separation of \mathcal{H}_{mnp} and \mathcal{H}_{m0}

In an np formalism \mathcal{H}_{mnp} is \mathcal{H}_{mT} under another guise; neutron and proton shells are differentiated and the operators T_{rs} and S_{rs} are written in terms of four scalars $S_{r_x s_y}$; $x, y = n$ or p .

We may also be interested in extracting only the purely isoscalar contribution to \mathcal{H}_{mT} , which we call \mathcal{H}_{m0} . The power of French's product notation becomes particularly evident here, because the form of both terms is identical. It demands some algebraic manipulation to find (Zuker, 1994)

$$\mathcal{H}_{mnp} \text{ or } \mathcal{H}_{m0} = \mathcal{K} + \sum_{\alpha} \left(\bar{\mathcal{V}}_{\alpha} S_{\alpha} [1 - \Phi(e)] + \frac{1}{2} [(\bar{\mathcal{V}}_{\alpha}^{+} + \bar{\mathcal{V}}_{\alpha}^{-}) S_{\alpha} + (\bar{\mathcal{V}}_{\alpha}^{-} - \bar{\mathcal{V}}_{\alpha}^{+}) S_{\bar{\alpha}}] \Phi(e) \right) \quad (\text{B15})$$

with

$$\begin{aligned} \bar{\mathcal{V}}_{rstu} &= \sum_{(\Gamma)} \mathcal{V}_{rstu}^{\Gamma} [\Gamma] / \sum_{(\Gamma)} [\Gamma], \\ \sum_{(\Gamma)} [\Gamma] &= D_r [D_s - \Phi(P)] / [1 + \Phi(P)], \\ \bar{\mathcal{V}}_{rstu}^{\pm} &= \sum_{\Gamma} \mathcal{V}_{rstu}^{\Gamma} [\Gamma] [1 \pm (-1)^{\Gamma+2r}], \\ \sum_{\Gamma} [\Gamma] [1 \pm (-1)^{\Gamma+2r}] &= D_r [D_r \mp (-1)^{2r}]. \end{aligned} \quad (\text{B16})$$

Of course we must remember that, for \mathcal{H}_{mnp} ,

$$D_r = 2j_r + 1, \quad (-1)^{2r} = -1, \quad \Gamma \equiv J, \text{ etc.},$$

while for \mathcal{H}_{m0}

$$D_r = 2(2j_r + 1), \quad (-1)^{2r} = +1, \quad \Gamma \equiv JT, \text{ etc.}$$

It should be noted that \mathcal{H}_{m0} is not obtained by simply discarding the b coefficients in Eqs. (B14), because we can extract some $\gamma=00$ contribution from the T_{α} operators. The point will become quite clear when considering the diagonal contributions.

2. Diagonal forms of \mathcal{H}_m

\mathcal{H}_m is unique, but its diagonal part \mathcal{H}_m^d , which contains only m and T operators, can take two forms that reproduce average energies of configurations either at fixed m and T (\mathcal{H}_{mT}^d in a “ T ” formalism) or at fixed number of protons and neutrons (\mathcal{H}_{np}^d in an “ np ” formalism). Only $\mathcal{V}_{rsrs}^{\Gamma}$ matrix elements are involved, whose centroids will be called simply \mathcal{V}_{rs} and \mathcal{V}_{rs}^T (the overbar in $\bar{\mathcal{V}}_{rstu}^T$ was meant to avoid confusion with possible matrix elements \mathcal{V}_{rstu}^1 or \mathcal{V}_{rstu}^0 ; it can be safely dropped now). Then Eq. (B14) becomes Eq. (11), and Eq. (B15) becomes

$$\mathcal{H}_{mnp}^d \text{ or } \mathcal{H}_{m0}^d = \mathcal{K} + \sum_{r \leq s} \mathcal{V}_{rs} n_r (n_s - \delta_{rs}) / (1 + \delta_{rs}). \quad (\text{B17})$$

We rewrite the relevant centroids incorporating explicitly the Pauli restrictions,

$$\mathcal{V}_{rs} = \frac{\sum_{\Gamma} \mathcal{V}_{rsrs}^{\Gamma} [\Gamma] [1 - (-1)^{\Gamma} \delta_{rs}]}{D_r (D_s - \delta_{rs})}, \quad (\text{B18a})$$

$$\mathcal{V}_{rs}^T = \frac{4 \sum_J \mathcal{V}_{rsrs}^{JT} [J] [1 - (-1)^{J+T} \delta_{rs}]}{D_r [D_s + 2\delta_{rs} (-1)^T]}, \quad (\text{B18b})$$

$$\begin{aligned} a_{rs} &= \frac{1}{4} (3\mathcal{V}_{rs}^1 + \mathcal{V}_{rs}^0) = \mathcal{V}_{rs} + \frac{3}{4} \frac{\delta_{rs}}{D_r - 1} b_{rs}, \\ b_{rs} &= \mathcal{V}_{rs}^1 - \mathcal{V}_{rs}^0. \end{aligned} \quad (\text{B18c})$$

The relationship between a_{rs} and \mathcal{V}_{rs} makes it possible to combine Eqs. (11) and (B17) and in a single form:

$$\mathcal{H}_m^d = \mathcal{K} + \sum \frac{1}{(1 + \delta_{rs})} \left[\mathcal{V}_{rs} n_r (n_s - \delta_{rs}) + b_{rs} \left(T_r \cdot T_s - \frac{3n_r n_r}{4(D_r - 1)} \delta_{rs} \right) \right], \quad (\text{B19})$$

where now the b_{rs} term can be dropped to obtain \mathcal{H}_{m0}^d or \mathcal{H}_{mnp}^d .

In the np scheme each orbit r goes into two r_n and r_p , and the centroids can be obtained through $(x, y = n$ or $p, x \neq y)$

$$\begin{aligned} \mathcal{V}_{r_x s_y} &= \frac{1}{2} \left[\mathcal{V}_{rs}^1 \left(1 - \frac{2\delta_{rs}}{D_r} \right) + \mathcal{V}_{rs}^0 \left(1 + \frac{2\delta_{rs}}{D_r} \right) \right], \\ \mathcal{V}_{r_x s_x} &= \mathcal{V}_{rs}^1. \end{aligned} \quad (\text{B20})$$

Note that the diagonal terms depend on the representation $\mathcal{H}_{mnp}^d \neq \mathcal{H}_{mT}^d$ in general.

APPENDIX C: THE CENTER-OF-MASS PROBLEM

“What do you do about center of mass?” is probably the standard question most shell-model practitioners prefer to ignore or dismiss. Even if we may be tempted to do so, there is no excuse for ignoring what the problem is, and here we would like to explain it in sufficient detail to dispel some common misconceptions.

The center-of-mass (c.m.) problem arises because in a many-body treatment it is most convenient to work with A coordinates and momenta, while only $A-1$ of them can be linearly independent since the solutions cannot depend on the center-of-mass coordinate $R = (\sum_i r_i) / \sqrt{A}$ or momentum $P = (\sum_i p_i) / \sqrt{A}$. The way out is to impose a factorization of the wave functions into relative and c.m. parts: $\Phi(r_1 r_2 \cdots r_A) = \Phi_{rel} \phi_{c.m.}$. The potential energy is naturally given in terms of relative values, and for the kinetic energy we should do the same by referring to the c.m. momentum,

$$\sum_i \left(p_i - \frac{P}{\sqrt{A}} \right)^2 = \sum_i p_i^2 - P^2 = \frac{1}{A} \sum_{ij} (p_i - p_j)^2, \quad (\text{C1})$$

and change accordingly \mathcal{K}_{ij} in Eq. (2). As we are only interested in wave functions in which the center of mass is at rest (or in its lowest possible state), we can add a c.m. operator to the Hamiltonian $\mathcal{H} \Rightarrow \mathcal{H} + \lambda (R^2 + P^2)$, and calling $r_{ij} = r_i - r_j$ we have

$$R^2 + P^2 = \sum_i (r_i^2 + p_i^2) - \frac{1}{A} \sum_{ij} (r_{ij}^2 + p_{ij}^2), \quad (\text{C2})$$

so that upon diagonalization the eigenvalues will be of the form $E = E_{rel} + \lambda(N_{c.m.} + 3/2)$, and it only remains to select the states with $N_{c.m.} = 0$. We are taking for granted separation of c.m. and relative coordinates. Unfortunately, this happens only for spaces that are *closed* under the c.m. operator [Eq. (C2)]. For $N_{c.m.}$ to be a good quantum number the space must include all possible states with $N_{c.m.}$ oscillator quanta. The problem was raised by Elliott and Skyrme (1955), who initiated the study of “particle-hole” (*ph*) excitations on closed shells. They noted that acting with $R - iP$ on the IPM ground state of ^{16}O ($|0\rangle$) leads to

$$\sqrt{\frac{1}{18}}(\bar{p}_1 s_1 - \sqrt{2}\bar{p}_3 s_1 - \sqrt{5}\bar{p}_1 d_3 + \bar{p}_3 d_3 + 3\bar{p}_3 d_5)|0\rangle, \quad (\text{C3})$$

where \bar{p}_{2j} removes a particle and s_1 or d_{2j} add a particle on $|0\rangle$. As $R - iP$ has tensorial rank $J^\pi T = 1^-0$, Eq. (C3) is telling us that out of five possible 1^-0 excitations, one is “spurious” and has to be discarded.

Assume now that we are interested in $2p-2p$ excitations. They involve jumps of two oscillator quanta ($2\hbar\omega$), and the c.m. eigenstates $(R - iP)^2|0\rangle$ involve the operator in Eq. (C3), but also jumps to other shells, of the type $\bar{s}p\bar{p}(sd) \equiv \bar{s}(sd)$ or $(\bar{s}d)(p\bar{f})\bar{p}(sd) \equiv \bar{p}(p\bar{f})$. Therefore, as anticipated, relative-c.m. factorization can be achieved only by including all states involving a given number of oscillator quanta. The clean way to proceed is through complete $N\hbar\omega$ spaces, discussed in Secs. II.A and III.F. The $0\hbar\omega$ and EI spaces are also free of problems (the latter because no $1\hbar\omega$ 1^-0 states exist). It remains to analyze the EEI valence spaces, where c.m. spuriousness is always present but strongly suppressed because the main contributors to $R - iP$ —of the type $pj \Rightarrow p+1j \pm 1$, with the largest j —are always excluded. Consider $\text{EEI}(1) = p_{1/2}, d_{5/2}, s_{1/2}$. The only possible $1\hbar\omega$ 1^-0 state is $\bar{p}_1 s_1$, which according to Eq. (C3) accounts for $(1/18)\% = 5.6\%$ of the spurious state. This apparently minor problem was unduly transformed into a serious one through a proposal by Gloeckner and Lawson (1974). It amounts to projecting c.m. spuriousness through the $\mathcal{H} \Rightarrow \mathcal{H} + \lambda(R^2 + P^2)$ prescription in the $\text{EEI}(1)$ space by identifying $R - iP \equiv \bar{p}_1 s_1$. The procedure is manifestly incorrect, as was repeatedly pointed out (see, for instance, Whitehead *et al.*, 1977), but the misconception persists. An interesting and viable alternative was put forward by Dean *et al.* (1999) in calculations with two contiguous major shells. Further work on the subject would be welcome.

REFERENCES

- Abgrall, Y., G. Baron, E. Caurier, and G. Monsonego, 1967, Phys. Lett. **26B**, 53.
 Abgrall, Y., E. Caurier, and G. Monsonego, 1967, Phys. Lett. **24B**, 609.

- Abzouzi, A., E. Caurier, and A. P. Zuker, 1991, Phys. Rev. Lett. **66**, 1134.
 Ahmad, Q. R., *et al.* (SNO collaboration), 2002, Phys. Rev. Lett. **89**, 011301.
 Alford, W. P., *et al.*, 1993, Phys. Rev. C **48**, 2818.
 Alhassid, Y., G. F. Bertch, D. J. Dean, and S. E. Koonin, 1996, Phys. Rev. Lett. **77**, 1444.
 Alhassid, Y., D. J. Dean, S. E. Koonin, G. Lang, and W. E. Ormand, 1994, Phys. Rev. Lett. **72**, 613.
 Alhassid, Y., S. Liu, and H. Nakada, 1999, Phys. Rev. Lett. **83**, 4265.
 Altshuler, B. L., Y. Gefenand, A. Kamenevand, and L. S. Levitov, 1997, Phys. Rev. Lett. **78**, 2803.
 Anderson, B. D., T. Chittrakarn, A. R. Baldwin, C. Lebo, R. Madey, P. C. Tandy, J. W. Watson, B. A. Brown, and C. C. Foster, 1985, Phys. Rev. C **31**, 1161.
 Anderson, B. D., C. Lebo, A. R. Baldwin, T. Chittrakarn, R. Madey, and J. W. Watson, 1990, Phys. Rev. C **41**, 1474.
 Andreozzi, F., N. Lo Iudice, and A. Porrino, 2003, J. Phys. G **29**, 2319.
 Arima, A., 2001, Prog. Part. Nucl. Phys. **46**, 119.
 Arima, A., M. Harvey, and K. Shimuzi, 1969, Phys. Lett. **30B**, 517.
 Arima, A., and F. Iachello, 1975, Phys. Rev. Lett. **35**, 1069.
 Aumann, T., *et al.*, 2001, Phys. Rev. Lett. **84**, 35.
 Axel, O., J. H. D. Jensen, and H. E. Suess, 1949, Phys. Rev. **75**, 1766.
 Azaiez, F., 1999, in *Experimental Nuclear Physics in Europe*, AIP Conference Proceedings No. 495, edited by B. Rubio, M. Lozano, and W. Gelletly (AIP, Melville, NY), p. 171.
 Balysh, A., A. De Silva, V. I. Lebedev, K. Lou, M. K. Moe, M. A. Nelson, A. Piepke, A. Pronskiy, M. A. Vient, and P. Vogel, 1996, Phys. Rev. Lett. **77**, 5186.
 Bambynek, W., H. Behrens, M. H. Chen, B. Crasemann, M. L. Fitzpatrick, K. W. D. Ledingham, H. Genz, M. Mutterer, and R. L. Intermann, 1977, Rev. Mod. Phys. **49**, 77; **49**, 961(E) 1977.
 Bansal, R. K., and J. B. French, 1964, Phys. Lett. **11**, 145.
 Baranger, M., and K. Kumar, 1968, Nucl. Phys. A **110**, 490.
 Bardin, R. K., P. J. Gollon, J. D. Ullman, and C. S. Wu, 1970, Nucl. Phys. A **158**, 337.
 Bäumer, C., *et al.*, 2003, Phys. Rev. C **68**, 031303.
 Behrens, H., and W. Bühring, 1982, *Electron Radial Wave Functions and Nuclear Beta-decay* (Clarendon, Oxford).
 Bender, M., H. Flocard, and P.-H. Heenen, 2003, Phys. Rev. C **68**, 044321.
 Bender, M., P.-H. Heenen, and P. G. Reinhard, 2003, Rev. Mod. Phys. **75**, 121.
 Bennaceur, K., F. Nowacki, J. Okolowicz, and M. Ploszajczak, 1999, Nucl. Phys. A **651**, 289.
 Bennaceur, K., F. Nowacki, J. Okolowicz, and M. Ploszajczak, 2000, Nucl. Phys. A **671**, 203.
 Bentley, M. A., C. D. O’Leary, A. Poves, G. Martínez-Pinedo, D. E. Appelbe, R. A. Bark, D. M. Cullen, S. Ertürk, and A. Maj, 1998, Phys. Lett. B **437**, 243.
 Bentley, M. A., C. D. O’Leary, A. Poves, G. Martínez-Pinedo, D. E. Appelbe, R. A. Bark, D. M. Cullen, S. Ertürk, and A. Maj, 1999, Phys. Lett. B **451**, 445.
 Bentley, M. A., S. J. Williams, *et al.*, 2000, Phys. Rev. C **62**, 051303.
 Bertsch, G. F., and I. Hamamoto, 1982, Phys. Rev. C **26**, 1323.
 Bes, D. R., and R. A. Sorensen, 1969, in *Advances in Nuclear Physics*, edited by M. Baranger and E. Vogt (Plenum, New

- York), p. 129.
- Bethe, H. A., 1936, *Phys. Rev.* **50**, 332.
- Bhattacharya, M., *et al.*, 1998, *Phys. Rev. C* **58**, 3677.
- Bijker, R., and A. Frank, 2000a, *Phys. Rev. Lett.* **84**, 420.
- Bijker, R., and A. Frank, 2000b, *Phys. Rev. C* **62**, 014303.
- Bijker, R., A. Frank, and S. Pittel, 1999, *Phys. Rev. C* **60**, 021302.
- Bloom, S. D. B., 1984, *Prog. Part. Nucl. Phys.* **11**, 505.
- Bogner, A. N. S., and A. Schwenk, 2004, *Phys. Rev. C* **70**, 061002(R).
- Bogner, S. K., T. T. S. Kuo, and A. Schwenk, 2003, *Phys. Rep.* **386**, 1.
- Bohr, A., 1952, *K. Dan. Vidensk. Selsk. Mat. Fys. Medd.* **26**, 14.
- Bohr, A., and B. R. Mottelson, 1953, *K. Dan. Vidensk. Selsk. Mat. Fys. Medd.* **27**, 16.
- Bohr, A., and B. R. Mottelson, 1969, *Nuclear Structure* (Benjamin, New York), Vol. 1.
- Bohr, A., B. R. Mottelson, and D. Pines, 1958, *Phys. Rev.* **110**, 936.
- Borcea, R., *et al.*, 2001, *Nucl. Phys. A* **695**, 69.
- Borge, M. J. G., *et al.*, 1997, *Phys. Rev. C* **55**, R8.
- Brandolini, F., S. M. Lenzi, *et al.*, 1998, *Nucl. Phys. A* **642**, 387.
- Brandolini, F., N. Marginean, *et al.*, 2002, *Phys. Rev. C* **66**, 024304.
- Brandolini, F., N. H. Medina, *et al.*, 1999, *Phys. Rev. C* **60**, 041305.
- Brandolini, F., N. H. Medina, *et al.*, 2001, *Phys. Rev. C* **64**, 044307.
- Brandolini, F., J. Sánchez Solano, *et al.*, 2002, *Phys. Rev. C* **66**, 021302.
- Brown, B. A., 2001, *Prog. Part. Nucl. Phys.* **47**, 517.
- Brown, B. A., R. Clement, H. Schatz, J. Giansiracusa, W. A. Richter, M. Hjorth-Jensen, K. L. Kratz, B. Pfeiffer, and W. B. Walters, 2003, *Nucl. Phys. A* **719**, 177c.
- Brown, B. A., A. Etchegoyen, W. D. M. Rae, N. S. Godwin, W. A. Richter, C. H. Zimmerman, W. E. Ormand, and J. S. Winfield, 1985, OXBASH Code, Technical Report No. 524, MSU-NSCL available at <ftp://ftp.nscp.msu.edu/pub/oxbash>
- Brown, B. A., and B. H. Wildenthal, 1988, *Annu. Rev. Nucl. Part. Sci.* **38**, 29.
- Brueckner, K., 1954, *Phys. Rev.* **96**, 508.
- Cameron, J. A., M. A. Bentley, A. M. Bruce, R. A. Cunningham, W. Gelletly, H. G. Price, J. Simpson, D. D. Warner, and A. N. James, 1991, *Phys. Rev. C* **44**, 1882.
- Cameron, J. A., M. A. Bentley, A. M. Bruce, R. A. Cunningham, W. Gelletly, H. G. Price, J. Simpson, D. D. Warner, and A. N. James, 1994, *Phys. Rev. C* **49**, 1347.
- Cameron, J. A., M. A. Bentley, A. M. Bruce, R. A. Cunningham, H. G. Price, J. Simpson, D. D. Warner, A. N. James, W. Gelletly, and P. V. Isacker, 1993, *Phys. Lett. B* **319**, 58.
- Campi, X., H. Flocard, A. K. Kerman, and S. Koonin, 1975, *Nucl. Phys. A* **251**, 193.
- Carter, E. B., G. E. Mitchell, and R. H. Davis, 1964, *Phys. Rev.* **133**, B1421.
- Caurier, E., J. L. Egido, G. Martínez-Pinedo, A. Poves, J. Retamosa, L. M. Robledo, and A. P. Zuker, 1995, *Phys. Rev. Lett.* **75**, 2466.
- Caurier, E., K. Langanke, G. Martínez-Pinedo, and F. Nowacki, 1999, *Nucl. Phys. A* **653**, 439.
- Caurier, E., K. Langanke, G. Martínez-Pinedo, F. Nowacki, and P. Vogel, 2001, *Phys. Lett. B* **522**, 240.
- Caurier, E., G. Martínez-Pinedo, F. Nowacki, A. Poves, J. Retamosa, and A. P. Zuker, 1999a, *Phys. Rev. C* **59**, 2033.
- Caurier, E., G. Martínez-Pinedo, F. Nowacki, A. Poves, J. Retamosa, and A. P. Zuker, 1999b, in *Proceedings of the International Nuclear Physics Conference INPC/98*, edited by B. Frois (*Nucl. Phys. A* **164**, 747c).
- Caurier, E., P. Navrátil, W. E. Ormand, and J. P. Vary, 2001, *Phys. Rev. C* **64**, 051301(R).
- Caurier, E., P. Navrátil, W. E. Ormand, and J. P. Vary, 2002, *Phys. Rev. C* **66**, 024314.
- Caurier, E., and F. Nowacki, 1999, *Acta Phys. Pol. B* **30**, 705.
- Caurier, E., F. Nowacki, and A. Poves, 2001, *Nucl. Phys. A* **693**, 374.
- Caurier, E., F. Nowacki, and A. Poves, 2002, *Eur. Phys. J. A* **15**, 145.
- Caurier, E., F. Nowacki, A. Poves, and J. Retamosa, 1996, *Phys. Rev. Lett.* **77**, 1954.
- Caurier, E., F. Nowacki, A. Poves, and J. Retamosa, 1998, *Phys. Rev. C* **58**, 2033.
- Caurier, E., A. Poves, and A. P. Zuker, 1989, Report No. CRN/PN 89-22, Strasbourg.
- Caurier, E., A. Poves, and A. P. Zuker, 1990, *Phys. Lett. B* **252**, 13.
- Caurier, E., A. Poves, and A. P. Zuker, 1995, *Phys. Rev. Lett.* **74**, 1517.
- Caurier, E., M. Rejmund, and H. Grawe, 2003, *Phys. Rev. C* **67**, 054310.
- Caurier, E., A. P. Zuker, A. Poves, and G. Martínez-Pinedo, 1994, *Phys. Rev. C* **50**, 225.
- Cavedon, J. M., *et al.*, 1982, *Phys. Rev. Lett.* **49**, 978.
- Chau Huu-Tai, P., A. Frank, N. A. Smirnova, and P. Van Isacker, 2002, *Phys. Rev. C* **66**, 061302.
- Chevallier, P., F. Scheibling, G. Goldring, I. Plesser, and M. W. Sachs, 1967, *Phys. Rev.* **160**, 827.
- Chiara, C. J., *et al.*, 2003, *Phys. Rev. C* **67**, 041303.
- Chou, W.-T., E. K. Warburton, and B. A. Brown, 1993, *Phys. Rev. C* **47**, 163.
- Coester, F., and H. Kümmel, 1960, *Nucl. Phys.* **17**, 477.
- Cohen, S., and D. Kurath, 1965, *Nucl. Phys.* **73**, 1.
- Coraggio, L., N. Itaco, A. Covello, A. Gargano, and T. T. S. Kuo, 2003, *Phys. Rev. C* **68**, 034320.
- Cortes, A., R. U. Haq, and A. P. Zuker, 1982, *Phys. Lett.* **115B**, 1.
- Covello, A., F. Andreozzi, L. Coraggio, A. Gargano, T. T. S. Kuo, and A. Porrino, 1997, *Prog. Part. Nucl. Phys.* **18**, 165.
- Dang, N. D., A. Arima, T. Suzuki, and S. Yamaji, 1997, *Nucl. Phys. A* **621**, 719.
- Davidson, E. R., 1975, *J. Comput. Phys.* **17**, 87.
- Dean, D. J., S. E. Koonin, K. Langanke, P. B. Radha, and Y. Alhassid, 1995, *Phys. Rev. Lett.* **74**, 2909.
- Dean, D. J., M. T. Russell, M. Hjorth-Jensen, S. E. Koonin, K. Langanke, and A. P. Zuker, 1999, *Phys. Rev. C* **59**, 2474.
- Dechargé, J., and D. Gogny, 1980, *Phys. Rev. C* **21**, 1568.
- Descouvremont, P., 2002, *Nucl. Phys. A* **709**, 275.
- Detraz, C., D. Guillemaud, G. Huber, R. Klapisch, M. de Saint-Simon, C. Thibault, and F. Touchard, 1979, *Phys. Rev. C* **19**, 164.
- Dillmann, I., *et al.*, 2003, *Phys. Rev. Lett.* **91**, 162503.
- Doi, M., T. Kotani, and E. Takasugi, 1985, *Prog. Theor. Phys. Suppl.* **83**, 1.
- Drożdż, S., V. Klemt, J. Speth, and J. Wambach, 1986, *Phys. Lett.* **166B**, 18.
- Duflo, J., and A. P. Zuker, 1995, *Phys. Rev. C* **52**, R23.
- Duflo, J., and A. P. Zuker, 1999, *Phys. Rev. C* **59**, R2347.

- Duflo, J., and A. P. Zuker, 2002, *Phys. Rev. C* **66**, 051303(R).
- Dufour, M., and A. P. Zuker, 1996, *Phys. Rev. C* **54**, 1641.
- Dukelsky, J., and S. Pittel, 2001, *Phys. Rev. C* **63**, 061303.
- Dukelsky, J., S. Pittel, S. S. Dimitrova, and M. V. Stoistov, 2002, *Phys. Rev. C* **65**, 054319.
- Duvernois, M. A., 1997, *Astrophys. J.* **481**, 241.
- Eguchi, K., *et al.* (KamLAND Collaboration), 2003, *Phys. Rev. Lett.* **90**, 021802.
- El-Kateb, S., *et al.*, 1994, *Phys. Rev. C* **49**, 3128.
- Elliott, J. P., 1958a, *Proc. R. Soc. London, Ser. A* **245**, 128.
- Elliott, J. P., 1958b, *Proc. R. Soc. London, Ser. A* **245**, 562.
- Elliott, J. P., A. D. Jackson, H. A. Mavromantis, E. A. Sanderson, and B. Sing, 1968, *Nucl. Phys. A* **121**, 241.
- Elliott, J. P., and A. M. Lane, 1957, in *Handbuch der Physik XXXIX*, edited by S. Fluegge (Springer Verlag, Berlin), p. 241.
- Elliott, J. P., and T. H. R. Skyrme, 1955, *Proc. R. Soc. London, Ser. A* **232**, 561.
- Endt, P. M., and C. van der Leun, 1990, *Nucl. Phys. A* **521**, 1.
- Entem, D. R., and R. Machleidt, 2002, *Phys. Lett. B* **524**, 93.
- Entem, D. R., R. Machleidt, and H. Witala, 2002, *Phys. Rev. C* **65**, 064005.
- Fiase, J., A. Hamoudi, J. M. Irvine, and F. Yazici, 1988, *J. Phys. G* **14**, 27.
- Firestone, R. B., 1996, *Table of Isotopes* (Wiley, New York).
- Fisker, J. L., V. Barnard, J. Görres, K. Langanke, G. Martínez-Pinedo, and M. C. Wiescher, 2001, *At. Data Nucl. Data Tables* **79**, 241.
- Fisker, J. L., G. Martínez-Pinedo, and K. Langanke, 1999, *Eur. Phys. J. A* **5**, 229.
- French, J. B., 1966, in *Enrico Fermi Lectures XXXVI*, edited by C. Bloch (Academic, New York), p. 278.
- French, J. B., 1969, in *Isospin in Nuclear Physics*, edited by D. H. Wilkinson (North-Holland, Amsterdam).
- French, J. B., E. C. Halbert, J. B. McGrory, and S. S. M. Wong, 1969, in *Advances in Nuclear Physics*, edited by M. Baranger and E. Vogt (Plenum, New York), p. 193.
- Fricke, G., C. Bernhardt, K. Heilig, L. A. Schaller, L. Schellenberg, E. B. Shera, and C. W. D. Jager, 1995, *At. Data Nucl. Data Tables* **60**, 177.
- Fujita, Y., *et al.*, 2002, *Eur. Phys. J. A* **13**, 411.
- Fukuda, Y., *et al.* (Super-Kamiokande Collaboration), 1998, *Phys. Rev. Lett.* **81**, 1562.
- Fukunishi, N., T. Otsuka, and T. Sebe, 1992, *Phys. Lett. B* **296**, 279.
- Fuller, G. M., W. A. Fowler, and M. J. Newman, 1980, *Astrophys. J., Suppl.* **42**, 447.
- Fuller, G. M., W. A. Fowler, and M. J. Newman, 1982a, *Astrophys. J.* **252**, 715.
- Fuller, G. M., W. A. Fowler, and M. J. Newman, 1982b, *Astrophys. J., Suppl. Ser.* **48**, 279.
- Fuller, G. M., W. A. Fowler, and M. J. Newman, 1985, *Astrophys. J.* **293**, 1.
- Garrett, P. E., *et al.*, 2001, *Phys. Rev. Lett.* **87**, 132502.
- Glasmacher, T., 1998, *Annu. Rev. Nucl. Part. Sci.* **48**, 1.
- Gloeckner, D., and R. Lawson, 1974, *Phys. Lett.* **53B**, 313.
- Guillemaud-Mueller, D., C. Detraz, M. Langevin, F. Naulin, M. de Saint-Simon, C. Thibault, F. Touchard, and M. Epherre, 1984, *Nucl. Phys. A* **426**, 37.
- Hagiwara, K., *et al.* (Particle Data Group), 2002, *Phys. Rev. D* **66**, 010001.
- Halbert, E. C., J. B. McGrory, B. H. Wildenthal, and S. Pandya, 1971, in *Advances in Nuclear Physics*, edited by M. Baranger and E. Vogt (Plenum, New York), p. 316.
- Hannawald M., *et al.*, 1999, *Phys. Rev. Lett.* **82**, 1391.
- Hansen, P. G., and B. Jonson, 1987, *Europhys. Lett.* **4**, 409.
- Hara, K., and Y. Sun, 1995, *Int. J. Mod. Phys. E* **4**, 637.
- Hara, K., Y. Sun, and T. Mizusaki, 1999, *Phys. Rev. Lett.* **83**, 1922.
- Hauschild, K., M. Rejmund, and H. Grawe, 2001, *Phys. Rev. Lett.* **87**, 072501.
- Haxton, W. C., 1987, *Phys. Rev. D* **36**, 2283.
- Haxton, W. C., 1998, *Phys. Lett. B* **431**, 110.
- Haxton, W. C., and C. Johnson, 1990, *Phys. Rev. Lett.* **65**, 1325.
- Hayes, A. C., and I. S. Towner, 2000, *Phys. Rev. C* **61**, 044603.
- Hecht, K. T., and A. Adler, 1969, *Nucl. Phys. A* **137**, 129.
- Heger, A., E. Kolbe, W. C. Haxton, K. Langanke, G. Martínez-Pinedo, and S. E. Woosley, 2005, *Phys. Lett. B* **606**, 258.
- Heger, A., K. Langanke, G. Martínez-Pinedo, and S. E. Woosley, 2001, *Phys. Rev. Lett.* **86**, 1678.
- Heger, A., S. E. Woosley, G. Martínez-Pinedo, and K. Langanke, 2001, *Astrophys. J.* **560**, 307.
- Heisenberg, J. H., and B. M. Mihaila, 1999, *Phys. Rev. C* **59**, 1440.
- Hernnd, H., J. Görres, M. Wiescher, B. A. Brown, and L. van Wormer, 1995, *Phys. Rev. C* **52**, 1078.
- Heyde, K., and J. L. Woods, 1991, *J. Phys. G* **17**, 135.
- Hix, W. R., O. E. B. Messer, A. Mezzacappa, M. Liebendörfer, J. Sampaio, K. Langanke, D. J. Dean, and G. Martínez-Pinedo, 2003, *Phys. Rev. Lett.* **91**, 201102.
- Hjorth-Jensen, M., 1996, private communication.
- Hjorth-Jensen, M., T. T. S. Kuo, and E. Osnes, 1995, *Phys. Rep.* **261**, 126.
- Honma, M., T. Mizusaki, and T. Otsuka, 1996, *Phys. Rev. Lett.* **77**, 3315.
- Honma, M., T. Otsuka, B. A. Brown, and T. Mizusaki, 2002, *Phys. Rev. C* **65**, 061301.
- Honma, M., T. Otsuka, B. A. Brown, and T. Mizusaki, 2004, *Phys. Rev. C* **69**, 034335.
- Horoi, M., B. A. Brown, and V. Zelevinsky, 2001, *Phys. Rev. Lett.* **87**, 062501.
- Horoi, M., B. A. Brown, and V. Zelevinsky, 2002, *Phys. Rev. C* **65**, 027303.
- Horoi, M., B. A. Brown, and V. Zelevinsky, 2003, *Phys. Rev. C* **67**, 034303.
- Horoi, M., A. Volya, and V. Zelevinsky, 1999, *Phys. Rev. Lett.* **82**, 2064.
- Iachello, F., and A. Arima, 1987, *The Interacting Boson Model* (Cambridge University Press, Cambridge, England).
- Ibbotson, R. W., T. Glasmacher, P. F. Mantica, and H. Scheit, 1999, *Phys. Rev. C* **59**, 642.
- Ichimura, M., and A. Arima, 1966, *Prog. Theor. Phys.* **36**, 296.
- Id Betan, R., R. J. Liotta, N. Sandulescu, and T. Vertse, 2002, *Phys. Rev. Lett.* **89**, 042501.
- Ideguchi, E., *et al.*, 2001, *Phys. Rev. Lett.* **87**, 222501.
- Ikeda, K. I., S. Fujii, and J. I. Fujita, 1963, *Phys. Lett.* **3**, 271.
- Ilijin, A. S., M. V. Mebel, N. Bianchi, E. de Sanctis, C. Guaraldo, V. Lucherini, V. Muccifora, E. Polli, A. R. Reolon, and P. Rossi, 1992, *Nucl. Phys. A* **543**, 517.
- Iwasaki, H., *et al.*, 2001, *Phys. Lett. B* **522**, 227.
- Janssens, R. V. F., *et al.*, 2002, *Phys. Lett. B* **546**, 55.
- Jiang, M. F., R. Machleidt, D. B. Stout, and T. T. S. Kuo, 1989, *Phys. Rev. C* **40**, 1857.
- Johnson, C. W., G. F. Bertsch, and D. J. Dean, 1998, *Phys. Rev. Lett.* **80**, 2749.
- Johnson, C. W., G. F. Bertsch, D. J. Dean, and I. Talmi, 1999,

- Phys. Rev. C **61**, 014311.
- Juodagalvis, A., and S. Åberg, 1998, Phys. Lett. B **428**, 227.
- Kahana, S., H. Lee, and C. Scott, 1969a, Phys. Rev. **180**, 956.
- Kahana, S., H. Lee, and C. Scott, 1969b, Phys. Rev. **185**, 1378.
- Käppeler, F., F.-K. Thielemann, and M. Wiescher, 1998, Annu. Rev. Nucl. Part. Sci. **48**, 175.
- Kawarada, H., and A. Arima, 1964, J. Phys. Soc. Jpn. **19**, 1768.
- Klotz, G., P. Baumann, M. Bounajma, A. Huck, A. Knipper, G. Walter, G. Marguier, C. Richard-Serre, A. Poves, and J. Retamosa, 1993, Phys. Rev. C **47**, 2502.
- Kolbe, E., K. Langanke, and G. Martínez-Pinedo, 1999, Phys. Rev. C **60**, 052801.
- Kolbe, E., K. Langanke, G. Martínez-Pinedo, and P. Vogel, 2003, J. Phys. G **29**, 2569.
- Koonin, S. E., D. J. Dean, and K. Langanke, 1997a, Phys. Rep. **278**, 2.
- Koonin, S. E., D. J. Dean, and K. Langanke, 1997b, Annu. Rev. Nucl. Part. Sci. **47**, 463.
- Kowalski, K., D. J. Dean, M. Hjorth-Jensen, T. Papenbrock, and P. Piecuch, 2004, Phys. Rev. Lett. **92**, 132501.
- Kratz, K.-L., B. Pfeiffer, and F.-K. Thielemann, 1998, Nucl. Phys. A **630**, 352.
- Kumar, K., and M. Baranger, 1968, Nucl. Phys. A **110**, 529.
- Kümmel, H. K., K. H. Lührmann, and J. G. Zabolitzky, 1978, Phys. Rep. **36**, 1.
- Kuo, T. T. S., and G. Brown, 1968, Nucl. Phys. A **114**, 241.
- Kuo, T. T. S., and G. E. Brown, 1966, Nucl. Phys. **85**, 40.
- Kuo, T. T. S., and G. H. Herling, 1971, NRL Memorandum Report No. 2258.
- Lanczos, C., 1950, J. Res. Natl. Bur. Stand. **45**, 252.
- Langanke, K., 1998, Phys. Lett. B **438**, 235.
- Langanke, K., D. J. Dean, P. B. Radha, Y. Alhasid, and S. E. Koonin, 1995, Phys. Rev. C **52**, 718.
- Langanke, K., E. Kolbe, and D. J. Dean, 2001, Phys. Rev. C **63**, 032801.
- Langanke, K., and G. Martínez-Pinedo, 2000, Nucl. Phys. A **673**, 481.
- Langanke, K., and G. Martínez-Pinedo, 2001, At. Data Nucl. Data Tables **79**, 1.
- Langanke, K., and G. Martínez-Pinedo, 2003, Rev. Mod. Phys. **75**, 819.
- Langanke, K., G. Martínez-Pinedo, O. E. B. Messer, J. M. Sampaio, D. J. Dean, W. R. Hix, A. Mezzacappa, M. Liebendörfer, H.-T. Janka, and M. Rampp, 2003, Phys. Rev. Lett. **90**, 241102.
- Langanke, K., J. Terasaki, F. Nowacki, D. J. Dean, and W. Nazarewicz, 2003, Phys. Rev. C **67**, 044314.
- Lawson, R. D., and M. H. Macfarlane, 1965, Nucl. Phys. **66**, 80.
- Lee, H. C., 1969, code made available to A.P.Z.
- Lenzi, S. M., N. Marginean, *et al.*, 2001, Phys. Rev. Lett. **87**, 122501.
- Lenzi, S. M., D. R. Napoli, *et al.*, 1996, Z. Phys. A **354**, 117.
- Lenzi, S. M., D. R. Napoli, *et al.*, 1999, Phys. Rev. C **60**, 021303.
- Lenzi, S. M., C. A. Ur, *et al.*, 1997, Phys. Rev. C **56**, 1313.
- Liddick, S. N., *et al.*, 2004, Phys. Rev. Lett. **92**, 072502.
- Long, G.-L., and Y. Sun, 2001, Phys. Rev. C **63**, 021305.
- Machleidt, R., 2001, Phys. Rev. C **63**, 024001.
- Machleidt, R., F. Sammaruca, and Y. Song, 1996, Phys. Rev. C **53**, R1483.
- Mantica, P. F., *et al.*, 2003, Phys. Rev. C **67**, 014311.
- Marsden, D. C. J., P. Navrátil, S. A. Coon, and B. R. Barrett, 2002, Phys. Rev. C **66**, 044007.
- Martínez-Pinedo, G., 2001, Nucl. Phys. A **688**, 357c.
- Martínez-Pinedo, G., and K. Langanke, 1999, Phys. Rev. Lett. **83**, 4502.
- Martínez-Pinedo, G., A. Poves, E. Caurier, and A. P. Zuker, 1996, Phys. Rev. C **53**, R2602.
- Martínez-Pinedo, G., A. Poves, L. M. Robledo, E. Caurier, F. Nowacki, J. Retamosa, and A. P. Zuker, 1996, Phys. Rev. C **54**, R2150.
- Martínez-Pinedo, G., and P. Vogel, 1998, Phys. Rev. Lett. **81**, 281.
- Martínez-Pinedo, G., A. P. Zuker, A. Poves, and E. Caurier, 1997, Phys. Rev. C **55**, 187.
- Mayer, M., 1949, Phys. Rev. **75**, 1969.
- Mazzocchi, C., *et al.*, 2001, Eur. Phys. J. A **12**, 269.
- McCullen, J. D., B. F. Bayman, and L. Zamick, 1964, Phys. Rev. **134**, A515.
- Michel, N., W. Nazarewicz, M. Płoszajczak, and K. Bennaceur, 2002, Phys. Rev. Lett. **89**, 042502.
- Michel, N., W. Nazarewicz, M. Płoszajczak, and J. Okolowicz, 2003, Phys. Rev. C **67**, 054311.
- Mihaila, B. M., and J. H. Heisenberg, 2000, Phys. Rev. C **61**, 054309.
- Mizusaki, T., 2000, RIKEN Accel. Prog. Rep. **33**, 14.
- Mizusaki, T., and M. Imada, 2002, Phys. Rev. C **65**, 064319.
- Mizusaki, T., and M. Imada, 2003, Phys. Rev. C **67**, 041301.
- Mizusaki, T., T. Otsuka, M. Honma, and B. A. Brown, 2001, Phys. Rev. C **63**, 044306.
- Mizusaki, T., T. Otsuka, M. Honma, and B. A. Brown, 2002, Nucl. Phys. A **704**, 190c.
- Mizusaki, T., T. Otsuka, Y. Utsuno, M. Honma, and T. Sebe, 1999, Phys. Rev. C **59**, 1846.
- Mon, K. K., and J. B. French, 1975, Ann. Phys. (N.Y.) **95**, 90.
- Motobayashi, T., *et al.*, 1995, Phys. Lett. B **346**, 9.
- Mulhall, D., A. Volya, and V. Zelevinsky, 2000, Phys. Rev. Lett. **85**, 4916.
- Nakada, H., and Y. Alhassid, 1997, Phys. Rev. Lett. **79**, 2939.
- Navin, A., *et al.*, 2000, Phys. Rev. Lett. **85**, 266.
- Navrátil, P., and B. R. Barrett, 1996, Phys. Rev. C **54**, 2986.
- Navrátil, P., and B. R. Barrett, 1998, Phys. Rev. C **57**, 562.
- Navrátil, P., and B. R. Barrett, 1999, Phys. Rev. C **59**, 1906.
- Navrátil, P., G. P. Kamuntavičius, and B. R. Barrett, 2000, Phys. Rev. C **61**, 044001.
- Navrátil, P., and W. E. Ormand, 2002, Phys. Rev. Lett. **88**, 152502.
- Navrátil, P., W. E. Ormand, J. P. Vary, and B. R. Barrett, 2001, Phys. Rev. Lett. **87**, 172502.
- Navrátil, P., J. P. Vary, and B. R. Barrett, 2000a, Phys. Rev. Lett. **84**, 5728.
- Navrátil, P., J. P. Vary, and B. R. Barrett, 2000b, Phys. Rev. C **62**, 054311.
- Nilsson, S. G., 1955, K. Dan. Vidensk. Selsk. Mat. Fys. Medd. **29**, 16.
- Novoselsky, A., and M. Vallières, 1997, Drexel University shell-model code DUPSM.
- Novoselsky, A., M. Vallières, and O. La'adan, 1997, Phys. Rev. Lett. **79**, 4341.
- Novoselsky, A., M. Vallières, and O. La'adan, 1998a, Phys. Rev. C **57**, R19.
- Novoselsky, A., M. Vallières, and O. La'adan, 1998b, Phys. Rev. Lett. **81**, 5955.
- Nowacki, F., 1996, Ph.D. thesis (Institut de Recherches Subatomiques, Strasbourg).
- Nummela, S., P. Baumann, *et al.*, 2001, Phys. Rev. C **63**, 044316.
- Nummela, S., F. Nowacki, *et al.*, 2001, Phys. Rev. C **64**, 054313.

- Oda, T., M. Hino, K. Muto, M. Takahara, and K. Sato, 1994, *At. Data Nucl. Data Tables* **56**, 231.
- O'Leary, C. D., M. A. Bentley, D. E. Appelbe, D. M. Cullen, S. Ertürk, R. A. Bark, A. Maj, and T. Saitoh, 1997, *Phys. Rev. Lett.* **79**, 4349.
- O'Leary, C. D., *et al.*, 2002, *Phys. Lett. B* **525**, 49.
- Ormand, W. E., and C. W. Johnson, 2002, REDSTICK code.
- Ormand, W. E., 1997, *Phys. Rev. C* **55**, 2407.
- Ormand, W. E., and B. A. Brown, 1995, *Phys. Rev. C* **52**, 2455.
- Ormand, W. E., P. M. Pizzochero, P. F. Bortignon, and R. A. Broglia, 1995, *Phys. Lett. B* **345**, 343.
- Osterfeld, F., 1992, *Rev. Mod. Phys.* **64**, 491.
- Otsuka, T., R. Fujimoto, Y. Utsuno, B. A. Brown, M. Honma, and T. Mizusaki, 2001, *Phys. Rev. Lett.* **87**, 082502.
- Otsuka, T., and N. Fukunishi, 1996, *Phys. Rep.* **264**, 297.
- Otsuka, T., M. Honma, and T. Mizusaki, 1998, *Phys. Rev. Lett.* **81**, 1588.
- Otsuka, T., M. Honma, T. Mizusaki, N. Shimizu, and Y. Utsuno, 2001, *Prog. Part. Nucl. Phys.* **47**, 319.
- Palmer, C. W. P., *et al.*, 1984, *J. Phys. B* **17**, 2197.
- Pandharipande, V. R., I. Sick, and P. K. A. deWitt Huberts, 1997, *Rev. Mod. Phys.* **69**, 981.
- Papenbrock, T., and D. J. Dean, 2003, *Phys. Rev. C* **67**, 051303.
- Pasquini, E., 1976, Ph.D. thesis (Université Louis Pasteur, Strasbourg), Report No. CRN/PT 76-14.
- Pasquini, E., and A. P. Zuker, 1978, in *Physics of Medium Light Nuclei: Proceedings of the Topical Conference on Physics of Medium Light Nuclei*, Florence, 1977, edited by P. Blasi, and R. A. Ricci (Editrice Compositori, Bologna).
- Peierls, R. E., and J. Yoccoz, 1957, *Proc. Phys. Soc., London, Sect. A* **70**, 381.
- Péru, S., M. Girod, and J. F. Berger, 2000, *Eur. Phys. J. A* **9**, 35.
- Petrovici, A., K. W. Schmid, A. Faessler, J. H. Hamilton, and A. V. Ramay, 1999, *Prog. Part. Nucl. Phys.* **43**, 485.
- Pfeiffer, B., K.-L. Kratz, F.-K. Thielemann, and W. B. Walters, 2001, *Nucl. Phys. A* **693**, 282.
- Pieper, S. C., V. R. Pandharipande, R. B. Wiringa, and J. Carlson, 2001, *Phys. Rev. C* **64**, 014001.
- Pieper, S. C., K. Varga, and R. B. Wiringa, 2002, *Phys. Rev. C* **66**, 044310.
- Pieper, S. C., and R. B. Wiringa, 2001, *Annu. Rev. Nucl. Part. Sci.* **51**, 53.
- Porter, C. E., 1965, Ed., *Statistical Theories of Spectra: Fluctuations* (Academic, New York).
- Poves, A., and G. Martínez-Pinedo, 1998, *Phys. Lett. B* **430**, 203.
- Poves, A., and J. Retamosa, 1987, *Phys. Lett. B* **184**, 311.
- Poves, A., and J. Retamosa, 1994, *Nucl. Phys. A* **571**, 221.
- Poves, A., and J. Sánchez Solano, 1998, *Phys. Rev. C* **58**, 179.
- Poves, A., J. Sánchez-Solano, E. Caurier, and F. Nowacki, 2001, *Nucl. Phys. A* **694**, 157.
- Poves, A., and A. P. Zuker, 1981a, *Phys. Rep.* **71**, 141.
- Poves, A., and A. P. Zuker, 1981b, *Phys. Rep.* **70**, 235.
- Priyachenko, B. V., *et al.*, 1999, *Phys. Lett. B* **461**, 322.
- Pudliner, B. S., V. R. Pandharipande, J. Carlson, S. Pieper, and R. W. Wiringa, 1997, *Phys. Rev. C* **56**, 1720.
- Radha, P. B., D. J. Dean, S. E. Koonin, T. T. S. Kuo, K. Langanke, A. Poves, J. Retamosa, and P. Vogel, 1996, *Phys. Rev. Lett.* **76**, 2642.
- Raju, R. D. R., J. P. Draayer, and K. T. Hecht, 1973, *Nucl. Phys. A* **202**, 433.
- Rakers, S., *et al.*, 2002, *Phys. Rev. C* **65**, 044323.
- Raman, S., C. W. Nestor, S. Kahane, and K. H. Bhatt, 1989, *At. Data Nucl. Data Tables* **42**, 1.
- Rapaport, J., *et al.*, 1983, *Nucl. Phys. A* **410**, 371.
- Rauscher, T., and F.-K. Thielemann, 2000, *At. Data Nucl. Data Tables* **75**, 1.
- Retamosa, J., E. Caurier, and F. Nowacki, 1995, *Phys. Rev. C* **51**, 371.
- Retamosa, J., E. Caurier, F. Nowacki, and A. Poves, 1997, *Phys. Rev. C* **55**, 1266.
- Richter, A., 1995, *Prog. Part. Nucl. Phys.* **34**, 261.
- Richter, W. A., M. J. van der Merwe, R. E. Julies, and B. A. Brown, 1991, *Nucl. Phys. A* **523**, 325.
- Rodriguez-Guzmán, R., J. L. Egido, and L. M. Robledo, 2000, *Phys. Lett. B* **474**, 15.
- Rönnqvist, T., *et al.*, 1993, *Nucl. Phys. A* **563**, 225.
- Rudolph, D., *et al.*, 1999, *Phys. Rev. Lett.* **82**, 3763.
- Rutsgl, M. L., H. W. Kung, R. Raj, R. A. Nisley, and H. H. Hull, 1971, *Phys. Rev. C* **4**, 874.
- Sagawa, H., B. A. Brown, and H. Esbensen, 1993, *Phys. Lett. B* **309**, 1.
- Sakurai, H., *et al.*, 1999, *Phys. Lett. B* **448**, 180.
- Sampaio, J. M., K. Langanke, and G. Martínez-Pinedo, 2001, *Phys. Lett. B* **511**, 11.
- Sampaio, J. M., K. Langanke, G. Martínez-Pinedo, and D. J. Dean, 2002, *Phys. Lett. B* **529**, 19.
- Sarazin, F., *et al.*, 2000, *Phys. Rev. Lett.* **84**, 5062.
- Sawicka, M., *et al.*, 2003, *Eur. Phys. J. A* **16**, 51.
- Schmid K. W., 2001, *Prog. Part. Nucl. Phys.* **46**, 145.
- Schopper, H. W., 1966, *Weak Interactions and Nuclear Beta Decay* (North-Holland, Amsterdam).
- Schwenk, A., and A. P. Zuker, 2005, nucl-th/0501038.
- Serot, B. D., and J. D. Walecka, 1986, *Adv. Nucl. Phys.* **16**, 1.
- Shimizu, N., T. Otsuka, T. Mizusaki, and M. Honma, 2001, *Phys. Rev. Lett.* **86**, 1171.
- Siiskonen, T., P. O. Lippas, and J. Rikowska, 1999, *Phys. Rev. C* **60**, 034312.
- Simon, H., *et al.*, 1999, *Phys. Rev. Lett.* **83**, 496.
- Sohler, D., *et al.*, 2002, *Phys. Rev. C* **66**, 054302.
- Sorlin, O., C. Donzaud, *et al.*, 2000, *Nucl. Phys. A* **669**, 351.
- Sorlin, O., C. Donzaud, *et al.*, 2003, *Eur. Phys. J. A* **16**, 55.
- Sorlin, O., S. Leenhardt, *et al.*, 2002, *Phys. Rev. Lett.* **88**, 092501.
- Stoks, V. G. J., R. A. M. Klomp, M. C. M. Rentmeester, and J. J. de Swart, 1993, *Phys. Rev. C* **48**, 792.
- Stoks, V. G. J., R. A. M. Klomp, C. P. F. Terheggen, and J. J. de Swart, 1994, *Phys. Rev. C* **49**, 2950.
- Storm, M. H., A. Watt, and R. R. Whitehead, 1983, *J. Phys. G* **9**, L165.
- Suhonen, J., and O. Civitarese, 1998, *Phys. Rep.* **300**, 123.
- Sur, B., E. B. Norman, K. T. Lesko, E. Browne, and R.-M. Larimer, 1990, *Phys. Rev. C* **42**, 573.
- Suzuki, K., 1982, *Prog. Theor. Phys.* **68**, 246.
- Suzuki, K., and S. Y. Lee, 1980, *Prog. Theor. Phys.* **64**, 2091.
- Suzuki, T., R. Fujimoto, and T. Otsuka, 2003, *Phys. Rev. C* **67**, 044302.
- Suzuki, T., and T. Otsuka, 1994, *Phys. Rev. C* **50**, R555.
- Svensson, C. E., S. M. Lenzi, *et al.*, 1998, *Phys. Rev. C* **58**, R2621.
- Svensson, C. E., A. O. Macchiavelli, *et al.*, 2000, *Phys. Rev. Lett.* **85**, 2693.
- Svensson, C. E., A. O. Macchiavelli, *et al.*, 2001, *Phys. Rev. C* **63**, 061301.
- Takasugi, E., 1981, *Phys. Lett.* **103B**, 219.
- Talmi, I., and I. Unna, 1960, *Annu. Rev. Nucl. Sci.* **10**, 353.
- Tanihata, I., H. Hamagaki, O. Hasimoto, N. Yoshikawa, K.

- Sugimoto, O. Yamakawa, T. K. Kobayashi, and N. Takahashi, 1985, *Phys. Rev. Lett.* **55**, 2676.
- Thibault, C., R. Klapisch, C. Rigaud, A. M. Poskancer, R. Prieels, L. Lesard, and W. Reisdorf, 1975, *Phys. Rev. C* **12**, 644.
- Toivanen, J., E. Kolbe, K. Langanke, G. Martínez-Pinedo, and P. Vogel, 2001, *Nucl. Phys. A* **694**, 395.
- Tonev, D., *et al.*, 2002, *Phys. Rev. C* **65**, 034314.
- Towner, I. S., and J. C. Hardy, 2002, *Phys. Rev. C* **66**, 035501.
- Tsuboi, T., K. Muto, and H. Horie, 1984, *Phys. Lett.* **143B**, 2122.
- Ur, C. A., *et al.*, 1998, *Phys. Rev. C* **58**, 3163.
- Utsuno, Y., T. Otsuka, T. Mizuzaki, and M. Honma, 1999, *Phys. Rev. C* **60**, 054315.
- Vargas, C. E., J. G. Hirsch, and J. P. Draayer, 2001, *Nucl. Phys. A* **690**, 409.
- Vargas, C. E., J. G. Hirsch, and J. P. Draayer, 2002a, *Nucl. Phys. A* **697**, 655.
- Vargas, C. E., J. G. Hirsch, and J. P. Draayer, 2002b, *Phys. Rev. C* **66**, 064309.
- Vautherin, D., and D. M. Brink, 1972, *Phys. Rev. C* **5**, 626.
- Velázquez, V., and A. P. Zuker, 2002, *Phys. Rev. Lett.* **88**, 072502.
- Vetterli, M. C., *et al.*, 1990, *Phys. Rev. C* **40**, 559.
- Vold, P. B., D. Cline, R. Boyd, H. Clement, W. Alford, and J. Kuehner, 1978, *Nucl. Phys. A* **302**, 12.
- Volpe, C., N. Auerbach, G. Colò, T. Suzuki, and N. van Giai, 2000, *Phys. Rev. C* **62**, 015501.
- von Neumann-Cosel, P., A. Poves, J. Retamosa, and A. Richter, 1998, *Phys. Lett. B* **443**, 1.
- Wakasa, T., *et al.*, 1997, *Phys. Rev. C* **55**, 2909.
- Wakasa, T., *et al.*, 1998, *Phys. Lett. B* **426**, 257.
- Wallerstein, G., *et al.*, 1997, *Rev. Mod. Phys.* **69**, 995.
- Warburton, E. K., J. A. Becker, and B. A. Brown, 1990, *Phys. Rev. C* **41**, 1147.
- Warburton, E. K., and B. A. Brown, 1991, *Phys. Rev. C* **43**, 602.
- Weidenmüller, H. A., 1990, *Nucl. Phys. A* **507**, 5c.
- White, J. A., S. E. Koonin, and D. J. Dean, 2000, *Phys. Rev. C* **61**, 034303.
- Whitehead, R. R., 1980, in *Moment Methods in Many Fermion Systems*, edited by B. J. Dalton, S. M. Grimes, J. D. Vary, and S. A. Williams (Plenum, New York), p. 235.
- Whitehead, R. R., A. Watt, B. J. Cole, and I. Morrison, 1977, *Adv. Nucl. Phys.* **9**, 123.
- Wildenthal, B. H., 1984, *Prog. Part. Nucl. Phys.* **11**, 5.
- Wildenthal, B. H., and W. Chung, 1979, *Phys. Rev. C* **19**, 164.
- Wildenthal, B. H., M. S. Curtin, and B. A. Brown, 1983, *Phys. Rev. C* **28**, 1343.
- Wilkinson, D. H., 2002a, *Nucl. Instrum. Methods Phys. Res. A* **495**, 65.
- Wilkinson, D. H., 2002b, *Nucl. Instrum. Methods Phys. Res. A* **488**, 654.
- Wilkinson, D. H., and B. E. F. Macefield, 1974, *Nucl. Phys. A* **58**, 58.
- Wilkinson, J. H., 1965, *The Algebraic Eigenvalue Problem* (Clarendon, Oxford).
- Williams, A. L., *et al.*, 1995, *Phys. Rev. C* **51**, 1144.
- Wiringa, R. B., and S. C. Pieper, 2002, *Phys. Rev. Lett.* **89**, 182501.
- Wiringa, R. B., S. C. Pieper, J. Carlson, and V. R. Pandharipande, 2000, *Phys. Rev. C* **62**, 014001.
- Wiringa, R. B., V. G. J. Stoks, and R. Schiavilla, 1995, *Phys. Rev. C* **51**, 38.
- Wuosmaa, A. H., *et al.*, 1998, *Phys. Rev. Lett.* **80**, 2085.
- Yanasak, N. E., *et al.*, 2001, *Astrophys. J.* **563**, 768.
- Yoneda, K., *et al.*, 2000, *Phys. Lett. B* **499**, 233.
- Zaerpoor, K., *et al.*, 1997, *Phys. Rev. Lett.* **79**, 4306.
- Zamick, L., 1965, *Phys. Lett.* **19**, 580.
- Zdesenko, Y., 2002, *Rev. Mod. Phys.* **74**, 663.
- Zhao, Y. M., and A. Arima, 2001, *Phys. Rev. C* **64**, 041301.
- Zhao, Y. M., A. Arima, and N. Yoshinaga, 2001, *Phys. Rev. C* **66**, 034302.
- Zheng, D. C., B. R. Barrett, L. Jaqua, J. P. Vary, and R. J. McCarthy, 1993, *Phys. Rev. C* **48**, 1083.
- Zheng, D. C., J. P. Vary, and B. R. Barrett, 1994, *Phys. Rev. C* **50**, 2841.
- Zuker, A. P., 1969, *Phys. Rev. Lett.* **23**, 983.
- Zuker, A. P., 1984, in *Mathematical and Computational Methods in Nuclear Physics: Proceedings of 6th Granada Workshop*, edited by J. S. Dehesa, J. M. G. Gómez, and A. Polls, Lecture Notes in Physics, No. 209 (Springer, Berlin), p. 157.
- Zuker, A. P., 1994, *Nucl. Phys. A* **576**, 65.
- Zuker, A. P., 2001, *Phys. Rev. C* **64**, 021303(R).
- Zuker, A. P., 2003, *Phys. Rev. Lett.* **90**, 042502.
- Zuker, A. P., B. Buck, and J. B. McGrory, 1968, *Phys. Rev. Lett.* **21**, 39.
- Zuker, A. P., B. Buck, and J. B. McGrory, 1969, *Shell Model Wave Functions for A=15-18 Nuclei*, Brookhaven National Laboratory, Technical Report No. PD-99 BNL 14085.
- Zuker, A. P., S. Lenzi, G. Martínez-Pinedo, and A. Poves, 2002, *Phys. Rev. Lett.* **89**, 142502.
- Zuker, A. P., J. Retamosa, A. Poves, and E. Caurier, 1995, *Phys. Rev. C* **52**, R1741.
- Zuker, A. P., L. Waha-Ndeuna, F. Nowacki, and E. Caurier, 2001, *Phys. Rev. C* **64**, 021304(R).